

UNIVERSITAT POLITÈCNICA DE VALÈNCIA  
DEPARTAMENT DE COMUNICACIONS

**Design of optical fiber sensors  
and interrogation schemes**



UNIVERSITAT  
POLITÈCNICA  
DE VALÈNCIA

Ph.D THESIS

Demetrio Sartiano

Supervisors:

Salvador Sales Maicas

David Barrera Vilar

Universitat Politècnica de València

October, 2020



## **Acknowledgment**

First, I would like to thank my supervisor Salvador Sales and the co-director of the thesis David Barrera for their help and guidance along these years and their help reviewing this thesis. It has been a pleasure working with them.

I would like to thank all the members of the PRL especially Javier, Gloria, Luis, Dani, Jesus for the time we spent together inside and outside the university. I would like to thank all my colleagues from FINESSE for the great time we spent during the training events and the secondments.

I am grateful to the supervisors of my secondments in Lausanne and Brussels, Thomas Geernaert and Luc Thevenaz for welcoming in their research groups.

I would like to greatly thank the European Union's Horizon 2020 Research and Innovation Program that funded the research described in this thesis under the Marie Skłodowska-Curie Action Grant Agreement N° 722509.

I would like to express my gratefulness to my family for their love, without their support it would not be possible to achieve this goal. I dedicate this work to them.



## Resumen

Las fibras ópticas son dispositivos muy utilizados en el campo de las telecomunicaciones desde su descubrimiento. En las últimas décadas, las fibras ópticas comenzaron a utilizarse como sensores fotónicos. Los primeros trabajos se centraron en la medición de unas dimensiones físicas en un punto específico. Posteriormente, surgió la posibilidad de medir las propiedades de la fibra óptica en diferentes puntos a lo largo de la fibra. Este tipo de sensores se definen como sensores distribuidos. Los componentes optoelectrónicos fueron desarrollados e investigados para telecomunicaciones. Los avances en las telecomunicaciones hicieron posible el desarrollo de sistemas de interrogación para sensores de fibra óptica, creciendo en paralelo con los avances de las telecomunicaciones.

Se desarrollaron sistemas de interrogación de fibra óptica que permiten el uso de una única fibra óptica monomodo estándar como sensor que puede monitorear decenas de miles de puntos de detección al mismo tiempo. Los métodos que extraen la información de detección de la señal reflejada en la fibra óptica son los más empleados debido a la facilidad de acceso al sensor y la flexibilidad de estos sistemas. Los más estudiados son la reflectometría en dominios de tiempo y frecuencia. La reflectometría óptica en el dominio del tiempo (OTDR) fue la primera técnica utilizada para detectar la posición de los fallos en las redes de comunicación de fibra óptica. El OTDR sensible a la fase hizo posible detectar la elongación y la temperatura en una posición específica. Paralelamente, los gratings de Bragg (FBG) se convirtieron en los dispositivos más utilizados para implementar sensores en fibra óptica discretos. Se desarrollaron técnicas de multiplexación para realizar la detección en múltiples puntos utilizando FBGs. La reflectometría realizada interrogando arrays de FBG débiles demuestra que mejora el rendimiento del sistema en comparación al uso de una fibra monomodo.

Los sistemas de interrogatorio actuales tienen algunos inconvenientes. Algunos de ellos son velocidad de interrogatorio limitada, grandes dimensiones y alto costo. En esta tesis doctoral se desarrollaron nuevos sistemas de interrogación y sensores de fibra óptica para superar algunos de estos inconvenientes. Los sensores de fibra óptica de plástico demuestran ser una plataforma innovadora para desarrollar nuevos sensores y sistemas de interrogación de bajo costo y fáciles de implementar para fibras de plástico comerciales. Se investigó la reflectometría en el dominio del tiempo y las técnicas fotónicas de microondas para la interrogación de una matriz de rejillas débiles que permitieron simplificar el sistema de interrogación para la detección de temperatura y vibración.



## **Abstract**

Optical fibers are devices largely used in telecommunication field since their discovery. In the last decades, optical fibers started to be used as photonic sensors. The first works were focused on the measurement of physical dimensions to a specific point. Afterward, emerged the possibility to measure the optical fiber properties at different locations along the fiber. These kinds of sensors are defined as distributed sensors. The optoelectronic components were developed and investigated for telecommunications. The progress in telecommunication made possible the development of optical fiber sensors interrogation systems, growing in parallel with the advances of telecommunications.

Optical fiber interrogation systems were developed to use a single standard mono-mode optical fiber as a sensor that can monitor tens of thousands of sensing points at the same time. The methods that extract the sensing information from the backscattered signal in the optical fiber are widely employed because of the easiness of access to the sensor element and the flexibility of these systems. The most studied are the reflectometry in time and frequency domains. The optical time domain reflectometry (OTDR) was the first technique used to detect the position of the failures in the optical fiber communication networks. Using phase sensitive OTDR it is possible to sense strain and temperature at a specific position. In parallel, fiber Bragg gratings (FBGs) became the most widely used devices to implement discrete optical fiber sensors. Multiplexing techniques were developed to perform multi points sensing using these gratings. The reflectometry performed interrogating weak FBGs arrays demonstrate to improve the performance of the system employing a single mode fiber.

The interrogation systems nowadays have some drawbacks. Some of them are limited speed of interrogation, bulkiness, and high cost. New interrogation systems and optical fiber sensors were developed in this doctoral thesis to overcome some of these drawbacks. Plastic optical fiber sensors demonstrate to be an innovative platform to develop both new sensors and low cost, easy to implement interrogation systems for commercial plastic fibers. Reflectometry in time domain and microwave photonic techniques were investigated for the interrogation of weak gratings array allowed to simplify the interrogation system for the sensing of temperature and vibration.





## Resum

Les fibres òptiques són dispositius molt utilitzats en el camp de les telecomunicacions des del seu descobriment. En les últimes dècades, les fibres òptiques van començar a utilitzar-se com a sensors fotònics. Els primers treballs es van centrar en el mesurament d'unes dimensions físiques en un punt específic. Posteriorment, va sorgir la possibilitat de mesurar les propietats de la fibra òptica en diferents punts al llarg de la fibra. Aquest tipus de sensors es defineixen com a sensors distribuïts. Els components optoelectrònics van ser desenvolupats i investigats per a telecomunicacions. Els avanços en les telecomunicacions van fer possible el desenvolupament de sistemes d'interrogació per a sensors de fibra òptica, creixent en paral·lel amb els avanços de les telecomunicacions.

Es van desenvolupar sistemes d'interrogació de fibra òptica que permeten l'ús d'una única fibra òptica monomodo estàndard com a sensor que pot monitorar desenes de milers de punts de detecció al mateix temps. Els mètodes que extreuen la informació de detecció del senyal reflectit en la fibra òptica són els més utilitzats a causa de la facilitat d'accés al sensor i la flexibilitat d'aquests sistemes. Els més estudiats són la reflectometria en dominis de temps i freqüència. La reflectometria òptica en el domini del temps (OTDR) va ser la primera tècnica utilitzada per a detectar la posició de les fallades en les xarxes de comunicació de fibra òptica. El OTDR sensible a la fase va fer possible detectar l'elongació i la temperatura en una posició específica. Paral·lelament, els gratings de Bragg (FBG) es van convertir en els dispositius més utilitzats per a implementar sensors en fibra òptica discrets. Es van desenvolupar tècniques de multiplexació per a realitzar la detecció en múltiples punts utilitzant FBGs. La reflectometria realitzada interrogant arrays de FBG febles demostra que millora el rendiment del sistema en comparació a l'ús d'una fibra monomodo.

Els sistemes d'interrogatori actuals tenen alguns inconvenients. Alguns d'ells són velocitat d'interrogatori limitada, voluminositat i alt cost. En aquesta tesi doctoral es van desenvolupar nous sistemes d'interrogació i sensors de fibra òptica per a superar alguns d'aquests inconvenients. Els sensors de fibra òptica de plàstic demostren ser una plataforma innovadora per a desenvolupar nous sensors i sistemes d'interrogació de baix cost i fàcils d'implementar per a fibres de plàstic comercials. Es va investigar la reflectometria en el domini del temps i les tècniques fotòniques de microones per a la interrogació d'una matriu de reixetes febles que van permetre simplificar el sistema d'interrogació per a la detecció de temperatura i vibració.



# Index

## CHAPTER 1

<b>Introduction to optical fiber sensors.....</b>	<b>1</b>
1.1.Optical fiber sensors.....	2
1.2.Distributed.....	2
1.3.Discrete.....	5
1.3.1. Fabrication and types of optical fiber Bragg gratings....	7
1.3.2. Weak FBG arrays based sensors.....	10
1.4.Plastic optical fiber sensing.....	12
1.4.1. Wearable POF sensors for health care.....	15
1.5.Objective and structure of the thesis.....	17
Reference.....	19

## CHAPTER 2

<b>Plastic optical fiber sensor for vital signal monitoring.....</b>	<b>29</b>
2.1. Intensity based optical fiber sensors.....	30
2.2. Plastic optical sensor embedded in mattress for signal vital monitoring.....	32
2.2.1. Setup implementation.....	32
2.2.2. Measurements and discussion.....	39
2.3. Miniaturized plastic optical fiber interrogation system.....	45
2.4. Conclusions.....	46
Reference.....	48

## CHAPTER 3

<b>Trilobal plastic optical fiber sensors.....</b>	<b>52</b>
3.1. Trilobal plastic optical fiber sensor for curvature and rotation monitoring.....	53
3.1.1. Extrusion process.....	55
3.1.2. Numerical mode confinement simulation in non-circular POF...	59
3.1.3. Trilobal fiber fabrication and experimental results.....	61
3.2. Conclusions.....	68
Reference.....	69

## **CHAPTER 4**

### **Interrogation system for temperature/strain fiber-based sensor..... 73**

4.1. Discrete and distributed fiber sensor.....	74
4.1.1. FBG: discrete sensing and multiplexing.....	74
4.1.2. Time analysis: distributed sensing.....	75
4.1.3. Distributed sensing with FBGs.....	76
4.2. Interrogation setup and principle of operation.....	77
4.3. Temperature measurement.....	81
4.4. Vibration measurement.....	85
4.5. Conclusions.....	87
Reference.....	89

## **CHAPTER 5**

### **The role of laser coherence length in microwave photonics fiber sensing...94**

5.1. Microwave photonics.....	95
5.2. MWP in optical fiber sensing.....	96
5.2.1. Light source linewidth and coherence regime.....	99
5.2.2. Fiber Bragg gratings array fabrication.....	103
5.3. Coherence length influence on amplitude noise.....	104
5.3.1. Measurement of amplitude noise .....	104
5.5. Conclusions.....	108
Reference.....	109

## **CHAPTER 6**

### **Summary, conclusions and open research lines..... 114**

6.1. Summary and conclusions.....	115
6.2. Open research lines.....	117

## **APPENDIX 1**

### **Glossary.....118**

**APPENDIX 2: Author's publications**

**Scientific publications in journals.....119**  
**Scientific publications in congresses.....119**  
**Participation in research projects.....120**

## LIST OF FIGURES

Figure 1.1. Frequency response of light scattering in optical fibers. The frequency $f_0$ is the frequency of the injected light, $f_B$ is the Brillouin frequency ( $\approx 9-11$ GHz) and $f_R$ is the Raman frequency ( $\approx 13$ THz).....	3
Figure 1.2. Schematic representation of Rayleigh scattering inside optical fiber core. The imperfection inside the core is represented as a black spot, that scatter light in all direction.....	3
Figure 1.3. Representation of the effect of strain/temperature on the two component of the Brillouin scattering and on the anti-Stokes component of Raman.....	5
Figure 1.4. Schematic representation of the FBG as refractive index fluctuation in the core of the fiber. The incoming light is reflected at the Bragg wavelength $\lambda_B$ .....	6
Figure 1.5. A UV light is shined on a phase mask. The two order of diffraction (+1 and -1) generate an interference pattern. The fiber core is exposed to the interference pattern to fabricate an FBG.....	8
Figure 1.6. Draw tower fabrication of FBGs arrays: after the extrusion of the fiber from a preform the gratings are inscribed using a pulsed laser and an interferometric setup. Finally, the coating is applied to the gratings array.....	9
Figure 1.7. Figures taken from [59]. (a) Part of the setup with the gratings and the unbalanced Mach-Zender. (b) Operation principle used to generate interference between the reflected signals of adjacent FBGs.....	11

Figure 1.8. Image taken from [69], the process to fabricate mPOFs is schematically shown.....	13
Figure 1.9. Image taken from [81]: difference between extrinsic (up) and intrinsic (down) POF sensors.....	14
Figure 1.10. The three scenarios studied in [130], using a POF based multiplexed system for robot rehabilitation.....	17
Figure 2.1. The conversion of a measurand in an optical magnitude (in this case light intensity).....	31
Figure 2.2. (a) 3D model of the plastic holder used to cut the fibers. The hemicylindrical groove has the same diameter as the plastic fiber to limit the penetration of the blade into the fiber and obtain similar cuts of approximately 1.1 mm (half of the fiber diameter) depth. (b) Effect of a pressure exerted on a sensitized point of the POF ESKA.....	33
Figure 2.3. Normalized response to curvature of six sensitive points.....	34
Figure 2.4. (a) Schematic representation of the fiber matrix; and (b) sensor implementation: the arrows represent the communication between the computer, the board and the electronic components of the interrogation circuit.....	35
Figure 2.5. (a) Cross section of the LED used to inject light in the plastic fiber. (b) Schematic representation of the current driver circuit.....	36
Figure 2.6. (a) Photodetectors array TSL1402R; and (b) 3D model of the fiber holder, entire piece (left) and cross-section (right).....	37
Figure 2.7. (a) Plot of the light level detected by the two arrays of photodetectors, the eight peaks are the light outputs of the eight fibers bottom	

coupled to the photodetectors array; and (b) light signal post-processing: the software individuates and store the first and last pixel position that detect a light power above a certain threshold (noise level), any variation of light power in this area will be interpreted as a pressure applied in one of the sensitive points of the fiber.....38

Figure 2.8. (a) Experimental set-up; and (b) mattress cover with the integrated POFs, the points tested to measure the static response are highlighted.....41

Figure 2.9. (a) Time response of a fiber, after a pressure is applied: in blue is reported the response measured and in red the theoretical response calculated considering the frequency response of the electronics. (b) Frequency response retrieved from the time response data calculating the derivative of the Fourier transform. In red is represented the  $-3$  dB line, the theoretical impulse response of the system is plotted with red dots.....43

Figure 2.10. Cyclic loading test to verify the presence of a drift in the response, in red is represented the initial zero-pressure base line.....44

Figure 2.11. (a) SMD package with dome lens of the red LED used for the PCB. (b) Spatial distribution of the output power.....45

Figure 2.12. (a) Main PCB (front and rear) with microcontroller (1); LED matrix (2); Bluetooth module (3). (b) PCB with the photodetector array; the two boards are connected through the JTS pins observable in the upper part in the rear of the main PCB.....46

Figure 3.1. Scheme of the extrusion system: the plastic material is fed into the extruder in form of pellet, the material is melted into the chamber using variable heater. The motor moves the screw that push the melted materials through the extrusion die. The extrudate is then cool down and collected.....55



Figure 3.2. Output of the custom extrusion die designed to fabricate the trilobal fiber.....59

Figure 3.3. (a) Optical microscope image of the cross-section of the three-lobe plastic optical fiber. (b) Simulated light field intensity of the fundamental mode at 645 nm.....60

Figure 3.4. Normalized Light field intensity ( $<103$  V/m) at 645nm of the two lowest order modes calculated in the imported three-lobe structure cross-section for bending with curvature center placed: (a) on the upper surface of the fiber; (b) on the lower surface of the fiber; (c) on the right-hand surface of the fiber.....61

Figure 3.5. Photo of the cross-sections of the obtained plastic optical fibers.....62

Figure 3.6. Schematic representation of the experimental setup.....63

Figure 3.7. Method used to obtain constant curvature.....65

Figure 3.8. Images collected with the CCD camera after bending the three-lobe plastic fiber. Red stars indicate the position of the weighted centroid, found from the converted gray scale image. The curvature center placed: (a) on the upper surface of the fiber; (b) on the lower surface of the fiber; (c) on the right-hand surface of the fiber.....65

Figure 3.9. Images captured with the CCD camera of the POF with rotation. The circular asymmetry can observe the rotation of the fiber core and retrieve the rotation angles (reported below).....67

Figure 3.10. (a) Reference and rotated image superimposed before and after the registration algorithm is applied. (b) Comparison between the

retrieved angles using the registration algorithm and the rotation angles applied. The error bars show the average error of ten measurements.....67

Figure 4.1. Laser module and optical fiber cavity used for gain-switching implemented with polarization maintaining fiber and two partial reflectors.....78

Figure 4.2. Scheme of the interrogation system and array of 500 weak FBGs.....79

Figure 4.3. (a) Interrogation pulse after the dispersion element (green line) and back reflect-ed pulse from an FBG at different temperatures. (b) The points represent the maximum of the peaks plotted in figure 3a superimposed to the interrogation pulse (blue line).....80

Figure 4.4. Scheme of the closed loop temperature system. A Peltier with a heatsink was used to set the temperature of the hot spot. The thermistor monitors the temperature. The temperature controller (TEC) provides the current to the Peltier according to the voltage signal of the thermistor.....81

Figure 4.5. Reflected signal of the array portion under test. The two images show the heating of two points (first point showed in (a), second point showed in (b)) less than one centimeter apart. In both cases the time shift is visible due to the temperature rising from 10°C to 40°C.....82

Figure 4.6. (a) Evaluation of the response of the sensor to temperature. (b) When the temperature was swept from 10°C to 40°C there was linear relation between time stamps and temperature.....84

Figure 4.7. (a) Scheme of the interrogation system. (b) Recovered spectra of the photodetector electrical output when a vibration of 25 kHz is applied to the sensing element.....86

Figure 4.8. Frequency spectra of the photodetector electrical output when the frequency of the vibration is swept between 15 kHz and 245 kHz....87

Figure 5.1. Schematic representation of an MWP system for RF signal processing. The optical signal is represented in blue, while the electrical signal is represented with black lines.....96

Figure 5.2. Schematic representation of a generic MWP setup used for sensing.....97

Figure 5.3. Implementation of a generic MWP filter with  $n$  taps. LS: light source; PD: photodetector; EOM: electro-optical modulator;  $\alpha_n$ : weight of the  $n$ th tap;  $\tau_n$ : delay of the  $n$ th tap;  $H(f)$ : frequency response.....98

Figure 5.4. A generic scheme of an MWP based interrogation system for an array of FBGs. LS: light source; PD: photodetector; EOM: electro-optical modulator; EVNA: electric vector network analyzer.....99

Figure 5.5. Principle of operation of the interrogation system presented in [3]. Tuning the filter of the light source it is possible to retrieve information about the hot spot in a long FBG.....100

Figure 5.6. Schematic of the core tracking system. The 400 nm photoluminescence, generated by the UV irradiation, is sensed on one end of the optical fiber during the fabrication. The moving mirror deflect the laser beam to maximize the irradiation.....103

Figure 5.7. Spectra of a single FBG of the array. The transmitted power drop of 0.5 dB at the Bragg wavelength.....105

Figure 5.8. The time domain impulse response retrieved applying the IFFT to the frequency signal measured with the EVNA. In (a) is shown the response of the array with the FBGs spaced of 20 cm, in (b) the response of the array with 150 cm spacing.....106

Figure 5.9. Time average (blue line) and peak amplitudes (red circles) for the 10 measurements performed in the four configurations listed in table 1.....107

## LIST OF TABLES

Table 2.1. Results of the linear regression for the loading static test. The alpha is the first-degree term of the linear regression, the beta is the constant term. The  $R^2$  values are reported in the third columns.....40

Table 3.1. First samples of POFs fabricated: images of the cross-section, fabrication parameters and optical power losses in dB/m measured with the cut-back method .....57

Table 3.2. Samples of POFs fabricated: images of the cross-section, fabrication parameters and optical power losses in dB/m measured with the cut-back method.....58

Table 3.3. Properties of Plexiglass 6N and 8N.....63

Table 3.4. Samples of trilobal POFs fabricated: fabrication parameters and optical power losses in dB/m measured with the cut-back method.....63

Table 5.1. List of the configuration of FBGs spacing and coherence length for the four measurements.....106

Table 5.2. Maximum variance of the peak amplitude for the four configurations .....107

**Chapter 1**  
**Introduction to optical  
fiber sensors**

## **1.1. Optical fiber sensors**

Photonic sensors are devices where light is the sensing element. Intensity [1-17], polarization [18-19], phase [20], wavelength [21] of the light guided in a waveguide change in function of one or more measurands. Optical fibers are employed as well as photonic sensors. The cost of optical fibers, the lightweight and the good handling make them ideal devices to sense over a distance of tens of kilometers (as achieved in the last years with distributed sensors) and to embedded fibers in composite [22-24], structure [25-28] and aircraft [29-32]. A general overview is given in this first section of discrete and distributed sensors and how fiber Bragg gratings based sensors breakthrough opens new possibilities in the distributed sensing field. In the last section plastic optical fiber (POF) sensing is introduced together with the state of the art.

## **1.2. Distributed**

Distributed sensors enable simultaneous measurements of temperature, strain, and vibration at multiple locations along a sensing fiber, and typically employ scattering phenomena in the raw optical fiber [33]. The backscattered light is collected, and the intensity/frequency contains the information about the local temperature/strain of the fiber. The main scattering phenomena observable in optical fibers are Rayleigh, Brillouin, and Raman (figure 1).

Rayleigh scattering is a linear effect produced by the refractive index changes, that exists in the fiber core as imperfection in the silica crystal. The light is scattered in all directions and part of that light is back reflected and guided back in the fiber (figure 2).

As the backscattered signal is quite low powered ( $< -70$  dB/m), highly sensitive photodetectors must be used to sense the back reflected signal and use it for sensing applications. Optical reflectometry is extensively used in optical fiber sensing in the time domain (OTDR) and in the frequency domain (OFDR). OTDR was first adopted in the communication field to

locate damage in the optical fiber network, and later in the sensing field in the phase sensitive version ( $\Phi$ -OTDR). Lasers with high coherence are used to create a coherent interference of the light reflected in the optical fiber [34-36]. It is possible to sense temperature and strain for several kilometers of optical fiber with a relatively low spatial resolution using this technique, for this reason, is defined as distributed sensing.

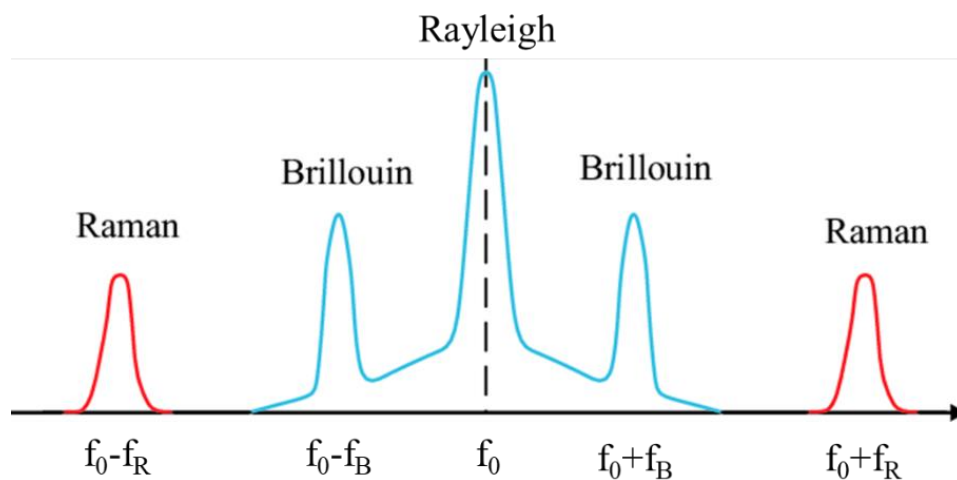


Figure 1. Frequency response of light scattering in optical fibers. The frequency  $f_0$  is the frequency of the injected light,  $f_B$  is the Brillouin frequency ( $\approx 9-11$  GHz) and  $f_R$  is the Raman frequency ( $\approx 13$  THz).

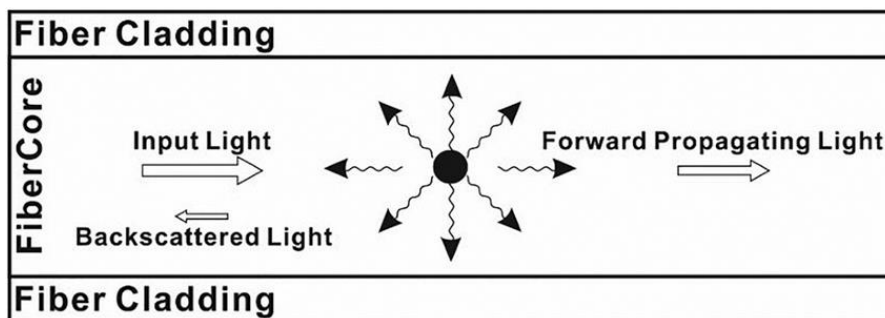


Figure 2. Schematic representation of Rayleigh scattering inside optical fiber core. The imperfections inside the core are represented as a black spot, that scatters light in all directions.

Brillouin scattering is due to the interaction of light with density fluctuations induced by the propagation of acoustic waves in the fiber. In silica-based optical fiber, the frequency of Stokes and anti-Stokes photon at 1550 nm is 9-11 GHz (figure 1). Pump and probe counter propagating waves are launched in the optical fiber. If the pump power is above the Brillouin threshold stimulated Brillouin scattering is produced. The peak frequency of the scattering wave has a linear dependence on strain and temperature according to the formula:

$$v_B = C_T \delta T + C_\varepsilon \delta \varepsilon + v_{B0} \quad (1)$$

where  $C_\varepsilon$  is the strain coefficient (MHz/ $\mu\varepsilon$ ),  $C_T$  is the temperature coefficient (MHz/ $^\circ\text{C}$ ) and  $v_{B0}$  the reference Brillouin frequency.  $C_T$  and  $C_\varepsilon$  are mostly determined by the fiber composition, pump wavelength, fiber coatings, and jackets [37]. Sensing the Brillouin frequency along the optical fiber it is possible to perform distributed sensing of temperature/strain [38].

Spontaneous Raman scattering is exploited for distributed temperature sensing in optical fibers. While temperature (and strain) affects both the Stokes and anti-Stokes component of the Brillouin scattering, for Raman scattering only the anti-Stokes component is sensitive to temperature variation while the Stokes component is only slightly dependent on the local temperature (figure 3) [33].

A laser pulse is launched inside the sensing fiber. The backscattered signal is filtered around the two Raman scattering components, that are detected using avalanche photodiodes and trans-impedance amplifiers. The temperature for each point in the fiber is obtained using the formula:

$$T = \left\{ \frac{1}{T_{ref}} - \frac{k_B}{h\nu_R} \ln \frac{R(T)}{R(T_{ref})} \right\}^{-1} \quad (2)$$



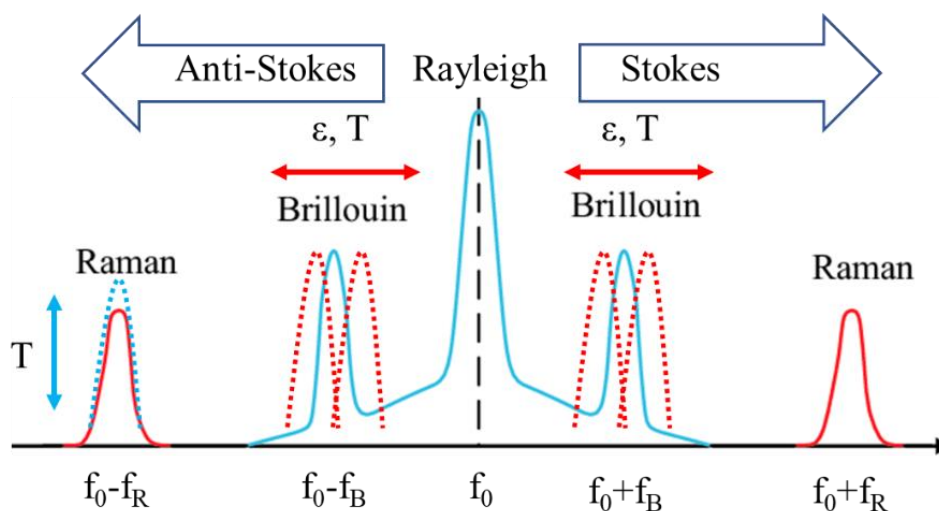


Figure 3. Representation of the effect of strain/temperature on the two components of the Brillouin scattering and on the anti-Stokes component of Raman.

Here  $k_B$  is the Boltzmann constant,  $h$  is the Planck constant,  $\nu_R$  the Raman frequency shift,  $R(T)$  the ratio between the two Raman components at a temperature  $T$  and  $T_{ref}$  a reference temperature.

### 1.3. Discrete

Discrete or multiplexed sensors sense temperature, strain, or vibration in a certain number of spots using reflectors and optical gratings. The spatial resolution is not dependent on the sampling frequency used to quantize the signal that is reflected in the core as in distributed sensing but on the position of the sensitive zones in the fiber. Fiber Bragg gratings (FBGs) are widely used as point sensors. FBG is a periodical modulation of the core refractive index (figure 4). The most common technique employed high power UV lasers to create a periodical grating inside the fiber core [39], that is photosensitive to UV light due to the high concentration of Germanium. The light traveling through the gratings partially scatters because of the refractive index modulation. The scattered light interferes

constructively at a certain wavelength (called Bragg wavelength ( $\lambda_B$ )) and propagates backward in the fiber core.

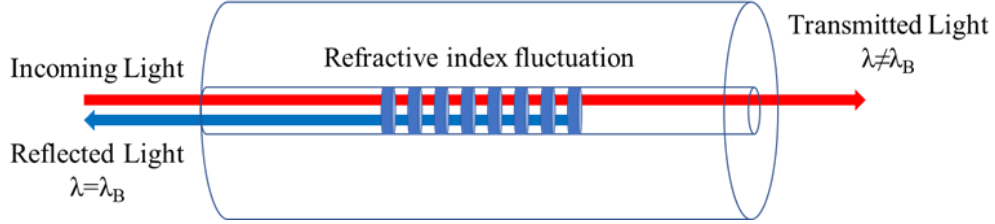


Figure 4. Schematic representation of the FBG as refractive index fluctuation in the core of the fiber. The incoming light is reflected at the Bragg wavelength  $\lambda_B$ .

The Bragg wavelength can be expressed as:

$$\lambda_B = 2n_{eff}\Lambda \quad (3)$$

Here  $n_{eff}$  is the effective refractive index of the optical fiber core and  $\Lambda$  is the pitch of the modulation of the refractive index. Modifications of refractive index or grating pitch change the reflected Bragg wavelength. This variation, mainly related to temperature and strain, can be expressed as:

$$\Delta\lambda_B = \frac{\delta\lambda_B}{\delta\varepsilon}\varepsilon + \frac{\lambda_B}{\delta T}\Delta T \quad (4)$$

Separating the two terms we obtain the sensitivity to temperature and strain:

$$\Delta\lambda_B = \lambda_B \left\{ 1 - \frac{n^2}{2} [p_{12} - \nu(p_{11} + p_{12})] \right\} \varepsilon \quad (5)$$

$$\Delta\lambda_B = \lambda_B \left( \alpha_\Lambda + \frac{1}{n_{eff}} \frac{\delta n_{eff}}{\delta T} \right) \Delta T \quad (6)$$

In (5)  $p_{11}$  and  $p_{12}$  are the elasto-optic tensor coefficients and  $\nu$  is the Poisson's coefficient and in (6)  $\alpha_\Lambda$  is the thermal expansion coefficient and  $\delta n_{eff}/\delta T$  the effective refractive index change in relation to temperature.

As the FBG spectrum shifts when a temperature or strain variation is exerted on the grating region, it is necessary to estimate the peak wavelength

(known as Bragg wavelength) from the FBG spectrum and then to track its shift from the reference position to effectively use an FBG to estimate a temperature or strain variation [40]. This method can reach a resolution of 10 pm/°C [41] for temperature measurement. One single grating inscribed on fiber can sense temperature or strain at one point. FBGs must be inscribed with different Bragg wavelengths and every peak must be tracked independently to sense at multiple points using peak tracking and single fiber. This method is commonly known as wavelength division multiplexing (WDM) [42].

### ***1.3.1. Fabrication and types of optical fiber Bragg gratings***

The photosensitivity in the optical fiber core was first reported in [43]. The radiation produced with a single mode Argon laser was injected inside the fiber core of an optical fiber. It was observed that the reflected power, due in principle to the Fresnel effect at the fiber end, was growing with the exposure time. This because after a certain exposure time, a permanent periodical reflecting element was permanently inscribed in the fiber core. These filters obtained were characterized afterward [44], and the tunability by stretching was characterized. The gratings obtained were formed with a long exposure procedure, and the reflected wavelength depended on the wavelength of the laser used to inject light in the fiber core.

After several years, in 1993, a more flexible method was introduced for the fabrication of optical fiber Bragg gratings: UV exposure through a phase mask [45]. A KrF excimer laser was modulated using a phase mask that generates a periodic pattern. The fiber core of a monomode fiber was exposed to the interference pattern producing a periodic refractive index change in the core (figure 5). Apodization demonstrates to lower the secondary lobes the spectral response.

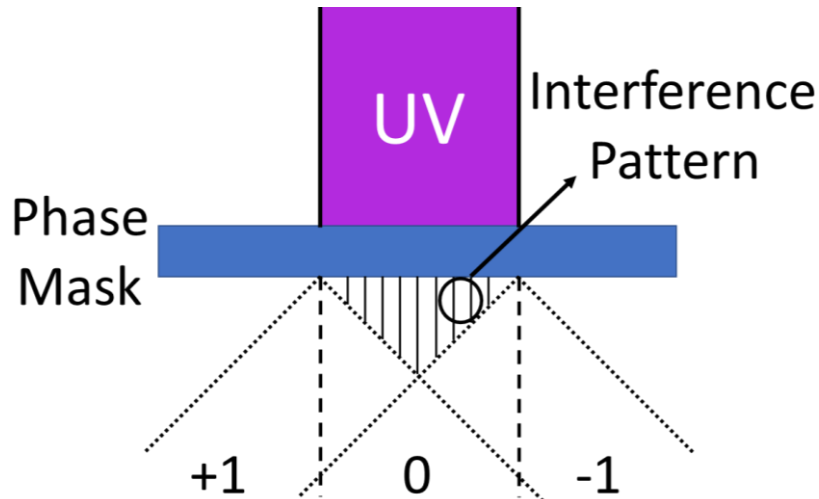


Figure 5. A UV light is shined on a phase mask. The two order of diffraction (+1 and -1) generate an interference pattern. The fiber core is exposed to the interference pattern to fabricate an FBG.

Depending on the formation mechanism different types of gratings are obtained:

- Type I gratings: they are obtained by single UV photon absorption. If the refractive index change is large, change in glass density was observed. The periodic fluctuation of the refractive index is annealed at high temperatures (450°C) in these gratings.
- Type II gratings: obtained using a pulsed laser with high power. High reflective gratings were fabricated using these mechanisms. The refractive index change is formed “damaging” the glass of the fiber core. These types of gratings can resist higher temperature than type I (over 1000°C)
- Type IIA gratings: these gratings are type I ones but with higher expose time. It was observed that if the exposure time is higher enough the type I gratings decrease in strength and a secondary grating growth. It was demonstrated that these gratings can temperature up to 700°C.
- Regenerated gratings: type I gratings can be thermally treated with a cycle of high temperatures. After temporary annealing of the original

gratings, a new grating is generated with a higher Bragg wavelength and lower reflectivity. This second grating is stable at high temperatures up to 1000°C [46].

The first demonstration of type II grating fabricated with draw tower is reported in [47]. Draw tower allows the fabrication of a large number of Bragg gratings in-line during the optical fiber extrusion. A pulsed KrF excimer was adopted to implement an interferometric inscription system (figure 6).

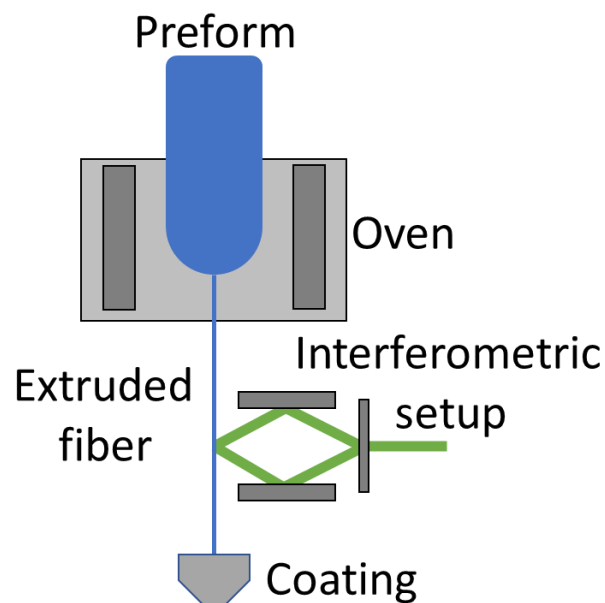
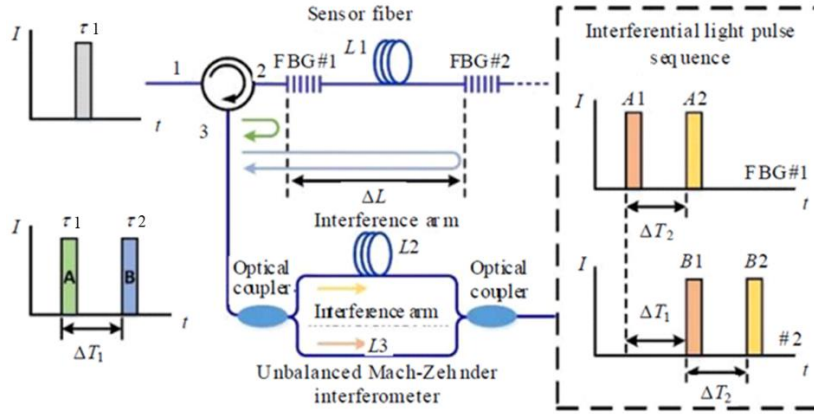


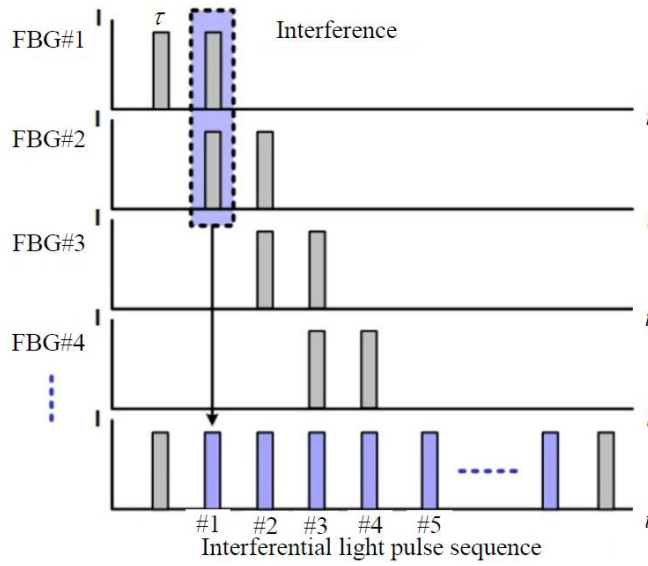
Figure 6. Draw tower fabrication of FBGs arrays: after the extrusion of the fiber from a preform the gratings are inscribed using a pulsed laser and an interferometric setup. Finally, the coating is applied to the gratings array.

### **1.3.2. Weak FBG arrays based sensors**

Implementing a system to perform distributed sensing with FBGs would require the grating to be inscribed along the length of the sensing fiber [48-49]. The idea is to enhance the back reflected signal in fiber using a weak uniform grating. The fabrication of a 1 meter long grating is reported in [50], two perpendicular cameras are used to track and actively compensate the deviation of the laser beam from the hanged fiber, this pointing procedure or other technique is crucial for fabricating high quality long gratings. Anyhow, the production of such a device for long distance is still a challenge and draw tower gratings fabrication offers an effective alternative: long arrays of weak gratings. The gratings are created during the drawing process of the optical fiber [51] enabling the production of long arrays with a large number of FBGs. If the FBGs are densely assembled in the array a higher backscattered signal can be obtained (as in using a Faint Long Optical Grating [48]) and a quasi-distributed sensor can be implemented [52-54]. Ultra-weak gratings arrays are employed to improve established distributed sensing systems as phase sensitive OTDR [54-55] or, in most cases, to be interrogated using interferometric interrogation setup [56-57]. Acoustic sensing is performed as well using these devices [58-61]. The basic principle of operation is based on the interference of the reflection of two gratings using an unbalanced Mach-Zender interferometer (figure 7a). The delays introduced by the grating spacing ( $L_1$ ) and the unbalanced arms ( $L_2-L_3$ ) are  $dT_1$  and  $dT_2$  respectively (figure 7b). When  $dT_1$  and  $dT_2$  are comparable the reflected pulses interfere. The interference of two consecutive gratings can be sampled and used to detect the vibration at a certain location.



(a)



(b)

Figure 7. Figures taken from [59]. (a) Part of the setup with the gratings and the unbalanced Mach-Zehnder. (b) Operation principle used to generate interference between the reflected signals of adjacent FBGs.

The interference intensity can be written as:

$$I = I_1 + I_2 + 2\sqrt{I_1 I_2} \cos[\Delta\varphi + \varphi_0] \quad (7)$$

With  $I_1$  and  $I_2$ , the intensity of the reflected pulse for grating 1 and 2,  $\Delta\varphi$  the phase shift and  $\varphi_0$  the starting phase. The signal is divided in a 1x3 coupler to avoid signal fading for phase value close to  $\pi$ , for an ideal splitting the signal in each branch of the coupler can be expressed as:

$$I_n = I_1 + I_2 + 2\sqrt{I_1 I_2} \cos \left[ \Delta\varphi(t) - (i - 1) \frac{2}{3} \pi \right], i = 1, 2, 3 \quad (8)$$

The phase difference introduced avoid signal fading in case of phase shift close to  $\pi$ . The three components are used to extract the phase shift module [62].

Advanced interrogation schemes allow quasi-distributed acoustic sensing over tens of meters [63]. The last mentioned interrogation techniques used to interrogate weak FBG arrays are OFDR [64] and microwave filtering photonic techniques that have also been used to interrogate a weak grating array [65] and a long weak grating [66].

#### **1.4.POF sensing**

Plastic optical fibers were researched in the last 50 years, initially for telecommunication. The improvement achieved in transparency and bandwidth made them a flexible and economical alternative to glass fibers for short distance communication. Plastic optical fibers are not only cheaper but also easy to handle.

POF are manufactured starting from a preform cylinder tens of centimeters long and with several centimeters of diameter. It is then extruded in a POF of several kilometers. The refractive index profile of the preform can be fabricated to obtain a specific refractive index profile for the final POF. Microstructured POFs (mPOF) were manufactured also in the last decades starting from long thin tubes stacked to create a preform and obtain the desired microstructure [67-69] (figure 8).



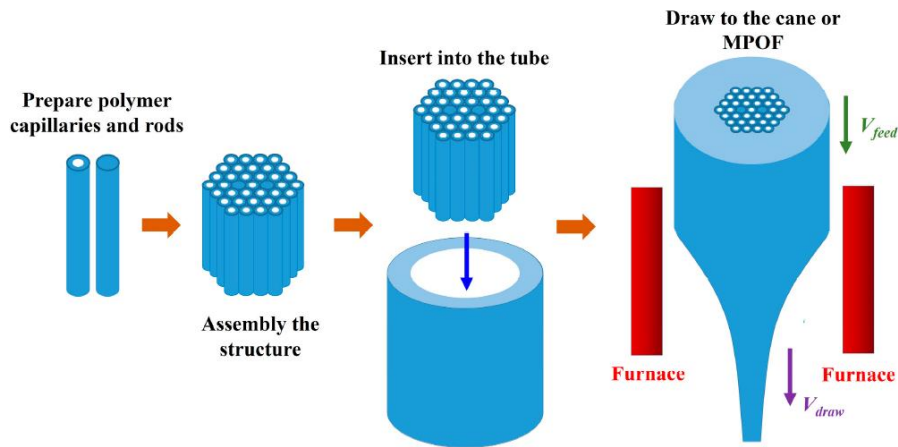


Figure 8. Image taken from [69], the process to fabricate mPOFs is schematically shown.

Some years later POFs were introduced in communication, their employment as sensors started to be investigated. In the scientific literature, several techniques to develop POF based sensors, are described together with the backscattering techniques, used as well with glass fiber (OTDR [70-73], OFDR [74-75]). Long and short period gratings have been fabricated in POF and mPOF [76-79]; the techniques used to monitor the shift of the wavelength spectra are the one used for FBG in glass fibers [80-81].

Anyhow, sensors based on intensity variation is the most common solution adopted when using POF [82]. Intensity-based sensing in transmission offers a cost-effective alternative that allows developing compact interrogation systems. A light source injects the light into the fiber core and a photodetector monitors the output power. The intensity-based sensors can be divided into two big groups: extrinsic and intrinsic. The first uses the fiber only to deliver and recollect the light to the sensing area, the second uses the fiber as a sensing element, so the light signal never leaves the optical fiber (figure 9).

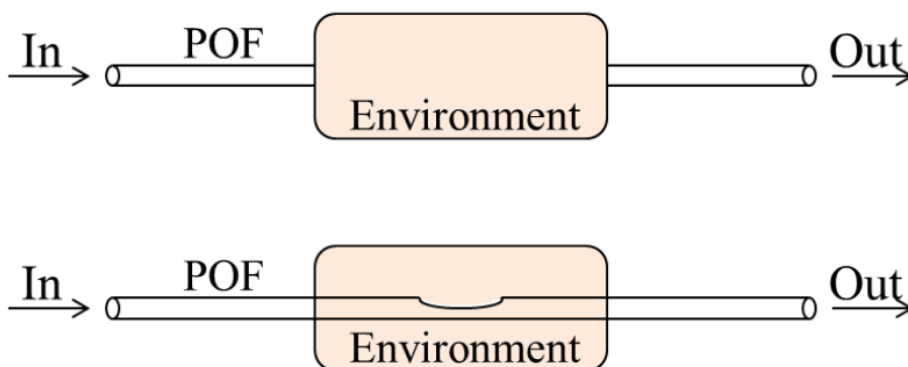


Figure 9. Image taken from [81]: difference between extrinsic (up) and intrinsic (down) POF sensors.

Turbidity measurements with POF are an example of an extrinsic sensor [83-87]. In this case, two plastic optical fiber are employed, one as a light source and the other to collect the reflected light: the higher the backscattered light the higher the turbidity of the water sample. Plastic fibers have large core thus allowing to maximize the backscattered light power guided in the collecting probe. For the intrinsic sensors, it is possible to differentiate between the sensor that used common POFs and modify their structure to make them sensitive and the waveguides fabricated for sensing purposes. Various techniques are reported in literature to make POFs sensitive to a specific measurand: one of the technique to implement curvature sensor is to polish a POF in order to enhance the evanescent radiation, that depends on the discontinuity in the core/cladding interface [6,11,82,88-90]; micro and macro bends are used as well to implement curvature, force and RI sensors [4,91-98]. Macro and microbending sensors rely on this interrogation scheme [1,5,99-101]; intensity monitoring is used as well to sense: the presence of liquid [7-11]; bending [12-14] and displacement [15-18]. Custom polymer waveguides can be fabricated with a specific characteristic that makes them ideal for sensing purposes [12,102-103].

### ***1.4.1. Wearable POF sensors for health care***

Wearable sensors have shown huge potential in health care monitoring. Studies presented in literature demonstrate the development of a smart shirt for activity monitoring as ECG [104-106], body fluid during exercise [107-108]. Beyond the activity monitoring, these smart sensor networks were developed for home care system for the elderly and disabled [109-111]

The mechanical properties of POF make them a good candidate for the development of wearable sensors. There are works in literature that present the integration of POF in textile and study the effect of multiple bending in POF produced with the manufacturing procedure to insert POF in warp and weft textile [98, 112-113]. The development of wearable sensors opened to new applications in health care. The possibility to develop new sensors that can push the “health home caring”, is a central topic, since a well-developed home-care and monitoring system can avoid part of the work that today is carried out in hospitals and other structures of national health care systems. One of the most researched sensing parameters is the breath rate [114.]. POF sensors, as all the photonic sensors, are immune to electromagnetic interference, so this feature makes possible to monitor vital parameter, as respiration, under magnetic resonance imaging or other environments where electronic sensors cannot be employed [115-118]. Modulation and the use of highly sensitive POF sensors allow monitoring both respiration and heart rate beat [119-121].

Another wide application field, exploiting the unique properties of POF, is the monitoring of posture, gait, and joint movements. One example of a wearable sensor for monitoring the seated spinal posture is reported in [13]. The spinal bending monitoring was furtherly improved in recent works to reach higher sensitivity and improve the power compensation system to ensure a longer stable behavior [122]; these new implementations allow to monitor the spinal position for some hours with a resolution less than  $2^\circ$ . Pressure POF sensors were used to implement an in-shoe

sensor for gait monitoring [123-126] since the pressure transmitted in different points of the shoe sole depends on the correct gaiting.

Curvature sensors implemented with POF are adopted for joint movements monitoring with wearable devices [127-128].

Wireless communication system allows the implementation of remote sensing using fibers. Remote sensing of physiological parameters with POF has been object of study since the beginning of 2000 [129]. The wide range of parameters that can be monitored using fibers and the lower power consumption allows the development of a multiplexed sensor for robot rehabilitation and a smart environment. The system proposed in [130] multiplexed in time up to five sensors (force, angle, breath rate) using a single board with five LED and two photodetectors. Commercial electronics components can be used to develop control boards to drive more than one LED and collect the data from the photodetectors. This is a cost effective alternative to implementing intensity based sensors, compared to the ones that need bulky equipment as optical spectrum analyzer. In [130] three different scenarios of rehabilitation are covered using photonic sensors: in the first scenario the subject is seated and perform flexion and extension cycles of the knee, the POF sensors provide information about the knee angle and the resistance force to the movement; in the second scenario the subject is walking at a constant speed while the sensor acquires the knee angle and the ground reaction force through in-sole POF sensors; in the third scenario POF sensors are used for gait event detection and breath monitoring while the subject is walking in a repetitive pattern of five meters (figure 10).

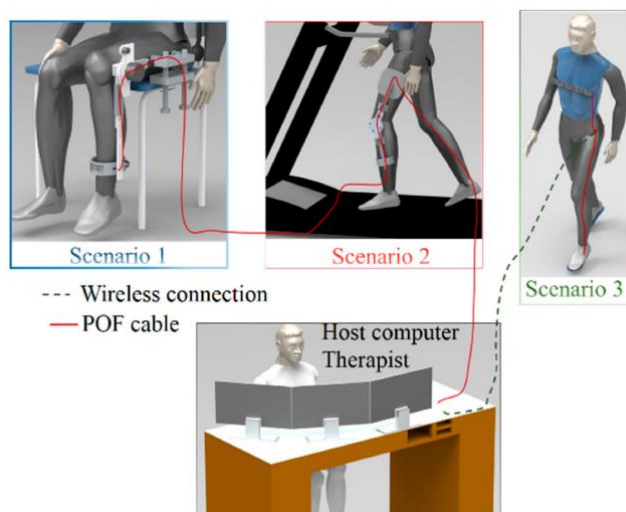


Figure 10. The three scenarios studied in [130], using a POF based multiplexed system for robot rehabilitation.

## 1.5. Objective and structure of the thesis

The objective of the thesis is to develop new interrogation systems and sensors employing plastic and glass optical fibers:

- Plastic optical fiber sensors:
  - POF interrogation system (Chapter 2): intensity based sensors have demonstrated to offer a wide range of applications. The possibility to implement low cost interrogation system developed with commercial electronic components was investigating, and a breath monitoring system was developed using a common microcontroller and commercial POF.
  - Fabrication of POF sensor (Chapter 3): extrusion is generally used to manufacture a preform and obtain a thinner optical fiber. The diameter of the filament is monitored and adjust modifying the wind-up speed. Uniform diameter and uniformity of the preform are crucial to obtain low loss optical fibers for communication. For sensing applications, where the loss requirements are not so crucial,

alternative fabrication systems can be explored. Extrusion from pellet is a cheaper alternative to avoid the fabrication of a preform. An extruder used in fiber textile fabrication was employed to fabricate a polymethyl methacrylate (PMMA) waveguide that demonstrate a potential application for curvature-direction and rotation sensing.

- Weak fiber gratings array interrogation systems
  - Time multiplexing (Chapter 4): time analysis demonstrates to simplify the interrogation system for distributed fiber sensing. Space resolution below the centimeter is still challenging in the time domain since the interrogation with short pulses produces very low optical backscattered power in raw fiber. A weak array was employed to enhance the light backscattered and a compact laser module was employed to develop a simple interrogation system for temperature and vibration sensing with sub-centimeter spatial resolution.
  - Microwave photonic techniques (Chapter 5): MWP offers new possibilities for optical fiber sensing. Incoherent and coherent regimes influence greatly the operation in the interrogation of weak fiber Bragg gratings array. The role of laser source coherence was studied with an approach that can be useful for sensing. The influence of gratings spacing and laser linewidth on the frequency response and the recovered time impulse response was assessed.
- In the last section, the conclusions and opened research lines are presented.

## References

- [1] Fegadolli, W. S., J. E. B. Oliveira, and V. R. Almeida. "Plastic optical fiber microbend sensors." *PIERS Proceedings, Cambridge, USA* (2008): 842-845.
- [2] Chen, Zhihao, et al. "Plastic optical fiber microbend sensor used as breathing sensor." *SENSORS, 2012 IEEE*. IEEE, 2012.
- [3] Linec, Matjaz, and Denis Donlagic. "A plastic optical fiber microbend sensor used as a low-cost anti-squeeze detector." *IEEE Sensors Journal* 7.9 (2007): 1262-1267.
- [4] Kulkarni, Atul, et al. "An evaluation of the optical fiber beam as a force sensor." *Optical Fiber Technology* 15.2 (2009): 131-135.
- [5] Yang, Xiufeng, et al. "Textile fiber optic microbend sensor used for heartbeat and respiration monitoring." *IEEE Sensors Journal* 15.2 (2014): 757-761.
- [6] Lomer, M., et al. "Lateral polishing of bends in plastic optical fibres applied to a multipoint liquid-level measurement sensor." *Sensors and Actuators A: Physical* 137.1 (2007): 68-73.
- [7] Rajamani, Allwyn S., M. Divagar, and V. V. R. Sai. "Plastic fiber optic sensor for continuous liquid level monitoring." *Sensors and Actuators A: Physical* 296 (2019): 192-199.
- [8] Jing, Ning, et al. "A liquid level sensor based on a race-track helical plastic optical fiber." *IEEE Photonics Technology Letters* 29.1 (2016): 158-160.
- [9] Lin, Xiao, et al. "Low-cost multipoint liquid-level sensor with plastic optical fiber." *IEEE Photonics Technology Letters* 26.16 (2014): 1613-1616.
- [10] Teng, Chuanxin, et al. "Liquid level sensor based on a V-groove structure plastic optical fiber." *Sensors* 18.9 (2018): 3111.
- [11] Kuang, Kevin SC, Wesley J. Cantwell, and Patricia J. Scully. "An evaluation of a novel plastic optical fibre sensor for axial strain and bend measurements." *Measurement Science and Technology* 13.10 (2002): 1523.
- [12] Nishiyama, Michiko, Mitsuo Miyamoto, and Kazuhiro Watanabe. "Respiration and body movement analysis during sleep in bed using hetero-core fiber optic pressure sensors without constraint to human activity." *Journal of biomedical optics* 16.1 (2011): 017002.
- [13] Salim, G. M., and M. A. Zawawi. "Knee joint movement monitoring device based on optical fiber bending sensor." *Journal of Telecommunication, Electronic and Computer Engineering (JTEC)* 10.1-3 (2018): 25-29.
- [14] Ghaffar, Abdul, et al. "Two-dimensional displacement optical fiber sensor based on macro-bending effect." *Optics & Laser Technology* 120 (2019): 105688.
- [15] Teng, Chuanxin, et al. "Investigation of a plastic optical fiber imprinted with V-groove structure for displacement sensing." *Optical Engineering* 58.7 (2019): 072002.

- [16] Ghaffar, Abdul, et al. "Optical Fiber Based Dynamic Displacement Measurement Sensor Using Polymer optical Fiber." *2019 2nd International Conference on Computing, Mathematics and Engineering Technologies (iCoMET)*. IEEE, 2019.
- [17] Teng, Chuanxin, et al. "Investigation of a plastic optical fiber imprinted with V-groove structure for displacement sensing." *Optical Engineering* 58.7 (2019): 072002.
- [18] Liu, Qiang, Liang Xin, and Zhaoxia Wu. "Refractive index sensor of a photonic crystal fiber Sagnac interferometer based on variable polarization states." *Applied Physics Express* 12.6 (2019): 062009.
- [19] Liu, Guohua, et al. "Polarization-dependent optical sensor based on reduced graphene oxide." *IEEE Photonics Technology Letters* 29.9 (2017): 767-770.
- [20] Bhatta, Hari Datta, et al. "Dynamic measurements of 1000 microstrains using chirped-pulse phase-sensitive optical time-domain reflectometry." *Journal of Lightwave Technology* 37.18 (2019): 4888-4895.
- [21] Guan, Zu-Guang, et al. "Wavelength detection of coherence-multiplexed fiber-optic sensors based on long-period grating pairs." *IEEE Sensors Journal* 7.1 (2006): 36-37.
- [22] Matveenko, V. P., et al. "Measurement of strains by optical fiber Bragg grating sensors embedded into polymer composite material." *Structural Control and Health Monitoring* 25.3 (2018): e2118.
- [23] Zhu, Pingyu, et al. "Distributed modular temperature-strain sensor based on optical fiber embedded in laminated composites." *Composites Part B: Engineering* 168 (2019): 267-273.
- [24] Ramakrishnan, Manjusha, et al. "Overview of fiber optic sensor technologies for strain/temperature sensing applications in composite materials." *Sensors* 16.1 (2016): 99.
- [25] Bremer, Kort, et al. "Structural health monitoring using textile reinforcement structures with integrated optical fiber sensors." *Sensors* 17.2 (2017): 345.
- [26] Güemes, Alfredo, et al. "Structural health monitoring in composite structures by fiber-optic sensors." *Sensors* 18.4 (2018): 1094.
- [27] Rajan, Ginu, and B. Gangadhara Prusty, eds. *Structural health monitoring of composite structures using fiber optic methods*. CRC press, 2016.
- [28] Laffont, Guillaume, et al. "Temperature resistant fiber Bragg gratings for on-line and structural health monitoring of the next-generation of nuclear reactors." *Sensors* 18.6 (2018): 1791.
- [29] Wada, Daichi, et al. "Flight demonstration of aircraft wing monitoring using optical fiber distributed sensing system." *Smart Materials and Structures* 28.5 (2019): 055007.
- [30] MAMIZU, HIROSHI, et al. "Optical Fiber Sensor based Aircraft Structural Health Monitoring System." *Structural Health Monitoring 2017 shm* (2017).



- [31] Zubia, J., et al. "Polymer optical fiber sensors for aircraft structural and engine health monitoring." *2017 19th International Conference on Transparent Optical Networks (ICTON)*. IEEE, 2017.
- [32] Ma, Zhen, and Xiyuan Chen. "Fiber Bragg gratings sensors for aircraft wing shape measurement: Recent applications and technical analysis." *Sensors* 19.1 (2019): 55.
- [33] Muanenda, Yonas, Claudio J. Oton, and Fabrizio Di Pasquale. "Application of Raman and Brillouin scattering phenomena in distributed optical fiber sensing." *Front Phys* 7 (2019): 155.
- [34] Lu, Yuelan, et al. "Distributed vibration sensor based on coherent detection of phase-OTDR." *Journal of lightwave Technology* 28.22 (2010): 3243-3249.
- [35] Pastor-Graells, Juan, et al. "Single-shot distributed temperature and strain tracking using direct detection phase-sensitive OTDR with chirped pulses." *Optics express* 24.12 (2016): 13121-13133
- [36] Martins, Hugo F., et al. "Distributed vibration sensing over 125 km with enhanced SNR using phi-OTDR over a URFL cavity." *Journal of Lightwave Technology* 33.12 (2015): 2628-2632
- [37] Zou, Weiwen, Xin Long, and Jianping Chen. "Brillouin Scattering in Optical Fibers and Its Application to Distributed Sensors." *Intech: Advances in Optical Fiber Technology: Fundamental Optical Phenomena and Applications* (2015): 1-53.
- [38] Zou, Weiwen, Xin Long, and Jianping Chen. "Brillouin Scattering in Optical Fibers and Its Application to Distributed Sensors." *Intech: Advances in Optical Fiber Technology: Fundamental Optical Phenomena and Applications* (2015): 1-53.
- [39] Meltz, G., W\_W Morey, and W. H. Glenn. "Formation of Bragg gratings in optical fibers by a transverse holographic method." *Optics letters* 14.15 (1989): 823-825.
- [40] Hill, Kenneth O., and Gerald Meltz. "Fiber Bragg grating technology fundamentals and overview." *Journal of lightwave technology* 15.8 (1997): 1263-1276.
- [41] Tosi, Daniele. "Review and analysis of peak tracking techniques for fiber Bragg grating sensors." *Sensors* 17.10 (2017): 2368.
- [42] Mihailov, Stephen J. "Fiber Bragg grating sensors for harsh environments." *Sensors* 12.2 (2012): 1898-1918.
- [43] Hill, K. O., et al. "Photosensitivity in optical fiber waveguides: Application to reflection filter fabrication." *Applied physics letters* 32.10 (1978): 647-649.
- [44] Kawasaki, Brian S., et al. "Narrow-band Bragg reflectors in optical fibers." *Optics Letters* 3.2 (1978): 66-68.
- [45] Hill, Kenneth O., et al. "Bragg gratings fabricated in monomode photosensitive optical fiber by UV exposure through a phase mask." *Applied Physics Letters* 62.10 (1993): 1035-1037.

- [46] Mihailov, Stephen J. "Fiber Bragg grating sensors for harsh environments." *Sensors* 12.2 (2012): 1898-1918.
- [47] Askins, C. G., et al. "Stepped-wavelength optical-fiber Bragg grating arrays fabricated in line on a draw tower." *Optics Letters* 19.2 (1994): 147-149.
- [48] Thévenaz, Luc, et al. "Novel technique for distributed fibre sensing based on faint long gratings (FLOGs)." *23rd International Conference on Optical Fibre Sensors*. Vol. 9157. International Society for Optics and Photonics, 2014.
- [49] Sancho, Juan, et al. "Time-frequency analysis of long fiber Bragg gratings with low reflectivity." *Optics express* 21.6 (2013): 7171-7179. [45]
- [50] Gagné, Mathieu, et al. "Fabrication of high quality, ultra-long fiber Bragg gratings: up to 2 million periods in phase." *Optics express* 22.1 (2014): 387-398.
- [51] Rothhardt, Manfred, et al. "Fabrication and applications of draw tower gratings." *Bragg Gratings, Photosensitivity, and Poling in Glass Waveguides*. Optical Society of America, 2016.
- [52] Westbrook, Paul S., et al. "Continuous multicore optical fiber grating arrays for distributed sensing applications." *Journal of Lightwave Technology* 35.6 (2017): 1248-1252.
- [53] Westbrook, Paul S., et al. "Improving distributed sensing with continuous gratings in single and multi-core fibers." *Optical Fiber Communication Conference*. Optical Society of America, 2018.
- [54] Zhu, Fan, et al. "Improved  $\Phi$ -OTDR sensing system for high-precision dynamic strain measurement based on ultra-weak fiber Bragg grating array." *Journal of Lightwave Technology* 33.23 (2015): 4775-4780.
- [55] Zhang, Xuping, et al. "Enhanced  $\Phi$ -OTDR system for quantitative strain measurement based on ultra-weak fiber Bragg grating array." *Optical Engineering* 55.5 (2016): 054103
- [56] Wang, Chen, et al. "Distributed OTDR-interferometric sensing network with identical ultra-weak fiber Bragg gratings." *Optics express* 23.22 (2015): 29038-29046.
- [57] Ou, Yiwen, et al. "Large-capacity multiplexing of near-identical weak fiber Bragg gratings using frequency-shifted interferometry." *Optics express* 23.24 (2015): 31484-31495.
- [58] Ai, Fan, et al. "Simultaneous distributed temperature and vibration measurement with UWFBG based coherent OTDR." *Optical Fiber Communication Conference*. Optical Society of America, 2018.
- [59] Tong, Yuheng, et al. "High-speed Mach-Zehnder-OTDR distributed optical fiber vibration sensor using medium-coherence laser." *Photonic Sensors* 8.3 (2018): 203-212.
- [60] Tang, Jianguan, et al. "Distributed acoustic sensing system based on continuous wide-band ultra-weak fiber Bragg grating array." *2017 25th Optical Fiber Sensors Conference (OFS)*. IEEE, 2017.

- [61] Wang, Chen, et al. "Distributed acoustic sensor using broadband weak FBG array for large temperature tolerance." *IEEE Sensors Journal* 18.7 (2018): 2796-2800.
- [62] Brown, David A. "A symmetric 3x3 coupler based demodulator for fiber optic interferometric sensors." *Fiber Optic and Laser Sensors IX*. Vol. 1584. International Society for Optics and Photonics, 1991.
- [63] Liang, Guanhua, et al. "Phase demodulation method based on a dual-identical-chirped-pulse and weak fiber Bragg gratings for quasi-distributed acoustic sensing." *Photonics Research* 8.7 (2020): 1093-1099.
- [64] Clement, Juan, et al. "Interrogation of a sensor array of identical weak FBGs using dispersive incoherent OFDR." *IEEE Photonics Technology Letters* 28.10 (2016): 1154-1156.
- [65] Hervás, Javier, et al. "Microwave Photonics filtering interrogation technique under coherent regime for hot spot detection on a weak FBGs array." *Journal of Lightwave Technology* 36.4 (2018): 1039-1045.
- [66] Ricchiuti, Amelia L., Javier Hervás, and Salvador Sales. "Cascade FBGs distributed sensors interrogation using microwave photonics filtering techniques." *Optics & Laser Technology* 77 (2016): 144-150.
- [67] Van Eijkelenborg, Martijn A., et al. "Microstructured polymer optical fibre." *Optics express* 9.7 (2001): 319-327.
- [68] Zubia, Joseba, and Jon Arrue. "Plastic optical fibers: An introduction to their technological processes and applications." *Optical fiber technology* 7.2 (2001): 101-140.
- [69] Talataisong, Wanvisa, et al. "Suspended-core microstructured polymer optical fibers and potential applications in sensing." *Sensors* 19.16 (2019): 3449.
- [70] Liehr, Sascha, Mathias Breithaupt, and Katerina Krebber. "Distributed humidity sensing in PMMA optical fibers at 500 nm and 650 nm wavelengths." *Sensors* 17.4 (2017): 738.
- [71] Liehr, Sascha, et al. "Distributed strain measurement with polymer optical fibers integrated into multifunctional geotextiles." *Optical Sensors 2008*. Vol. 7003. International Society for Optics and Photonics, 2008.
- [72] Fukumoto, Takuji, Kentaro Nakamura, and Sadayuki Ueha. "A POF-based distributed strain sensor with intrinsic memory effect." *Fiber Optic Sensors and Applications V*. Vol. 6770. International Society for Optics and Photonics, 2007.
- [73] Liehr, Sascha, et al. "Polymer optical fiber sensors for distributed strain measurement and application in structural health monitoring." *IEEE Sensors Journal* 9.11 (2009): 1330-1338.
- [74] Liehr, Sascha, Nils Nöther, and Katerina Krebber. "Incoherent optical frequency domain reflectometry and distributed strain detection in polymer optical fibers." *Measurement Science and Technology* 21.1 (2009): 017001.

- [75] Liehr, Sascha, Mario Wendt, and Katerina Krebber. "Distributed strain measurement in perfluorinated polymer optical fibres using optical frequency domain reflectometry." *Measurement Science and Technology* 21.9 (2010): 094023.
- [76] Min, Rui, Beatriz Ortega, and Carlos Marques. "Latest achievements in polymer optical fiber gratings: Fabrication and applications." *Photonics*. Vol. 6. No. 2. Multidisciplinary Digital Publishing Institute, 2019.
- [77] Ishikawa, Ryo, et al. "Perfluorinated graded-index plastic optical fiber Bragg gratings: Observation and theoretical analysis of unique dependence on pressure." *2017 22nd Microoptics Conference (MOC)*. IEEE, 2017.
- [78] Luo, Yanhua, et al. "Fabrication of polymer optical fibre (POF) gratings." *Sensors* 17.3 (2017): 511.
- [79] Fasano, Andrea, et al. "Fabrication and characterization of polycarbonate microstructured polymer optical fibers for high-temperature-resistant fiber Bragg grating strain sensors." *Optical Materials Express* 6.2 (2016): 649-659.
- [80] Haseda, Yuki, et al. "Measurement of pulse wave signals and blood pressure by a plastic optical fiber FBG sensor." *Sensors* 19.23 (2019): 5088.
- [81] Bundalo, Ivan-Lazar, et al. "All-plastic fiber-based pressure sensor." *Applied Optics* 55.4 (2016): 811-816.
- [82] Bilro, Lúcia, et al. "Optical sensors based on plastic fibers." *Sensors* 12.9 (2012): 12184-12207.
- [83] Aiestaran, Pedro, Jon Arrue, and Joseba Zubia. "Design of a sensor based on plastic optical fibre (POF) to measure fluid flow and turbidity." *Sensors* 9.5 (2009): 3790-3800.
- [84] Arifin, A., et al. "Design of sensor water turbidity based on polymer optical fiber." *2017 International Seminar on Sensors, Instrumentation, Measurement and Metrology (IS-SIMM)*. IEEE, 2017.
- [85] Yeoh, S., et al. "Plastic fiber evanescent sensor in measurement of turbidity." *Sensors and Actuators A: Physical* 285 (2019): 1-7.
- [86] Bin Omar, Ahmad Fairuz, and Mohd Zubir Bin MatJafri. "Turbidimeter design and analysis: a review on optical fiber sensors for the measurement of water turbidity." *Sensors* 9.10 (2009): 8311-8335.
- [87] Omar, A. F., and M. Z. MatJafri. "Water quality measurement using transmittance and 90° scattering techniques through optical fiber sensor." *2008 6th National Conference on Telecommunication Technologies and 2008 2nd Malaysia Conference on Photonics*. IEEE, 2008.
- [88] Bilro, Lúcia, et al. "Analytical analysis of side-polished plastic optical fiber as curvature and refractive index sensor." *Journal of lightwave technology* 29.6 (2011): 864-870

- [89] Leal-Junior, Arnaldo G., et al. "Polymer optical fiber-based sensor for simultaneous measurement of breath and heart rate under dynamic movements." *Optics & Laser Technology* 109 (2019): 429-436.
- [90] Babchenko, Anatoly, and Jonathan Maryles. "Graded-index plastic optical fiber for deformation sensing." *Optics and lasers in engineering* 45.7 (2007): 757-760.
- [91] Teng, Chuanxin, et al. "Investigation of a macro-bending tapered plastic optical fiber for refractive index sensing." *IEEE Sensors Journal* 16.20 (2016): 7521-7525
- [92] Ghaffar, Abdul, et al. "Two-dimensional displacement optical fiber sensor based on macro-bending effect." *Optics & Laser Technology* 120 (2019): 105688
- [93] Jing, Ning, et al. "Refractive index sensing based on a side-polished macrobending plastic optical fiber." *IEEE Sensors Journal* 15.5 (2014): 2898-2901
- [94] Lacraz, Amedee, et al. "Femtosecond laser inscribed Bragg gratings in low loss CYTOP polymer optical fiber." *IEEE Photonics Technology Letters* 27.7 (2015): 693-696.
- [95] Leal-Junior, Arnaldo, et al. "Polymer optical fiber Bragg gratings in CYTOP fibers for angle measurement with dynamic compensation." *Polymers* 10.6 (2018): 674.
- [96] Ishikawa, Ryo, et al. "Pressure dependence of fiber Bragg grating inscribed in perfluorinated polymer fiber." *IEEE Photonics Technology Letters* 29.24 (2017): 2167-2170.
- [97] Min, Rui, et al. "Fabrication and characterization of Bragg grating in CYTOP POF at 600-nm wavelength." *IEEE sensors letters* 2.3 (2018): 1-4.
- [98] Hu, Xuehao, et al. "Highly reflective Bragg gratings in slightly etched step-index polymer optical fiber." *Optics express* 22.15 (2014): 18807-18817.
- [99] Chen, Zhihao, et al. "Plastic optical fiber microbend sensor used as breathing sensor." *SENSORS, 2012 IEEE*. IEEE, 2012.
- [100] Linec, Matjaz, and Denis Donlagic. "A plastic optical fiber microbend sensor used as a low-cost anti-squeeze detector." *IEEE Sensors Journal* 7.9 (2007): 1262-1267.
- [101] Yang, Xiufeng, et al. "Textile fiber optic microbend sensor used for heartbeat and respiration monitoring." *IEEE Sensors Journal* 15.2 (2014): 757-761.
- [102] Zhao, Huichan, et al. "Optoelectronically innervated soft prosthetic hand via stretchable optical waveguides." *Science robotics* 1.1 (2016).
- [103] Rothmaier, Markus, Minh Phi Luong, and Frank Clemens. "Textile pressure sensor made of flexible plastic optical fibers." *Sensors* 8.7 (2008): 4318-4329.
- [104] Lee, Young-Dong, and Wan-Young Chung. "Wireless sensor network based wearable smart shirt for ubiquitous health and activity monitoring." *Sensors and Actuators B: Chemical* 140.2 (2009): 390-395.
- [105] Yoon, Sunghyun, Jai Kyoung Sim, and Young-Ho Cho. "A flexible and wearable human stress monitoring patch." *Scientific reports* 6 (2016): 23468.

- [106] Liden, Craig B., et al. "Characterization and implications of the sensors incorporated into the SenseWear armband for energy expenditure and activity detection." *Bodymedia Inc. White Papers: 1 7* (2002).
- [107] Morris, Deirdre, et al. "Wearable technology for bio-chemical analysis of body fluids during exercise." *2008 30th Annual International Conference of the IEEE Engineering in Medicine and Biology Society*. IEEE, 2008.
- [108] Coyle, Shirley, et al. "BIOTEX—Biosensing textiles for personalised healthcare management." *IEEE transactions on information technology in biomedicine* 14.2 (2010): 364-370.
- [109] Zhu, Chun, and Weihua Sheng. "Wearable sensor-based hand gesture and daily activity recognition for robot-assisted living." *IEEE Transactions on Systems, Man, and Cybernetics-Part A: Systems and Humans* 41.3 (2011): 569-573.
- [110] Pastorino, M., et al. "Wearable sensor network for health monitoring: the case of Parkinson disease." *Journal of Physics: Conference Series*. Vol. 450. No. 1. IOP Publishing, 2013.
- [111] Alemdar, Hande, and Cem Ersoy. "Wireless sensor networks for healthcare: A survey." *Computer networks* 54.15 (2010): 2688-2710.
- [112] Endruweit, A., A. C. Long, and M. S. Johnson. "Textile composites with integrated optical fibres: quantification of the influence of single and multiple fibre bends on the light transmission using a Monte Carlo ray-tracing method." *Smart materials and structures* 17.1 (2007): 015004.
- [113] D'Angelo, L. T., et al. "A system for respiratory motion detection using optical fibers embedded into textiles." *2008 30th Annual International Conference of the IEEE Engineering in Medicine and Biology Society*. IEEE, 2008.
- [114] Aitkulov, Arman, and Daniele Tosi. "Optical fiber sensor based on plastic optical fiber and smartphone for measurement of the breathing rate." *IEEE Sensors Journal* 19.9 (2019): 3282-3287.
- [115] Grillet, Augustin, et al. "Optical fiber sensors embedded into medical textiles for healthcare monitoring." *IEEE Sensors Journal* 8.7 (2008): 1215-1222.
- [116] Yoo, Wook-Jae, et al. "Development of respiration sensors using plastic optical fiber for respiratory monitoring inside MRI system." *Journal of the Optical Society of Korea* 14.3 (2010): 235-239.
- [117] Ahn, Dohyun, et al. "Plastic optical fiber respiration sensor based on in-fiber micro-holes." *Microwave and Optical Technology Letters* 61.1 (2019): 120-124.
- [118] Kam, Wern, et al. "Compact and low-cost optical fiber respiratory monitoring sensor based on intensity interrogation." *Journal of Lightwave Technology* 35.20 (2017): 4567-4573.

- [119] Koyama, Yuya, Michiko Nishiyama, and Kazuhiro Watanabe. "Smart textile using hetero-core optical fiber for heartbeat and respiration monitoring." *IEEE Sensors Journal* 18.15 (2018): 6175-6180.
- [120] Arifin, A., et al. "Measurement heart rate based on plastic optical fiber sensor." *Journal of Physics: Conference Series*. Vol. 1170. No. 1. IOP Publishing, 2019.
- [121] Yasin, Moh, et al. "Bundled plastic optical fiber based sensor for ECG signal detection." *Optik* 203 (2020): 164077.
- [122] Zawawi, Mohd Anwar, Sinead O'Keeffe, and Elfed Lewis. "Plastic optical fibre sensor for spine bending monitoring with power fluctuation compensation." *Sensors* 13.11 (2013): 14466-14483.
- [123] Leal-Junior, Arnaldo G., et al. "Polymer optical fiber for in-shoe monitoring of ground reaction forces during the gait." *IEEE Sensors Journal* 18.6 (2018): 2362-2368.
- [124] De Rossi, S. M. M., et al. "Development of an in-shoe pressure-sensitive device for gait analysis." *2011 Annual International Conference of the IEEE Engineering in Medicine and Biology Society*. IEEE, 2011.
- [125] Leal-Junior, Arnaldo G., et al. "Polymer optical fiber sensors in wearable devices: Toward novel instrumentation approaches for gait assistance devices." *IEEE Sensors Journal* 18.17 (2018): 7085-7092.
- [126] Bilro, L., et al. "A reliable low-cost wireless and wearable gait monitoring system based on a plastic optical fibre sensor." *Measurement Science and Technology* 22.4 (2011): 045801.
- [127] Stupar, Dragan Z., et al. "Wearable low-cost system for human joint movements monitoring based on fiber-optic curvature sensor." *IEEE Sensors Journal* 12.12 (2012): 3424-3431.
- [128] Li, Jing, et al. "Wearable Wrist Movement Monitoring Using Dual Surface-Treated Plastic Optical Fibers." *Materials* 13.15 (2020): 3291.
- [129] Pandian, P. S., et al. "Smart Vest: Wearable multi-parameter remote physiological monitoring system." *Medical engineering & physics* 30.4 (2008): 466-477.
- [130] Leal-Junior, Arnaldo, et al. "Polymer Optical Fiber-Based Integrated Instrumentation in a Robot-Assisted Rehabilitation Smart Environment: A Proof of Concept." *Sensors* 20.11 (2020): 3199.





## Chapter 2

# Plastic optical fiber sensor for vital signal monitoring

*Plastic optical fibers (POF) are adopted as a complement for glass fibers in short-haul communications links because they are easy to handle, flexible, and economical [1]. In the last 30 years, plastic optical fibers have been exploited as sensors, their chemical and mechanical properties have opened new possibilities in the sensing field, as, for example, chemical gas sensor implemented with porous POF [2]. Interrogation of POF using optical setup originally used with glass fibers is reported in the early years [3]. POFs are employed as sensor also using cost effective interrogation systems since the dimension of POFs make the coupling easier to handle than glass fiber and allow the use of low-precision and low cost components. In this perspective, one sensor implemented using POF is presented in this chapter. The first section is an introduction to the interrogation scheme that was chosen for the two POF sensors and the principle of operation of intensity-based sensors. In the second section, the first sensor is reported: a cost effective solution for vital signal monitoring implemented with commercial POF and low cost electronic components for the interrogation system.*

## **2.1. Intensity based optical fiber sensors**

There are various techniques presented in literature to use POF as sensors. After the inscription of the first fiber Bragg grating (FBG) in a step index POF in 1999 [4], these fiber-based sensors were adopted for strain and temperature demonstrating a sensitivity of  $1.48 \text{ pm}/\mu\epsilon$  and  $55 \text{ pm}/^\circ\text{C}$  [5-6]. The inscription of gratings in POF with a resonant wavelength in the C-band allows using commercial FBG interrogator, coupling a glass fiber connector with the POF using UV resin. In recent works, pulse wave and blood pressure monitoring were demonstrated using this method [7]. Other techniques used for glass sensing, adopted for POFs as well, are the optical reflectometry in frequency and time domain. POFs were interrogated using OTDR and the reflected signal was observed in presence of mechanical splice, small bend, torsional, axial strains, and temperature [3]. Since then, POF and OTDR were adopted for a wide range of application, as pH sensing [8] or long-distance intrusion sensing [9] over 60 km of fiber. All the previous application required the use of bulky instrumentation to interrogate the sensors, and in the case of FBG-based sensor it should be taken into account that the inscription of gratings in POF required the use of special lasers [10-12].

On the other hand, intensity-based sensing offers a cost effective alternative that allows developing compact interrogation systems. The possibility to design compact electronic systems as interrogators make the intensity sensors feasible to create fiber based wearable sensor [13-15]. Thanks to the growing adoption of POFs in communication technologies it is possible to retrieve low cost optoelectronic components. The principle of operation is shown in figure 1. A light source, that can be a laser or an LED, is used to transmit the optical power in the POF, transducers convert the measurand, that must be sensed, in a light intensity variation, and finally, a photodetector detects the optical power variations.

Industrial POFs for telecommunications can be used as well as sensors. Simple methods to make sensitive industrial POFs are presented in

literature. These fibers are designed to have low bending losses. Bending modulation of the light intensity is detectable only if very stable coupling and low noise electronics are employed.

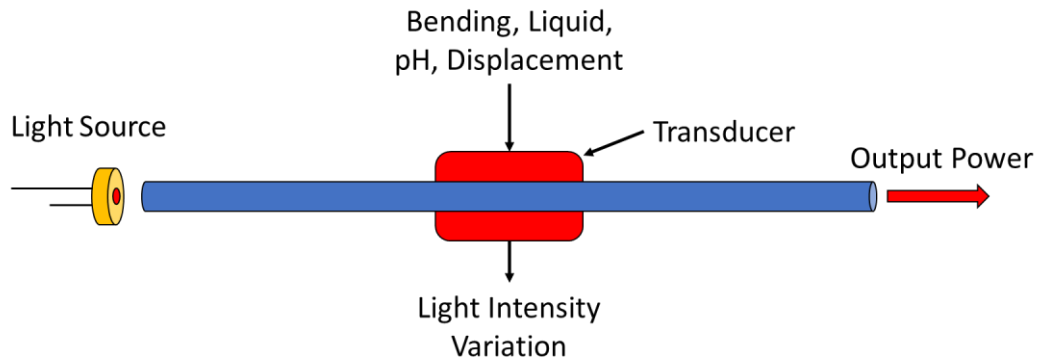


Figure 1. The conversion of a measurand in an optical magnitude (in this case light intensity).

If the easiness of implementation of the interrogation system is a key factor, industrial POFs need to be made sensitive to force [16-20], presence of liquid [21-25], bending [26-28], and displacement [29-32], abrading/segmenting part of the core/cladding or using micro/macro-bending. Fabrication of custom polymeric waveguides, specifically for intensity-based applications is an alternative to the sensitizing of existing fibers, less cost effective, but it offers more flexibility in the design of the sensor. The variety of materials with different refractive indexes and elasticity allows creating flexible optical waveguides as the ones integrated into the prosthetic hand in [33], made of a core of polyurethane and a silicone cladding, or in textile [34].

In this chapter, an intensity based plastic optical fiber sensor is presented: a POF sensor for vital signal monitoring is reported, implemented with standard POFs for telecommunication made sensitive to pressure cutting the fiber along the cross-section. A compact cost effective interrogation system was designed and implemented with LEDs as light source emitting around 645 nm (the center of the optical transmission window of POF

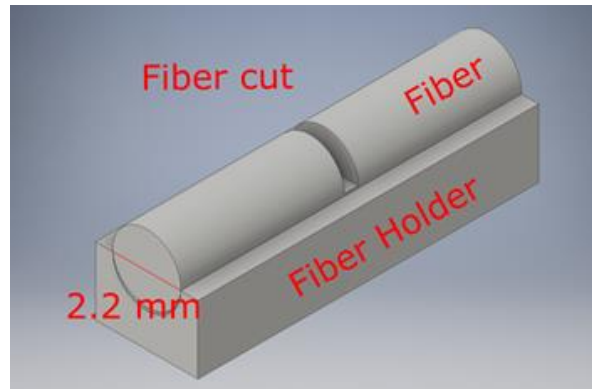
made of polymethyl methacrylate (PMMA) [35]), photodetectors arrays, microcontroller and additional components for the current driver of the LEDs.

## **2.2. Plastic optical fiber sensor embedded in mattress for signal vital monitoring**

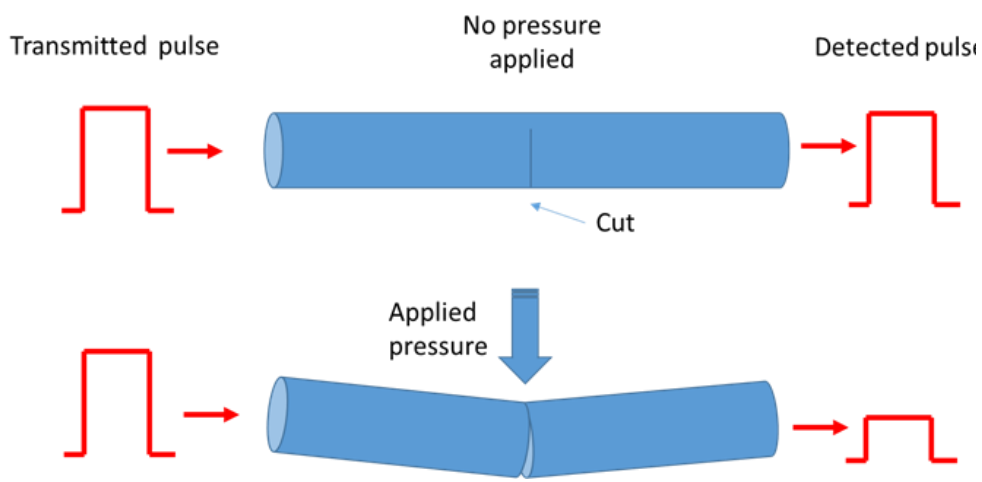
### ***2.2.1. Setup implementation***

The sensor developed with POFs was designed for non-invasive monitoring of vital signals of a patient lying on a bed [36]. The Super ESKA® (Mitsubishi Rayon Co. LTD., Tokyo, Japan) POF was employed. The fibers have a core of PMMA of 980  $\mu\text{m}$  and a cladding of fluorinated polymer with a diameter of 1000  $\mu\text{m}$ . The losses due to bending are of  $<0.5$  dB for radius bending  $>2.5$  cm, as reported in the datasheet. Different techniques were presented to make “sensitive” the POFs to bend: abrading part of the cladding [26-37], using a solvent that can attack the cladding without damaging the core [38]. In this case, the goal was to find a technique that can be reproduced in high-volume production; a cutting technique was developed that allows us to produce cuts in the fibers of approximately the same depth. The POF was cut for half of the cross section in some specific points in order to enhance the optical losses for bending. A fiber holder with a hemicylindrical groove with the same diameter of the fiber was used together with a razor blade to obtain cuts with approximately the same depth (figure 2a). The result and the intensity modulation when pressure is applied are shown in figure 2b.

After every cut, the fiber was mounted on an experimental setup for curvature response measurement, thus verify that every sensitive point has approximately the same response. Since the pressure applied bends the fiber at a certain angle, the curvature response is appropriate to verify the homogeneous response of the cut fibers.



(a)



(b)

Figure 2. (a) 3D model of the plastic holder used to cut the fibers. The hemicylindrical groove has the same diameter as the plastic fiber to limit the penetration of the blade into the fiber and obtain similar cuts of approximately 1.1 mm (half of the fiber diameter) depth. (b) Effect of a pressure exerted on a sensitized point of the POF ESKA.

Figure 3 shows the response of six different points to the curvature. As it can be observed, the standard deviation grows with the bend angle, so for

high pressure is expected not to have a homogeneous response for every sensitive point.

The fibers were then arranged in a matrix with the cuts positioned in the crossing points (figure 4a) and embedded in a mattress cover sample. The computer acquires the data from the board, that is the actual core of the sensor since it controls the current (light intensity) in the LEDs and converts the voltage values that are serially outputted from the photodetectors array (figure 4b).

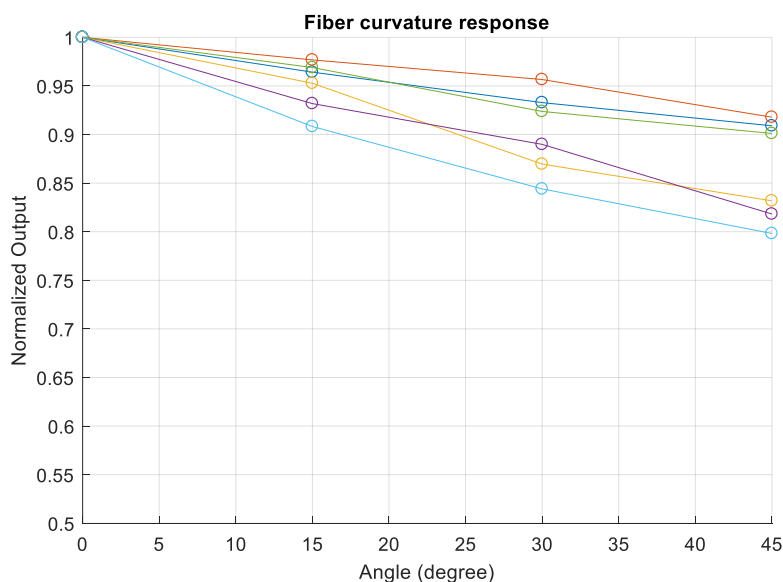


Figure 3. Normalized response to curvature of six sensitive points.

The position of the pressure applied can be retrieved from the simultaneous interrogation of the fibers in the matrix: each fiber is associated with an average light intensity, obtained processing the light data at the fiber end. An intensity variation for two different fibers is considered as a pressure applied on the crossing point between the latter; monitoring the output power of all the fibers, it is possible to reconstruct the pressure matrix.

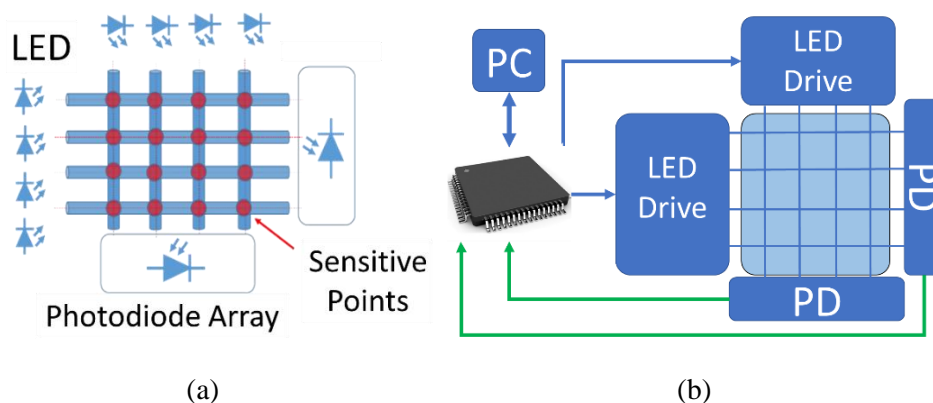


Figure 4. (a) Schematic representation of the fiber matrix; and (b) sensor implementation: the arrows represent the communication between the computer, the board, and the electronic components of the interrogation circuit.

The LED used to inject the light in the fiber is the IF E96E, a low-cost, high-speed, visible red LED housed in a “connector-less” style plastic fiber optic package (figure 5a). The output spectrum is produced by an Al-GaInP die which peaks at 645 nm. The LEDs are driven at constant current using the driver circuit shown in figure 5b, implemented with a 12-bit digital to analog converter (DAC) (MCP4822), a general-purpose operational amplifier (LM358), an NPN silicon BJT transistor (2N2222A), and one resistor. The microcontroller communicates through the SPI interface with a digital to analog converter that fixed the voltage at the (+) pin of the operational amplifier. The negative feedback of the system composed by the OpAmp, the BJT transistor, and the resistor “copy” the voltage of the (+) pin to the (-). In this way, the current of the LED is fixed since  $I_{LED} \approx V_{DAC}/R$ . The light is injected in the form of a pulse with constant duration. The duration of the pulses was chosen to maximize the full-scale range of the system. The lower pulse width is limited by the maximum operating frequency of the analog stage and of the LED bandwidth (maximum operation frequency 50 Mbps); the upper limit of the duration was chosen in order to not saturate the photodiodes. The duration was fixed to 50  $\mu$ s.

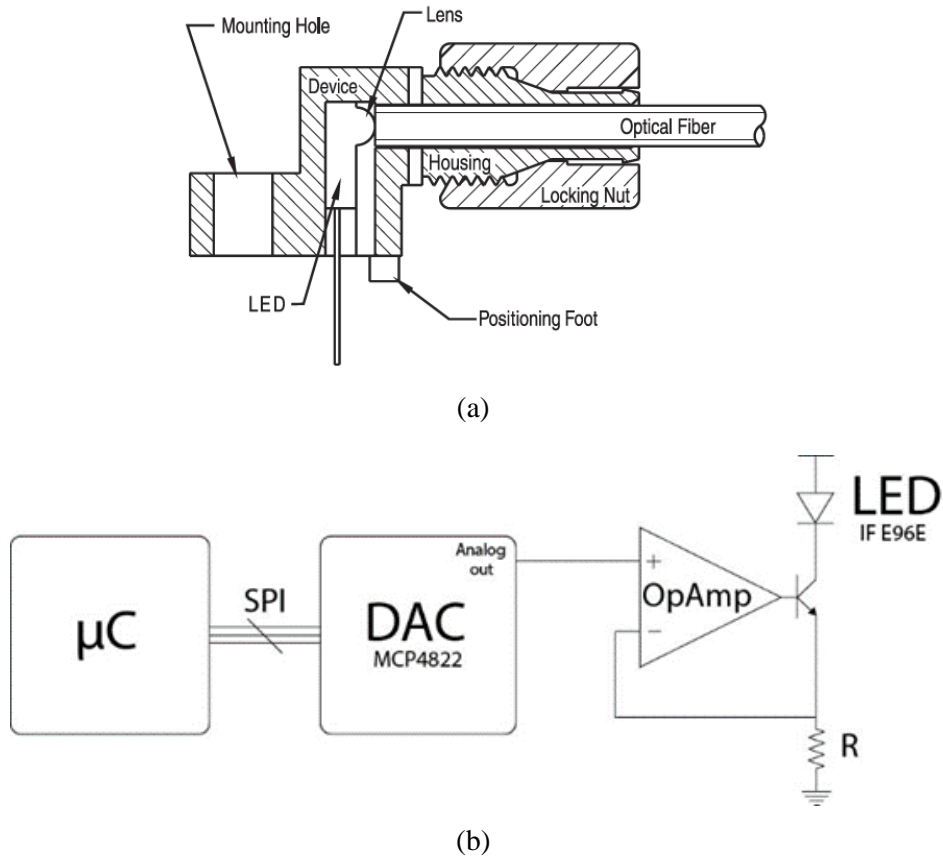


Figure 5. (a) Cross section of the LED used to inject light in the plastic fiber. (b) Schematic representation of the current driver circuit.

The photodetectors array is the TSL1402R, a linear array of 256 photodiodes. A plastic component was specifically designed, and 3D printed to bottom coupled the fibers ends to the light sensor (figure 6). The customized coupler holds the end of the fibers in front of the sensitive area of the linear sensor and insulates the photodiodes from the ambient light that could influence the measurement.



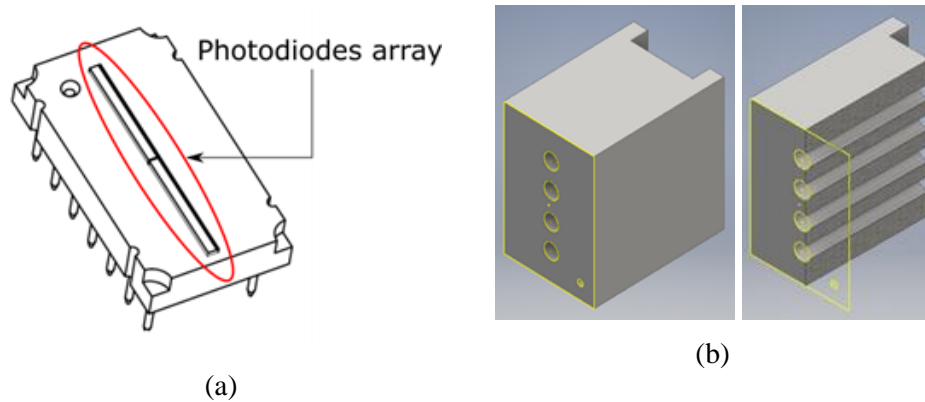


Figure 6. (a) Photodiodes array TSL1402R; and (b) 3D model of the fiber holder, entire piece (left) and cross-section (right).

Light energy impinging on a pixel generates a photocurrent, which is then integrated by the active integration circuitry associated with that pixel. The amount of charge accumulated at each pixel is directly proportional to the light intensity on that pixel and the integration time. The charge stored is sequentially connected to a charge-coupled output amplifier that generates a voltage on analog output. The output voltage of the sensor is converted through the build-in 12 bit analog to digital converter (ADC) of the microcontroller. The application chosen for this sensor is the monitoring of vital signals as respiration, opening new solutions for non-invasive monitoring of patients that suffer from respiratory problems (e.g. sleep apneas). The designed circuit works at an operating speed of kHz, a speed that allows averaging 10 times and still have enough bandwidth for vital signal monitoring (respiration rate), avoiding the use of a reference optical branch.

Every peak in the intensity graph is one of the 8 fibers output (figure 7a), the x-axis represents the pixel number of the linear photodiode array. In order to identify a change in the optical power the following algorithm was programmed: fixing a threshold, it determines the first and last pixel where a fiber end is coupled and operates an averaging of the voltage signals; the principle is shown in figure 7b. This permit obtaining a measurement less

sensitive to the optical power fluctuation due to the electronic noise and to the non-perfect fiber-photodetectors array coupling.

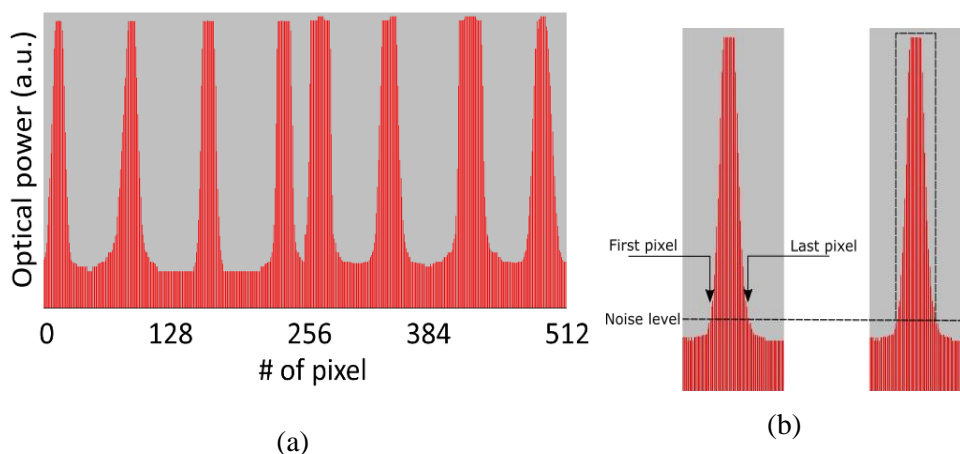


Figure 7. (a) Plot of the light level detected by the two arrays of photodetectors, the eight peaks are the light outputs of the eight fibers bottom coupled to the photodetectors array; and (b) light signal post-processing: the software individuates and store the first and last pixel position that detect a light power above a certain threshold (noise level), any variation of light power in this area will be interpreted as a pressure applied in one of the sensitive points of the fiber.

In order to verify the possibility to use the sensor three experiments were arranged to test, one static and two dynamic tests were carried out to analyze the performance of the sensor:

1. The first static test was made placing weights in a range 0–500 g (0–4.9 N) with steps of 100 g (force = 0.98 N) on the sensitive points of the matrix. This experiment confirmed that it would be possible to identify the pressure caused by the thorax during respiration of a person lying on the mattress where the sensor is embedded;
2. The second test is a dynamic test: a force step stimulus was applied on a point of the mattress sensor. From the time response data, the frequency response was obtained operating the Fourier transform. The sampling speed was tested to verify that it is sufficient to sense the respiration frequency (around 10 Hz);

3. The third is a cyclic loading test to study the effect of repetitive pressure cycles of charge and discharge. This last test is needed since the cut process changes the mechanical properties of the sensitive points. It is necessary to verify if the cyclic application of pressure changes the sensitivity or causes the appearance of hysteresis in the sensor response.

For the static tests, the force was applied on four different points, and the charge cycles were repeated three times. Since the idea is to use this sensor for the dynamic monitoring of vital signs, as the respiration rate (0.2–0.5 Hz), it is necessary to obtain a bandwidth of 10 Hz. The load cycle test was carried out to determine the short time drift or hysteresis of the sensor, which can be caused by the plastic deformation of the fibers. Weights for scale placed into a cylindrical weighing pan were used to apply the load on the sensitive points of the matrix both for static and dynamic measurements.

### **2.2.2. Measurements and discussion**

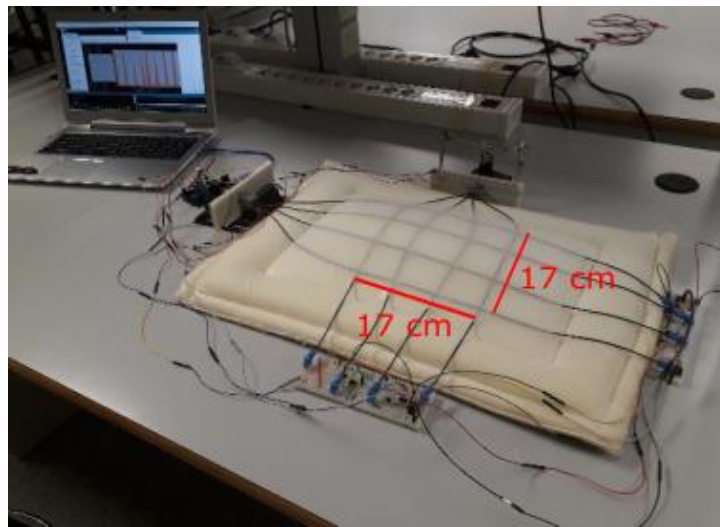
The charge cycles, for obtaining the static response, were repeated three times for every single sensitive point to verify the repeatability of the measurement. The step and the range of the measurement were chosen considering the pressure changes in the lungs during the breathing cycle, which are partially transmitted to the thorax. The pressure changes are in the order of 5 cm H<sub>2</sub>O ( $\approx 490$  Pa); considering the average thorax area for an adult, an applied force of about 50 N is obtained. As commented before, the pressure is only partially transmitted to the thorax expansion movement, so a resolution of 1 N could be a reasonable resolution to detect the force applied during respiration. The measurements show good linear responses: in table 1 are reported the linear regression results (alpha = first-degree term; beta = constant term and R<sup>2</sup> value). The resolutions obtained are slightly different for the four points, due to the different location of the tested points on the mattress cover sample.

Table 1. Results of the linear regression for the loading static test. The alpha is the first-degree term of the linear regression, the beta is the constant term. The  $R^2$  values are reported in the third column.

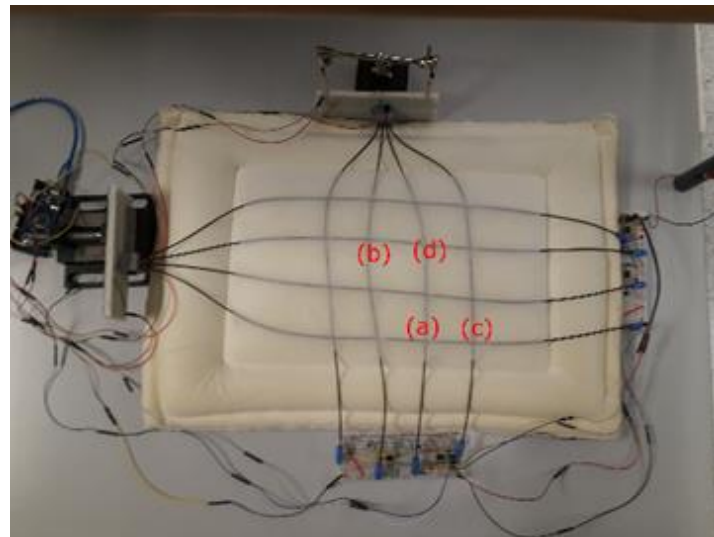
Sensitive Point	P= $\alpha$ x+ $\beta$ (P: power transmitted x: force applied)			$R^2$
	Repetition	Alpha	Beta	
(a)	1	-0.02283	0.98405	99.40%
	2	-0.02411	0.99762	99.60%
	3	-0.02246	0.98868	99.20%
(b)	1	-0.03279	0.98531	99.50%
	2	-0.03244	0.99224	99.50%
	3	-0.03263	0.97864	97.40%
(c)	1	-0.02840	1.01070	99.50%
	2	-0.02692	1.00920	99.80%
	3	-0.02809	1.00980	99.70%
(d)	1	-0.04494	0.98100	98.70%
	2	-0.04433	0.97798	98.70%
	3	-0.04346	0.97809	98.50%

The experimental setup is shown in figure 8a; in figure 8b it is presented from a different perspective, the points tested for the static response are highlighted.

The dynamic measurement is needed to test the response of the sensor for stimulus with frequencies lower than 10 Hz. Usually, to study the frequency behavior of a fiber sensor, piezo fiber stretchers are used; since it is necessary to study the response for very low frequencies, an analytical study of the time response data was carried out. The experimental result was compared to a theoretical result, computed considering the frequency response of the electronic light sensor and converter circuits (photodiode array-ADC).



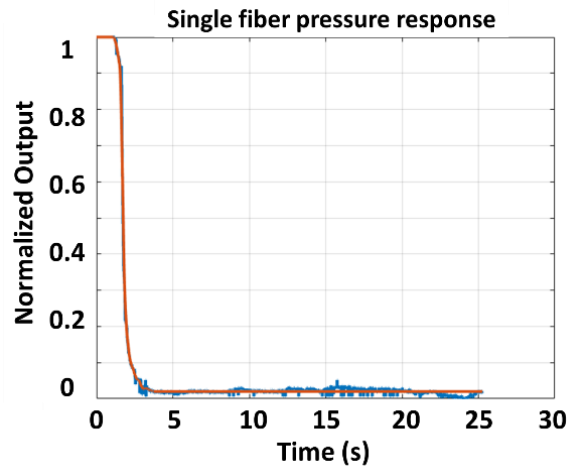
(a)



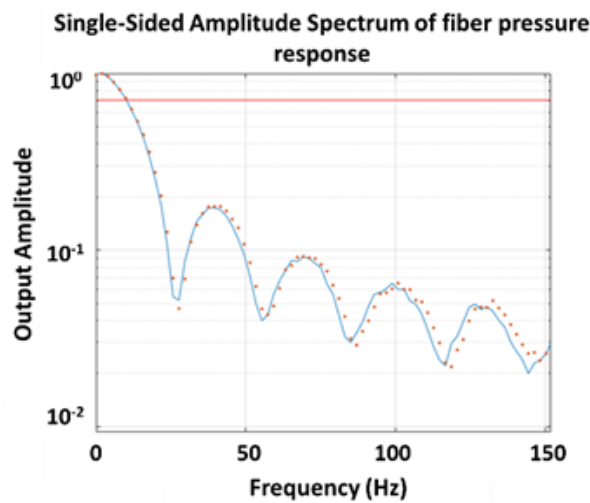
(b)

Figure 8. (a) Experimental set-up; and (b) mattress cover with the integrated POFs, the points tested to measure the static response are highlighted.

In figure 9a the blue represents the experimental response of our fiber sensor when a step-like pressure stimulus is applied, while in red is represented the simulated response for the same light attenuation obtained in the practical experiment. If the response of the sensor is linear for the load step applied, it is possible to obtain the frequency response of the sensor calculating the derivative of the Fourier transform of the time step response data. The result is shown in figure 9b (blue line). On the frequency plot is reported the  $-3$  dB line in red, as it can be observed that the response is  $>-3$  dB for frequencies  $<10$  Hz. This response proves that the sensor is feasible for detecting the respiration movement of a user in contact with the mattress sensor. As for the time response, the computed frequency response was compared to the ideal impulse response of our electronic system; the theoretical curve is reported in figure 9b plotted with red dots. One of the problems to address for plastic fibers is that often plastic deformation can occur, so the sensitive point cannot recover completely after pressure is applied, adding a constant offset that could adversely affect the sensor performance. Therefore, it is necessary to run a cyclic pressure test to verify that the zero-pressure level does not change significantly. In figure 10, in red, is reported the zero line (when no pressure is applied) and the response for a cyclic loading (in blue). The measurement demonstrates that substantially the zero-pressure level does not change after 25 short time load cycles with a force of 20 N. The performance obtained demonstrates the feasibility of the sensor for detecting movements and respiration.



(a)



(b)

Figure 9. (a) Time response of a fiber, after pressure is applied: in blue is reported the response measured and in red the theoretical response calculated considering the frequency response of the electronics. (b) Frequency response retrieved from the time response data calculating the derivative of the Fourier transform. In red is represented the  $-3$  dB line, the theoretical impulse response of the system is plotted with red dots.

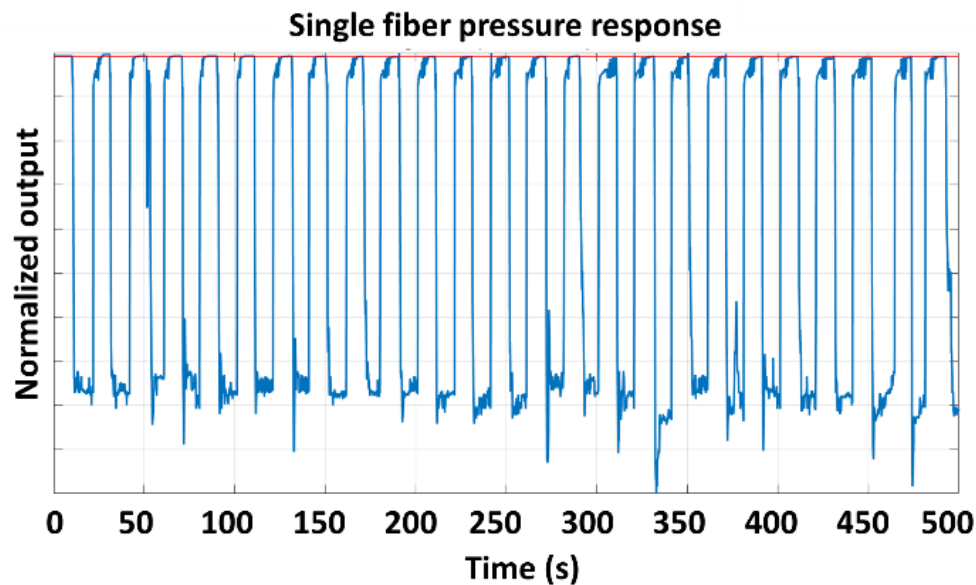


Figure 10. Cyclic loading test to verify the presence of a drift in the response, in red is represented the initial zero-pressure baseline.

As commented before, the pressure is only partially transmitted to the thorax expansion movement, so a resolution of 1 N could be a reasonable resolution to detect the force applied during respiration. The measurements show good linear responses ( $R^2$  values  $> 97.40\%$ ), and a resolution between  $2.2\%/N$  and  $4.5\%/N$ . The dynamic measurement is needed to test the response of the sensor for stimulus with frequencies lower than 10 Hz. Since it is necessary to study the response for very low frequencies, an analytical study of the time response data was carried out. The sensor has a response  $> -3$  dB for frequencies lower than 10 Hz. It was necessary to run a cyclic pressure test to verify that the zero-pressure level does not change significantly due to the plastic deformation: no significant drift due to loading cycles was observed. The results obtained make the sensor feasible for sleep apnea detection and in general for non-invasive cardiopulmonary monitoring.



### 2.3. Miniaturized POF interrogation system

In a second step, the interrogation system was redesigned to be integrated into a single printed circuit board (PCB). The bulky LEDs with a connector-less package were substituted with a red LED in a surface mount device (SMD) package manufactured by Kingbright. The upper part of the package is equipped with a dome lens (figure 11a) to enhance the light coupled inside the POF core, in figure 11b is reported the spatial distribution of the output power. These devices have a  $2*\phi_{1/2}=40^\circ$  (defined as double the angle from optical centerline where the luminous intensity is 1/2 of the optical peak value).

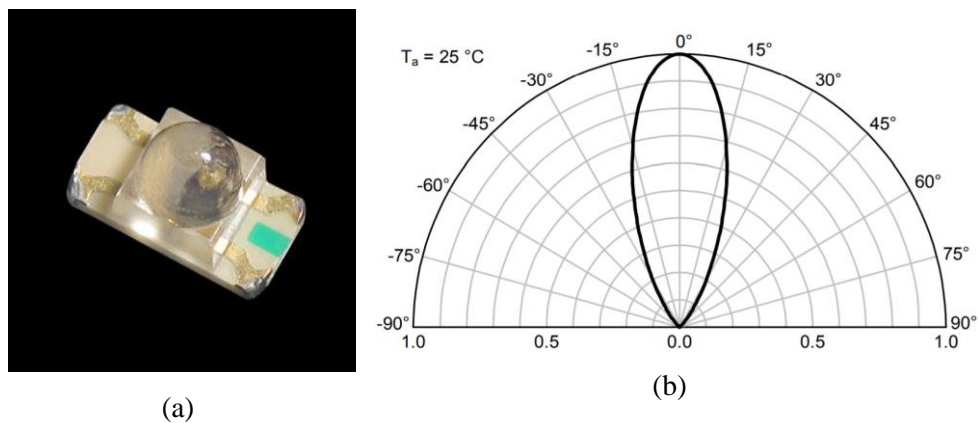


Figure 11. (a) SMD package with a dome lens of the red LED used for the PCB.  
(b) Spatial distribution of the output power.

The microcontroller chosen for the board is the dsPIC33EP16GS504 by Microchip with high frequency pulse width modulator, 12-bit high-speed built-in ADC. The new board is designed to be portable, for this reason, a Bluetooth interface was designed to send data of a portable device as a laptop/mobile phone. The UART serial interface of the microcontroller was used to communicate with the Bluetooth to serial port module HC-05. This module was chosen as well for the low power consumption. The TSL1402R, the same photodetector array used in the first implementation, was adopted as well for this new design. Two 3D plastic components were

printed and used to bottom-couple the fibers to the LEDs and the photodetector arrays. The final version of the PCBs was finally designed and manufactured (figure 12). In figure 12a is showed the PCB of 102x35 mm with microcontroller, LEDs, and Bluetooth module. In figure 12b is showed a smaller PCB used for the photodetectors array (dimension 33x22 mm). The two boards are connected with 5 pins JTS connectors.

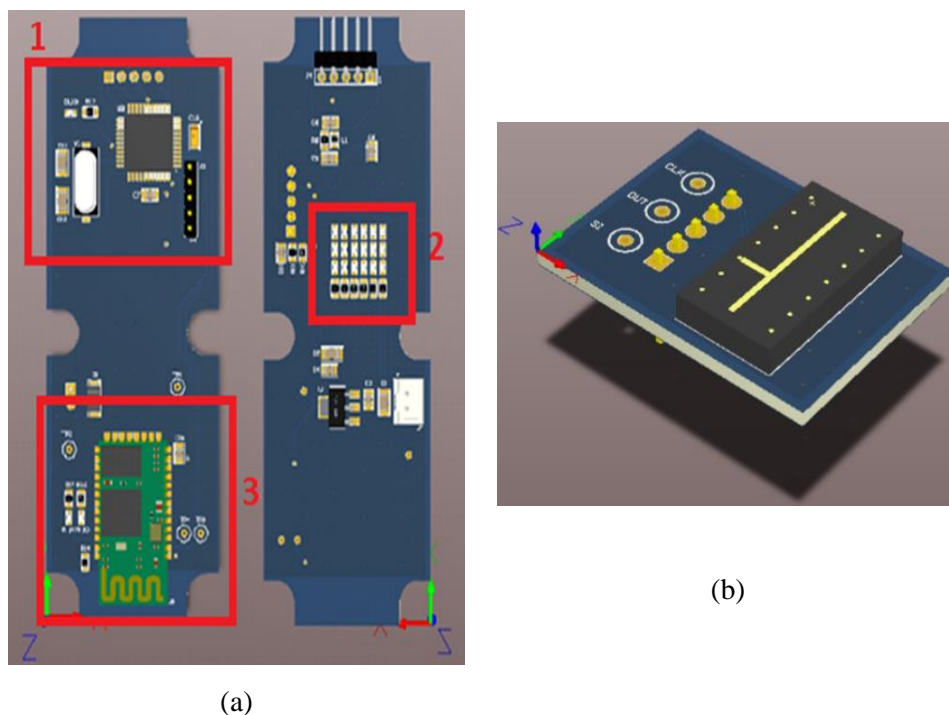


Figure 12. (a) Main PCB (front and rear) with a microcontroller (1); LED matrix (2); Bluetooth module (3). (b) PCB with the photodetector array; the two boards are connected through the JTS pins observable in the upper part in the rear of the main PCB.

## **2.4. Conclusions**

An intensity based POF based sensors were presented. The possibility to implement cost effective interrogation systems were described, thanks to the dimension of POFs that make the coupling easier to handle and allow to use of low-precision and cost-effective components. The first sensor

was tested and shows it could be feasible to monitor vital signal monitoring. This sensor was implemented with commercial POF and low-cost electronic components for the interrogation system. A repetitive method to make POF sensitive to bending was investigated, focus on finding a technique that can be reproduced in high-volume production; a cutting technique that allows us to produce cuts in the fibers of approximately the same depth was developed. After every cut, the fiber was mounted on an experimental setup for curvature response measurement, thus verify that every sensitive point has approximately the same response.

## References

- [1] Zubia, Joseba, and Jon Arrue. "Plastic optical fibers: An introduction to their technological processes and applications." *Optical fiber technology 7.2* (2001): 101-140.
- [2] Zhou, Quan, et al. "Porous plastic optical fiber sensor for ammonia measurement." *Applied optics* 28.11 (1989): 2022-2025.
- [3] Husdi, Irwan Rawal, Kentaro Nakamura, and Sadayuki Ueha. "Sensing characteristics of plastic optical fibres measured by optical time-domain reflectometry." *Measurement Science and Technology* 15.8 (2004): 1553.
- [4] Xiong, Z., et al. "Highly tunable Bragg gratings in single-mode polymer optical fibers." *IEEE Photonics technology letters* 11.3 (1999): 352-354.
- [5] Liu, H. Y., H. B. Liu, and G. D. Peng. "Tensile strain characterization of polymer optical fibre Bragg gratings." *Optics Communications* 251.1-3 (2005): 37-43.
- [6] Liu, H. Y., G. D. Peng, and P. L. Chu. "Thermal tuning of polymer optical fiber Bragg gratings." *IEEE Photonics Technology Letters* 13.8 (2001): 824-826.
- [7] Haseda, Yuki, et al. "Measurement of Pulse Wave Signals and Blood Pressure by a Plastic Optical Fiber FBG Sensor." *Sensors* 19.23 (2019): 5088.
- [8] Saunders, C., and P. J. Scully. "Distributed plastic optical fibre measurement of pH using a photon counting OTDR." *Journal of Physics: Conference Series*. Vol. 15. No. 1. IOP Publishing, 2005.
- [9] Rao, Yun-Jiang, et al. "Long-distance fiber-optic  $\Phi$ -OTDR intrusion sensing system." *20th international conference on optical fibre sensors*. Vol. 7503. International Society for Optics and Photonics, 2009.
- [10] Stajanca, Pavol, et al. "Strain sensing with femtosecond inscribed FBGs in perfluorinated polymer optical fibers." *Optical Sensing and Detection IV*. Vol. 9899. International Society for Optics and Photonics, 2016.
- [11] Kalli, Kyriacos, et al. "Femtosecond laser inscription of Bragg and complex gratings in coated and encapsulated silica and low-loss polymer optical fibers." *24th International Conference on Optical Fibre Sensors*. Vol. 9634. International Society for Optics and Photonics, 2015.
- [12] Theodosiou, Antreas, Amedee Lacraz, and Kyriacos Kalli. "Femtosecond laser inscription of multiplexed FBG sensors in CYTOP polymer optical fibres." *Bragg Gratings, Photosensitivity, and Poling in Glass Waveguides*. Optical Society of America, 2016.
- [13] Dunne, Lucy E., et al. "Design and evaluation of a wearable optical sensor for monitoring seated spinal posture." *2006 10th IEEE International Symposium on Wearable Computers*. IEEE, 2006.

- [14] Aitkulov, Arman, and Daniele Tosi. "Optical fiber sensor based on plastic optical fiber and smartphone for measurement of the breathing rate." *IEEE Sensors Journal* 19.9 (2019): 3282-3287.
- [15] Leal-Junior, Arnaldo G., et al. "Design considerations, analysis, and application of a low-cost, fully portable, wearable polymer optical fiber curvature sensor." *Applied optics* 57.24 (2018): 6927-6936.
- [16] Fegadolli, W. S., J. E. B. Oliveira, and V. R. Almeida. "Plastic optical fiber microbend sensors." *PIERS Proc.* (2008): 842-845.
- [17] Chen, Zhihao, et al. "Plastic optical fiber microbend sensor used as breathing sensor." *SENSORS, 2012 IEEE*. IEEE, 2012.
- [18] Linec, Matjaz, and Denis Donlagic. "A plastic optical fiber microbend sensor used as a low-cost anti-squeeze detector." *IEEE Sensors Journal* 7.9 (2007): 1262-1267.
- [19] Kulkarni, Atul, et al. "An evaluation of the optical fiber beam as a force sensor." *Optical Fiber Technology* 15.2 (2009): 131-135.
- [20] Yang, Xiufeng, et al. "Textile fiber optic microbend sensor used for heartbeat and respiration monitoring." *IEEE Sensors Journal* 15.2 (2014): 757-761.
- [21] Lomer, M., et al. "Lateral polishing of bends in plastic optical fibres applied to a multipoint liquid-level measurement sensor." *Sensors and Actuators A: Physical* 137.1 (2007): 68-73.
- [22] Rajamani, Allwyn S., M. Divagar, and V. V. R. Sai. "Plastic fiber optic sensor for continuous liquid level monitoring." *Sensors and Actuators A: Physical* 296 (2019): 192-199.
- [23] Jing, Ning, et al. "A liquid level sensor based on a race-track helical plastic optical fiber." *IEEE Photonics Technology Letters* 29.1 (2016): 158-160.
- [24] Lin, Xiao, et al. "Low-cost multipoint liquid-level sensor with plastic optical fiber." *IEEE Photonics Technology Letters* 26.16 (2014): 1613-1616.
- [25] Teng, Chuanxin, et al. "Liquid level sensor based on a V-groove structure plastic optical fiber." *Sensors* 18.9 (2018): 3111.
- [26] Kuang, Kevin SC, Wesley J. Cantwell, and Patricia J. Scully. "An evaluation of a novel plastic optical fibre sensor for axial strain and bend measurements." *Measurement Science and Technology* 13.10 (2002): 1523.
- [27] Nishiyama, Michiko, Mitsuo Miyamoto, and Kazuhiro Watanabe. "Respiration and body movement analysis during sleep in bed using hetero-core fiber optic pressure sensors without constraint to human activity." *Journal of biomedical optics* 16.1 (2011): 017002.
- [28] Salim, G. M., and M. A. Zawawi. "Knee joint movement monitoring device based on optical fiber bending sensor." *Journal of Telecommunication, Electronic and Computer Engineering (JTEC)* 10.1-3 (2018): 25-29.

- [29] Ghaffar, Abdul, et al. "Two-dimensional displacement optical fiber sensor based on macro-bending effect." *Optics & Laser Technology* 120 (2019): 105688.
- [30] Teng, Chuanxin, et al. "Investigation of a plastic optical fiber imprinted with V-groove structure for displacement sensing." *Optical Engineering* 58.7 (2019): 072002.
- [31] Ghaffar, Abdul, et al. "Optical Fiber Based Dynamic Displacement Measurement Sensor Using Polymer optical Fiber." *2019 2nd International Conference on Computing, Mathematics and Engineering Technologies (iCoMET)*. IEEE, 2019.
- [32] Teng, Chuanxin, et al. "Investigation of a plastic optical fiber imprinted with V-groove structure for displacement sensing." *Optical Engineering* 58.7 (2019): 072002.
- [33] Zhao, Huichan, et al. "Optoelectronically innervated soft prosthetic hand via stretchable optical waveguides." *Science Robotics* 1.1 (2016): eaai7529.
- [34] Rothmaier, Markus, Minh Phi Luong, and Frank Clemens. "Textile pressure sensor made of flexible plastic optical fibers." *Sensors* 8.7 (2008): 4318-4329.
- [35] Prajzler, Václav, et al. "Design, fabrication and properties of rib poly (methyl-methacrylimide) optical waveguides." (2011).
- [36] Sartiano, Demetrio, and Salvador Sales. "Low cost plastic optical fiber pressure sensor embedded in mattress for vital signal monitoring." *Sensors* 17.12 (2017): 2900.
- [37] Babchenko, Anatoly, and Jonathan Maryles. "Graded-index plastic optical fiber for deformation sensing." *Optics and lasers in engineering* 45.7 (2007): 757-760.
- [38] Grassini, Sabrina, et al. "Design and deployment of low-cost plastic optical fiber sensors for gas monitoring." *Sensors* 15.1 (2014): 485-498.



# Chapter 3

## Trilobal plastic optical fiber sensors

*In this chapter, the design and fabrication of a POF sensor are presented. For the second sensor implementation, non-circular polymeric fibers were designed and fabricated using the extrusion process from pellet. Custom optical fiber core shapes can be obtained using different extrusion dies. The fabrication process was first studied fabricating circular optical fiber with core and cladding. The fabrication parameters were studied related to optical losses. A three lobes shape was chosen as the shape of the fiber sensor. The possibility to monitor curvature using these types of fibers was investigated through numerical simulation, which results were experimentally validated. The extrusion process is described together with the tuning of the parameters to obtain polymeric filaments with low optical losses at a wavelength around 650 nm.*



### 3.1. Trilobal plastic optical fiber sensor for curvature and rotation monitoring

Fiber-based sensors have played an important role in many recent applications, including bridge security monitoring [1], biochemical sensing [2], gas detectors [3], and power system monitoring [4], due to their advantages, such as small size, immunity to electromagnetic interference, remote sensing capability and high sensitivity. Novel fiber sensors are implemented by innovating the fiber grating structure or inscribing gratings in specialty fibers instead of standard single-mode fibers (SMF). These designs are focused on solving the problem of cross-sensitivity between temperature and strain and implementing multi-parameter fiber sensors for new measurands. Baiou Guan et al. [5] used a superstructure fiber Bragg grating (FBG) to simultaneously measure strain and temperature; Maoqing Chen et al. [6] combined a micro extrinsic Fabry-Perot interferometer with an etched FBG for simultaneous measurement of strain and magnetic field. Multicore fibers (MCF) have also been used in sensing field: David Barrera et al. [7] inscribed a tilted fiber Bragg grating (TFBG) in a seven-core fiber by Argon-ion laser to measure strain, curvature direction and magnitude, and external RI. Strongly coupled MCF is an alternative to grating-based sensors: in [8] is reported a strain sensor implemented with an MCF with cores closer together than in a common MCF. The interference between two supermodes excited in the MCF has been used to obtain an interferometric strain sensor. Multiparameter sensors for rotation and bending are reported in literature as well [9-15]. Plastic optical fibers offer a valid cheap alternative to glass fibers in certain applications since they are manufactured with low-cost materials and processes and have good mechanical properties. Plastic fibers are preferable in applications in which high levels of mechanical strain are applied to the sensor since the Young's modulus value of bulk poly(methyl methacrylate) is 3.2 GPa (while it is 72 GPa in silica fibers) and it has high elastic deformation limits (10%). This polymer is also impact and vibration-resistant and has a lower density (1.195 kg/m<sup>3</sup>) than silica [26]. The material most frequently used to make POFs is PMMA thermoplastic polymer, commonly known as Plexiglas®, with a typical refractive index of 1.492 (Plexiglas® 6N at 589 nm

at 23 °C) [27], generally manufactured in two steps. Recent advances in polymer technology have allowed fabricating plastic optical fiber for sensing. The advantages of optical metrology with plastic optical fiber have attracted the attention of the scientific community, as they provide lower-cost systems than conventional technologies [27].

POF based curvature sensors were developed mostly as intensity sensors: for example, in [29-30], the core of the fiber is exposed abrading part of the cladding to enhance the irradiated light when a bend is applied. These sensors were used to monitor human joint and spine curvature[31-32]; as curvature sensors for structural health monitoring [33]; or sensor to monitor breathing [34]; nano displacement were sensed as well using a double core fiber and an interferometric approach [35].

In this chapter, a non-circular optical fiber was fabricated, consisting of a three-lobe PMMA fiber core without cladding. The work presented is the fabrication and experimental validation of a three lobes POF, used as curvature and rotation sensor. The polymeric filaments were fabricated with extrusion, a system normally used for textile fiber fabrication, it was employed to fabricate the PMMA filament with a custom-made extrusion die. Parameters tuning was carried out to obtain POF with low optical power losses.

An extensive experimental work was carried out in order to obtain optical polymeric fibers that can guide light with low optical losses. The extrusion process was adopted for the fabrication of the fibers in collaboration with AITEX (Textile Research Institute). In the first subsection, the fabrication process of the optical fibers is described together with the tuning of the machinery parameters to obtain low optical losses. In the second, is reported the results of numerical simulation for mode confinement and the effect of bending in non-circular POF. The fabrication of the final fiber prototypes is presented with the experimental results obtained for the novel curvature and rotation sensor in the last part.

### 3.1.1. Extrusion process

The extrusion is a flexible process used as well to fabricate plastic filament. The extrusion machine is presented schematically in figure 1. The two units (screw and heated chamber) interact together to convey the polymeric material, melt the material, and then push it through the die. The screw rotates at a predetermined speed with the electric motor drive unit. Temperature controllers are connected to heating/cooling elements on the heater bands to maintain the temperature at the set-point temperatures. The polymer filament is cooled down and collected with a rotating spool.

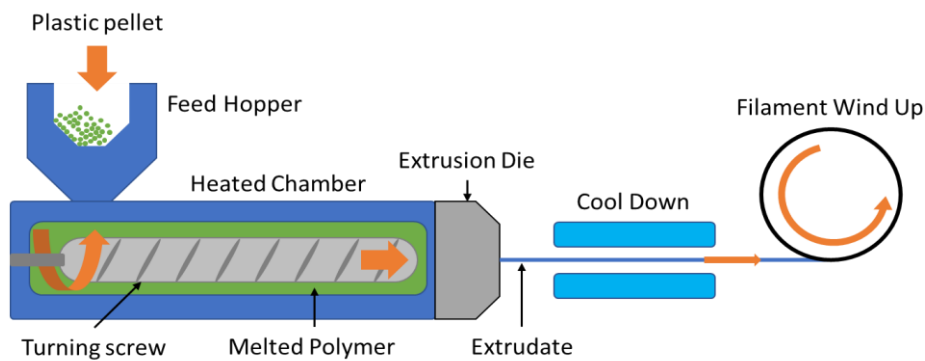


Figure 1. Scheme of the extrusion system: the plastic material is fed into the extruder in form of pellet, the material is melted into the chamber using a variable heater. The motor moves the screw that push the melted materials through the extrusion die. The extrudate is then cool down and collected.

A transparent material allows light to be transmitted through the material matrix with minimum attenuation. In semi crystalline polymers, such as PMMA, transparency is related to the crystallinity of the polymer [36]. Crystallinity is an intrinsic property of the polymeric material where molecular chains are aligned and folded together to form ordered regions called lamellae, which compose larger spheroidal structures named spherulites [37] and the refractive index of crystalline regions is higher than that of amorphous regions. When a light ray passing through an ordered region or spherulites with larger size than the wavelength of visible light (0.4–0.7  $\mu\text{m}$ ), a light scattering is produced. Therefore, amorphous materials will

transmit the light at a higher level compared with crystalline or semi-crystalline materials and a decrease in crystallinity in a semi-crystalline polymer enhances the clarity. The processability of the polymer influences the polymer crystallinity, however, reduction in crystallinity can result in a decrease in strength, stiffness, and resistance to bend.


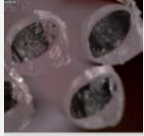



Different types of polymers, pressure, and temperature of the material, temperature, and velocity of the cooling process and speed of the rotating spool for wind up were studied in order to understand their influence on the crystallization process and consequently on the optical losses. The fabrication parameters were swept, and various samples were fabricated and tested to find the set of parameters that minimize the optical losses.

The first fabrication process was carried out using two polymers to obtain a fiber with different materials for core and cladding: polymethylmethacrylate (PMMA) and polypropylene (PP) respectively. As a first experiment circular POFs were fabricated: changing the position of the extrusion die with respect to the cooling down water bath; sweeping the pressure the cladding material is fed into the heated chamber acting on the pump speed; sweeping the speed of the spool for wind up. After the fabrication, the optical losses in the visible range were measured using the cut-back method [38]. The results and the images of the obtained PP/PMMA fibers are reported in table 1.

From these first data, it can be inferred that a lower wind-up speed permits to lower the optical losses of the light transmitted in the POF. Moreover considering the samples #2 and #5, the first fabricated with the extrusion die inclined with respect to the cooling bath and the second with the die perpendicular to the water bath, it is noticed that a circular-like shape for the core permits to lower the optical losses, as well. The main drawback of this fiber is the rigidity of the cladding material that make difficult the handling. For this reason, a more flexible polymer was chosen as cladding material: Polyvinylidene fluoride (PVDF), with its refractive index of 1.42

lower than the PMMA one of 1.49, guarantees the light confinement from the optical point of view.






Table 1. First samples of POFs fabricated: images of the cross-section, fabrication parameters and optical power losses in dB/m measured with the cut-back method.

Sample #	1	2	3	4	5
Photo					
Die position respect to the cooling bath	Inclined	Inclined	Perpendicular	Perpendicular	Perpendicular
Pump speed (rpm) PMMA	12	12	12	12	12
Pump speed (rpm) PP	26	49	49	49	49
Spool speed (m/min)	41	21	12	20	21
$\alpha$ (dB/m)	x	58.33	28.95	31.26	36.86

The work was again focused on the optimization of the extrusion process. For this second round of fabrication, the parameters swept were the spool speed and the temperature of the water of the cooling bath. The process of cooldown is known to directly influence the degree of crystallinity. The fiber and the optical losses are reported in table 2.

As expected, the temperature of the water tank greatly influenced the optical losses, water at 9°C ensure lower optical losses in the obtained fibers. So, at this stage it is possible to fabricate POF with reasonable optical losses, it is possible to design a specific POF with a specific geometry to use as a sensor. After the preliminary test with circular POF a three-lobe fiber was fabricated. The trilobal shape was obtained using the extrusion die showed in figure 2.

Table 2. Samples of POFs fabricated: images of the cross-section, fabrication parameters and optical power losses in dB/m measured with the cut-back method.

Sample #	1	2	3	4	5
Photo					
Pump speed (rpm) PMMA	6	6	6	6	6
Pump speed (rpm) PVDF	40	40	40	40	40
Spool speed (m/min)	8	8	8	8	16
Cool down Temperature (°C)	22	42	42	9	9
$\alpha$ (dB/m)	57.86	40.79	45.13	2.82	19.78

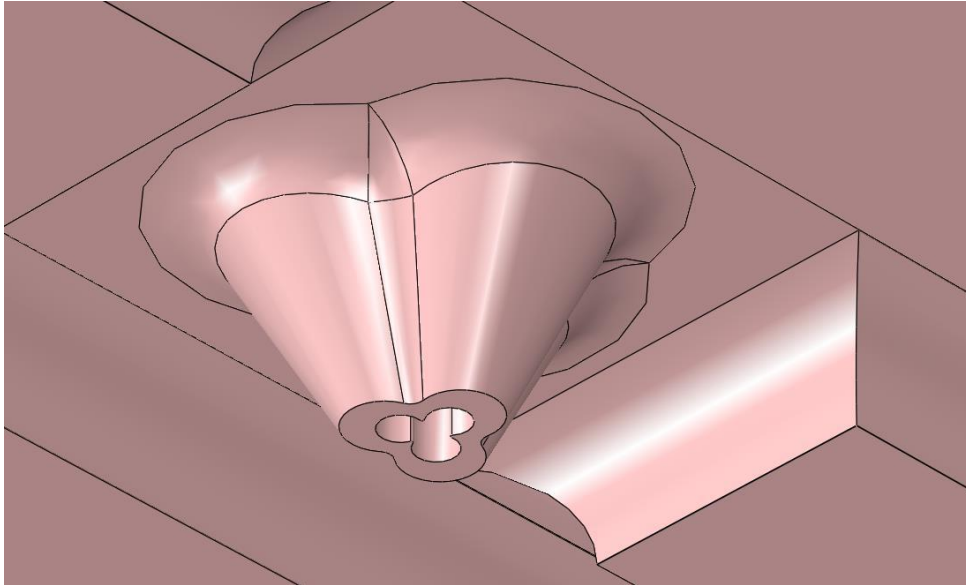


Figure 2. Output of the custom extrusion die designed to fabricate the trilobal fiber.

### ***3.1.2. Numerical mode confinement simulation in non-circular POF***

The shape chosen for our POF-sensor is a trilobal shape. The three-lobe shape was conceived to achieve a low-cost optical fiber bending direction and rotation sensor. The bend direction sensing principle is based on a shift of the mode fields in the cross-section of the three-lobe fiber when the plastic filament is bent. The transversal section of the three-lobe fiber was captured by an optical microscope (figure 3a), processed and then imported into Lumerical MODE software. Mode simulations were performed to calculate the light field distribution of the lowest order modes in both the straight and bent fiber. Figure 3b shows the light field intensity of the lowest order fiber mode simulated in the straight fiber.

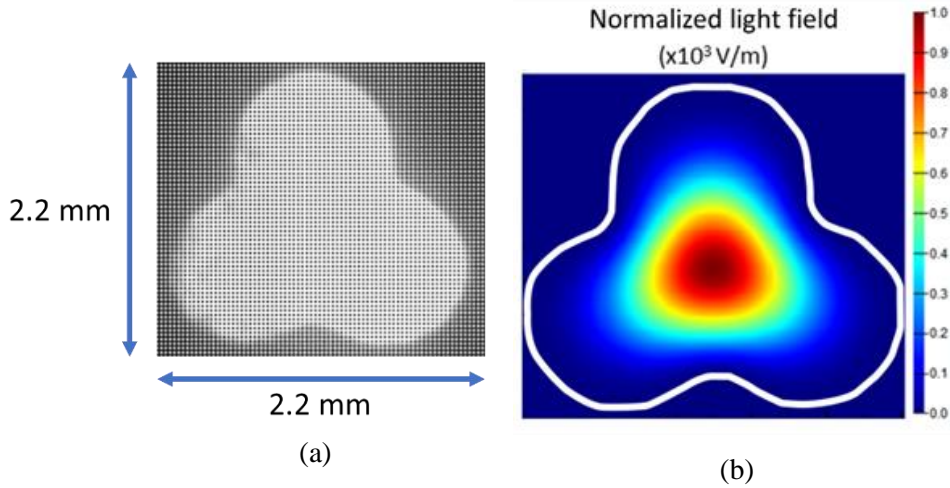


Figure 3. (a) Optical microscope image of the cross-section of the three-lobe plastic optical fiber. (b) Simulated light field intensity of the fundamental mode at 645 nm.

As observed in previous calculations and simulations on bent fibers, bending tends to distort the fiber modes and causes them to shift away from the center of curvature [39]. In the case of a bent waveguide Lumerical MODE software will solve for modes of the form:

$$E(\rho, \theta, z) = E_j(\rho, y)e^{i\beta_j\theta} \quad (1)$$

where  $\beta_j$  depicts the angular propagation constant of the  $j_{th}$  mode and has units of inverse radian, and  $(\rho, \theta, y)$  represents a cylindrical coordinate system. This constant is proportional to the effective index of the mode and the bending radius [40]. The simulated light field intensities for the lowest order modes under three-directional bending with a radius of 10 meters are shown in figure 4. The simulations confirmed that the guided modes in the bent three-lobe fiber shifted away from the center of curvature. The work was then focused on the fabrication of trilobal POF with low optical losses and validate the results of the simulation.



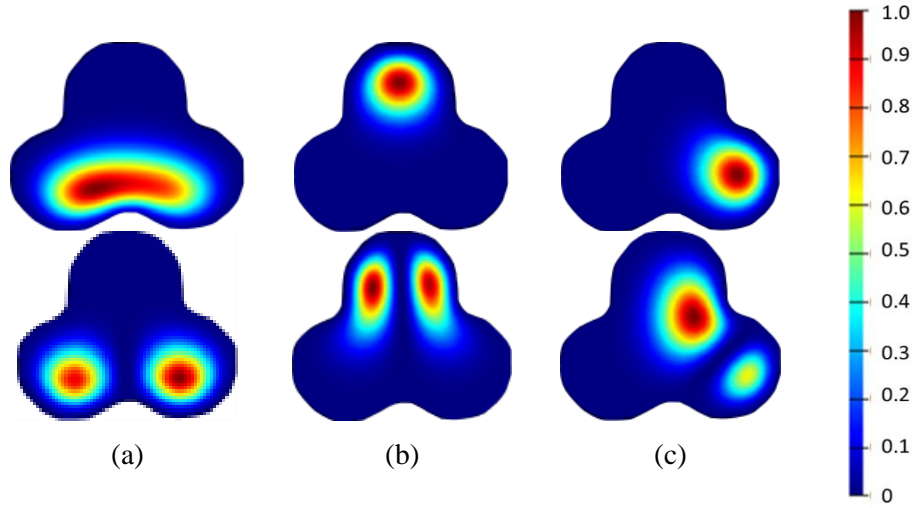


Figure 4. Normalized Light field intensity ( $<10^3 \text{ V/m}$ ) at 645nm of the two lowest order modes calculated in the imported three-lobe structure cross-section for bending with curvature center placed: (a) on the upper surface of the fiber; (b) on the lower surface of the fiber; (c) on the right-hand surface of the fiber.

The intensity variation, that shifts away from the bend centers, can be used to estimate the bending direction. The calculation of the weighted centroid is the algorithm chosen to process the intensity image and give an estimation of the curvature direction; the centroid is calculated using the intensity of the pixel as weight. For a 2D image  $N \times M$  it is possible to calculate the centroid coordinates using the formula (with  $I$ : intensity and  $x/y$ : horizontal/vertical coordinates):

$$x_f = \frac{\sum_{j=1}^M \sum_{i=1}^N I_{i,j} x_i}{\sum_{j=1}^M \sum_{i=1}^N I_{i,j}}; y_f = \frac{\sum_{i=1}^N \sum_{j=1}^M I_{i,j} y_j}{\sum_{j=1}^M \sum_{i=1}^N I_{i,j}} \quad (2)$$

### 3.1.3. Trilobal fiber fabrication and experimental results

The same fabrication procedure, presented in the previous paragraphs, was followed for the trilobal fibers. The first attempt was to fabricate a POF

composed of two materials for core and cladding, as for the circular POF, but adopting a custom extrusion die to obtain a trilobal fiber. The problem is that the hydrostatic pressure of the cladding material at the core/cladding interface made it impossible to maintain a three lobes shape for the core once the filament is extruded. For this reason, a PMMA trilobal filament was fabricated, with no cladding. The cooldown method was changed, since PMMA absorbs water it must be cool down at air; until this point, the cladding materials (PP, PVDF) avoid the absorbance of water. In figure 5 is shown the cross section of the obtained POF.



Figure 5. Photo of the cross-sections of the obtained plastic optical fibers.

Six samples were fabricated in order to study, even in this case, the effect of some parameters in the extrusion process on the optical losses of the obtained PMMA POFs, as PMMA pressure, wind-up speed, two different types of cool down both at room temperature with and without the employing of a cooling fan, and using two types of PMMA: the Plexiglas® 6N and 8N (which main characteristics are reported in table 3). In table 4 are reported the optical losses of the obtained polymeric optical fibers, measured using the cut-back method.

Table 3. Properties of Plexiglass 6N and 8N

Properties:	Plexiglas® 6N	Plexiglas® 6N
Tensile Modulus (MPa)	3200	3300
Stress @ break (MPa)	67	77
Strain @ break (%)	3	5.5
Refractive Index	1.49	1.49
Density (g/cm <sup>3</sup> )	1.19	1.19
Melt Volume Rate (cm <sup>3</sup> /10min)	12	3

Table 4. Samples of trilobal POFs fabricated: fabrication parameters and optical power losses in dB/m measured with the cut-back method.

Material	Plexiglas® 8N				Plexiglas® 6N	
	1	2	3	4	5	6
Pump speed (rpm) PMMA	12	12	8	8	10	10
Spool speed (m/min)	18	18	20	20	24	24
Cool down Temperature (°C)	RT	CF	RT	CF	RT	CF
$\alpha$ (dB/m)	27.66	28.18	25.29	19.61	21.58	20.28

It is noticed that the optical losses in this case are, on average, lower than the fiber made of two materials for core/cladding. This is because not only core material crystallinity affects the optical losses, but as well the irregularities at the core/cladding interface. Vacuum bubbles are formed during the cool down since the core and cladding materials have different thermic coefficients and contract at a different speed. These micro and macro bubbles are another major cause of losses in the two materials POFs.

The POF #4 was taken to prove that the intensity variations are observable when bending is applied, as supposed looking to the simulations results. The fiber was mounted in an intensity based interrogation system. The setup was implemented with a collimated red LED (645 nm peak wavelength), the fiber was fixed to a moving stage on one side, and an objective was used to focus the image of the fiber end on a charge coupled device (CCD) sensor (figure 6). In this case, a two-dimensional light sensor is needed because the light intensity distribution has to be monitored and not only the intensity as it is usual for intensity-based sensors. When the moving stage is moved a curvature is obtained, as shown in red in figure 7. A sample of 20 centimeters was fixed between the two holders and a curvature with a ray of approximately 1 meter was applied. The constant curvature was obtained using a moving stage and the curvature was approximated using the formula [41]:

$$\sin\left(\frac{LC}{2}\right) = \frac{(L - D)C}{2} \quad (3)$$

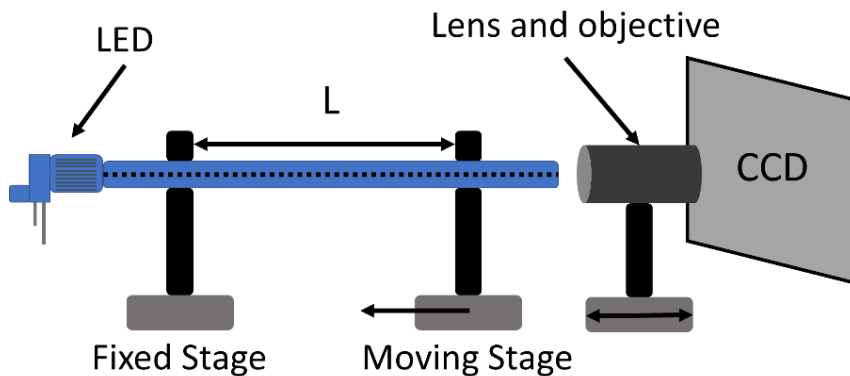


Figure 6. Schematic representation of the experimental setup.

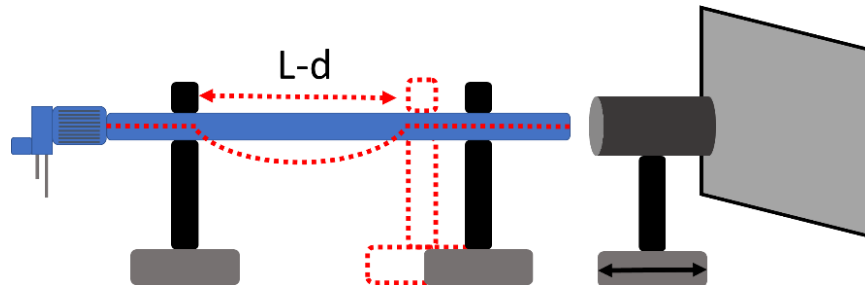


Figure 7. Method used to obtain constant curvature.

In order to verify if the curvature has a significant effect on the light intensity distribution inside the fiber core a reference image was acquired without curvature, after that a curvature was applied and another image was captured. Using MATLAB software, the two images were subtracted, and the results are shown in figure 8, three images obtained for bending orientation along the  $x$  and  $y$  axes (red stars represent the weighted centroid). As for the simulations, the light intensity variation is clearly observable in the exterior of the fiber, caused by the shift of the fiber modes due to the bending applied. This feature sensor can be used to estimate curvature direction.

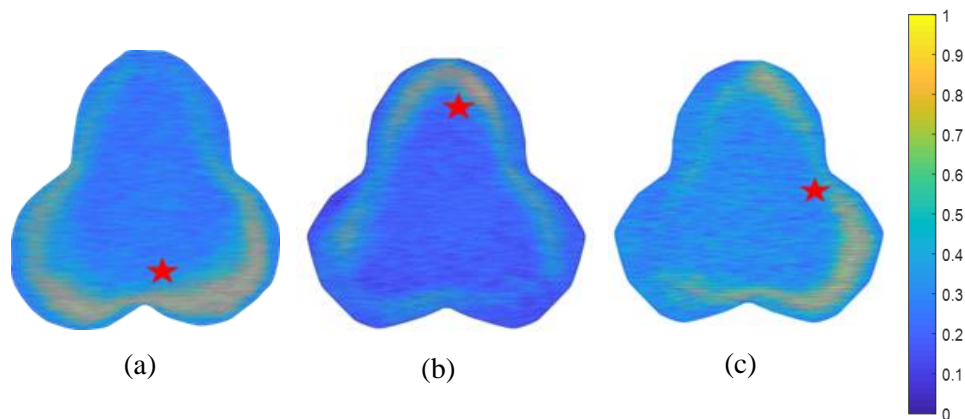


Figure 8. Images collected with the CCD camera after bending the three-lobe plastic fiber. Red stars indicate the position of the weighted centroid, found from the converted grayscale image. The curvature center placed: (a) on the upper surface of the fiber; (b) on the lower surface of the fiber; (c) on the right-hand surface of the fiber.

Another possible application for these fibers is rotation sensing. Since the fiber has a non-circular shape for the core, in principle, it is possible to retrieve the rotation angle of the filament around the normal axis of the end facet using a reference image and a rotated image. Due to the circular symmetry of the trilobal shape, the measurement is limited to a range between 0-120°. In order to demonstrate the possibility to sense rotation, the moving stage was substituted with a rotating clamp in the setup shown in figure 11. The fiber was then placed in a rotating clamp and rotated from 0° to 50° in 5° steps. An intensity-based automatic image registration algorithm was used to retrieve the rotation angle of the fiber through the images acquired by the camera. Intensity-based automatic image registration is an iterative process that requires a specified pair of images, a metric, an optimizer, and a transformation type. The image similarity metric takes two images and returns a scalar value that describes their similarity. The optimizer defines the method of minimizing or maximizing the similarity metric. The transformation type defines the type of 2-D transformation that aligns the misaligned image (known as the moving image) with the reference image (or fixed image) [42]. Registering the image of the rotated fiber (moving image) and the image of the fiber in the starting position (fixed image) it was possible to obtain the rotating angles. Figure 9 shows the images processed and the retrieved angles.

In this case, a rigid transformation was chosen since it includes translation and rotation. Registering the image of the rotated fiber (moving image) and the image of the fiber in the starting position (fixed image) it was possible to obtain the rotating angles. Figure 10a shows how the images were processed using the registration algorithm, on the left the two overlapped images and on the right the result of the algorithm processing. The rotation measurements were repeated 10 times: figure 10b shows the correspondence between the rotating angles and the retrieved angles, using the method described above, and the average error. It was possible to measure the rotation angle with an accuracy of 0.01° in our lab condition.

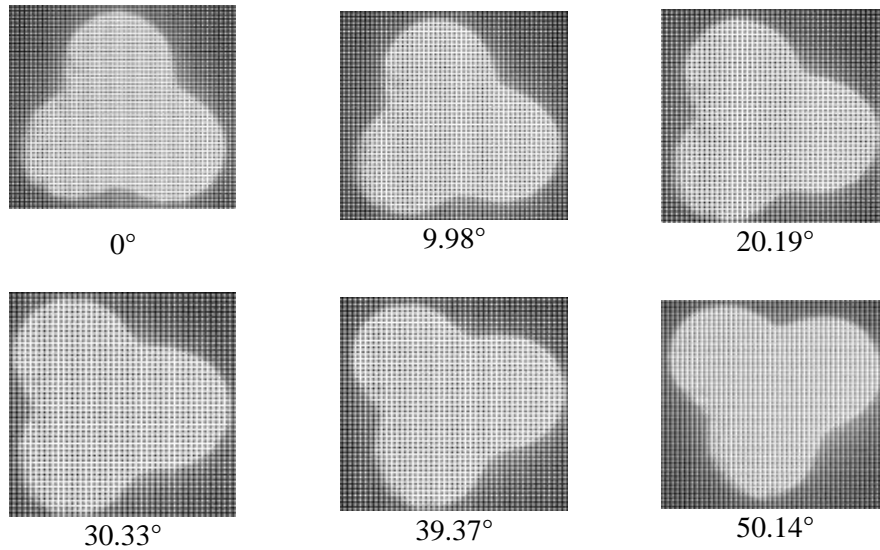


Figure 9. Images captured with the CCD camera of the POF with rotation. The circular asymmetry can observe the rotation of the fiber core and retrieve the rotation angles (reported below).

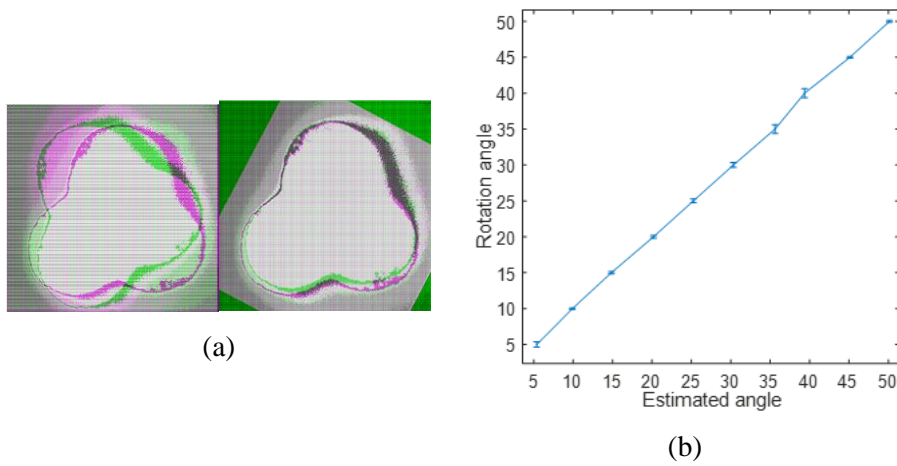


Figure 10. (a) Reference and rotated image superimposed before and after the registration algorithm is applied. (b) Comparison between the retrieved angles using the registration algorithm and the rotation angles applied. The error bars show the average error of ten measurements.

The circular POF fabricated were optimized not only in terms of optical losses but also regarding the mechanical properties to be integrated into textile. This textile can be integrated in composites, fiber carbon or other devices to implement new solutions for sensing pressure, force, bending and all the other parameters that can be sensed using intensity-based configuration. Other works in literature reported the integration of POF in textiles as thermoplastic silicone fibers [34] for pressure sensing. This work wants to propose a cost-effective platform for POF fabrication (extrusion) and integration in textiles. As well the interrogation system was miniaturized to permit the fabrication of portable POF-based sensors for wearable applications, for example.

### **3.2. Conclusions**

A sensor is presented for rotation and bend-direction sensing. The sensor was designed and fabricated using extrusion machinery, commonly used to extrude plastic fibers for textiles. The extrusion process was described together with the parameters swept to minimize the optical losses. The possibility to monitor curvature using these types of fibers was demonstrated validating the results of numerical simulation. The bend direction sensing principle is based on a shift of the mode fields in the cross-section of the three-lobe fiber when the plastic filament is bent.



## References

- [1] Maaskant, R., et al. "Fiber-optic Bragg grating sensors for bridge monitoring." *Cement and Concrete Composites* 19.1 (1997): 21-33.
- [2] Baldini, F., et al. "Optical fibre gratings as tools for chemical and biochemical sensing." *Analytical and bioanalytical chemistry* 402.1 (2012): 109-116.
- [3] Qin, Xiang, et al. "Molybdenum sulfide/citric acid composite membrane-coated long period fiber grating sensor for measuring trace hydrogen sulfide gas." *Sensors and Actuators B: Chemical* 272 (2018): 60-68.
- [4] Kim, Hyun-Jin, Hyoung-Jun Park, and Min-Ho Song. "A Quasi-Distributed Fiber-Optic Sensor System using an InGaAs PD Array and FBG Sensors for the Safety Monitoring of Electric Power Systems." *Journal of the Korean Institute of Illuminating and Electrical Installation Engineers* 24.2 (2010): 86-91.
- [5] Guan, Bai-Ou, et al. "Simultaneous strain and temperature measurement using a superstructure fiber Bragg grating." *IEEE Photonics Technology Letters* 12.6 (2000): 675-677.
- [6] Chen, Mao-qing, et al. "Hybrid MEFPI/FBG sensor for simultaneous measurement of strain and magnetic field." *Optical Fiber Technology* 39 (2017): 32-36.
- [7] Barrera, David, Javier Madrigal, and Salvador Sales. "Tilted fiber Bragg gratings in multicore optical fibers for optical sensing." *Optics Letters* 42.7 (2017): 1460-1463.
- [8] Villatoro, Joel, et al. "Accurate strain sensing based on super-mode interference in strongly coupled multi-core optical fibres." *Scientific reports* 7.1 (2017): 1-7.
- [9] Kisała, Piotr, Damian Harasim, and Janusz Mroczka. "Temperature-insensitive simultaneous rotation and displacement (bending) sensor based on tilted fiber Bragg grating." *Optics express* 24.26 (2016): 29922-29929.
- [10] Wang, Yi-Ping, and Yun-Jiang Rao. "A novel long period fiber grating sensor measuring curvature and determining bend-direction simultaneously." *IEEE Sensors Journal* 5.5 (2005): 839-843.
- [11] Salceda-Delgado, G., et al. "Compact fiber-optic curvature sensor based on super-mode interference in a seven-core fiber." *Optics letters* 40.7 (2015): 1468-1471.
- [12] Kissinger, Thomas, et al. "Dynamic fiber-optic shape sensing using fiber segment interferometry." *Journal of Lightwave Technology* 36.4 (2017): 917-925.
- [13] Ahmad, Raja, et al. "Probing micron-scale distributed contortions via a twisted multicore optical fiber." *APL Photonics* 4.6 (2019): 066101.
- [14] Moore, Jason P., and Matthew D. Rogge. "Shape sensing using multi-core fiber optic cable and parametric curve solutions." *Optics express* 20.3 (2012): 2967-2973.
- [15] Villatoro, Joel, et al. "Ultrasensitive vector bending sensor based on multicore optical fiber." *Optics Letters* 41.4 (2016): 832-835.

- [16] Xiong, Z., et al. "Highly tunable Bragg gratings in single-mode polymer optical fibers." *IEEE Photonics technology letters* 11.3 (1999): 352-354.
- [17] Liu, H. Y., H. B. Liu, and G. D. Peng. "Tensile strain characterization of polymer optical fibre Bragg gratings." *Optics Communications* 251.1-3 (2005): 37-43.
- [18] Liu, H. Y., G. D. Peng, and P. L. Chu. "Thermal tuning of polymer optical fiber Bragg gratings." *IEEE Photonics Technology Letters* 13.8 (2001): 824-826.
- [19] Haseda, Yuki, et al. "Measurement of pulse wave signals and blood pressure by a plastic optical fiber FBG sensor." *Sensors* 19.23 (2019): 5088.
- [20] Husdi, Irwan Rawal, Kentaro Nakamura, and Sadayuki Ueha. "Sensing characteristics of plastic optical fibres measured by optical time-domain reflectometry." *Measurement Science and Technology* 15.8 (2004): 1553..
- [21] Saunders, C., and P. J. Scully. "Distributed plastic optical fibre measurement of pH using a photon counting OTDR." *Journal of Physics: Conference Series*. Vol. 15. No. 15. 2005.
- [22] Rao, Yun-Jiang, et al. "Long-distance fiber-optic  $\Phi$ -OTDR intrusion sensing system." *20th international conference on optical fibre sensors*. Vol. 7503. International Society for Optics and Photonics, 2009.
- [23] Stajanca, Pavol, et al. "Strain sensing with femtosecond inscribed FBGs in perfluorinated polymer optical fibers." *Optical Sensing and Detection IV*. Vol. 9899. International Society for Optics and Photonics, 2016.
- [24] Kalli, Kyriacos, et al. "Femtosecond laser inscription of Bragg and complex gratings in coated and encapsulated silica and low-loss polymer optical fibers." *24th International Conference on Optical Fibre Sensors*. Vol. 9634. International Society for Optics and Photonics, 2015.
- [25] Theodosiou, Antreas, Amedee Lacraz, and Kyriacos Kalli. "Femtosecond laser inscription of multiplexed FBG sensors in CYTOP polymer optical fibres." *Bragg Gratings, Photosensitivity, and Poling in Glass Waveguides*. Optical Society of America, 2016.
- [26] Van Eijkelenborg, Martijn A., et al. "Microstructured polymer optical fibre." *Optics express* 9.7 (2001): 319-327.
- [27] Bilro, Lúcia, et al. "Optical sensors based on plastic fibers." *Sensors* 12.9 (2012): 12184-12207.
- [28] Zubia, Joseba, and Jon Arrue. "Plastic optical fibers: An introduction to their technological processes and applications." *Optical fiber technology* 7.2 (2001): 101-140.
- [29] Lomer, M., et al. "Lateral polishing of bends in plastic optical fibres applied to a multipoint liquid-level measurement sensor." *Sensors and Actuators A: Physical* 137.1 (2007): 68-73.
- [30] Kuang, Kevin SC, Wesley J. Cantwell, and Patricia J. Scully. "An evaluation of a novel plastic optical fibre sensor for axial strain and bend measurements." *Measurement Science and Technology* 13.10 (2002): 1523.

- [31] Stupar, Dragan Z., et al. "Wearable low-cost system for human joint movements monitoring based on fiber-optic curvature sensor." *IEEE Sensors Journal* 12.12 (2012): 3424-3431.
- [32] Zawawi, Mohd Anwar, Sinead O'Keeffe, and Elfed Lewis. "Plastic optical fibre sensor for spine bending monitoring with power fluctuation compensation." *Sensors* 13.11 (2013): 14466-14483.
- [33] Vallan, Alberto, et al. "Design and characterization of curvature sensors based on plastic optical fibers for structural monitoring." *2013 IEEE International Instrumentation and Measurement Technology Conference (I2MTC)*. IEEE, 2013.
- [34] Leal-Junior, Arnaldo G., et al. "Polymer optical fiber-based sensor for simultaneous measurement of breath and heart rate under dynamic movements." *Optics & Laser Technology* 109 (2019): 429-436.
- [35] Qu, H., G. F. Yan, and M. Skorobogatiy. "Interferometric fiber-optic bending/nano-displacement sensor using plastic dual-core fiber." *Optics letters* 39.16 (2014): 4835-4838.
- [36] Maier, Clive, and Theresa Calafut. *Polypropylene: the definitive user's guide and data-book*. William Andrew, 1998; pp. 194-198.
- [37] Carraher Jr, Charles E. *Seymour/Carraher's polymer chemistry*. Vol. 16. CRC press, 2003.
- [38] Ziemann, Olaf, et al. "POF handbook." *Springer* (2008).
- [39] Schermer, Ross T., and James H. Cole. "Improved bend loss formula verified for optical fiber by simulation and experiment." *IEEE Journal of Quantum Electronics* 43.10 (2007): 899-909.
- [40] Bent Waveguide Solver. Available online: [https://kb.lumerical.com/solvers\\_finite\\_difference\\_eigenmode\\_bend.html](https://kb.lumerical.com/solvers_finite_difference_eigenmode_bend.html) (Accessed on 10/09/2019)
- [41] Barrera, David, Javier Madrigal, and Salvador Sales. "Long period gratings in multicore optical fibers for directional curvature sensor implementation." *Journal of Lightwave Technology* 36.4 (2018): 1063-1068.



# Chapter 4

## Interrogation system for temperature/strain fiber-based sensor

*In the design of distributed and quasi-distributed fiber sensor, a tradeoff exists between the complexity of the fiber sensor and of the interrogation system. The advances in the fabrication of continuous grating and array of gratings allow performing distributed sensing, relaxing the design of the interrogation system. On the other hand, OTDR and OFDR based systems sense temperature and strain using a standard single mode fiber as a sensing element, much easier to employ and cheaper than fiber with gratings. In the first part of this chapter different approaches are presented: the state of the art of discrete and distributed fiber sensors is reported, together with the latest research works, where the FBGs (originally used as a discrete sensor) are employed together with OTDR/OFDR setup, in order to overcome the drawbacks of the classical wavelength division multiplexing, used for multiple points sensing with FBGs. Finally, the implementation and the experimental results of an interrogation system for an array of near identical FBGs to monitor temperature and mechanical vibration is presented. It was possible to sense temperature changes down to 1°C with sub-centimeter spatial resolution. The advantages of the fast interrogation setup were exploited, as the higher frequency limit of a dynamic measure that can be sensed is limited by the time needed to generate the optical pulse and to acquire the data from the sensor.*

## **4.1. Discrete and distributed fiber sensor**

Temperature and strain monitoring can be performed with fiber sensors at various points simultaneously, using a certain number of discrete sensors and multiplexing or using a distributed sensor. In the next section, FBGs are presented as discrete sensors together with multiplexing techniques that allow multipoint sensing. Then, the main distributed sensing technologies are described, as OTDR and OFDR; finally, the research work where FBGs array or long gratings are used to perform quasi-distributed and distributed sensing are presented. Distributed interrogation systems are often bulky and expensive, but they allow using a standard single mode fiber as a sensing element; on the other hand, inscribing continuous grating or array of weak gratings allows to move the complexity from the interrogation system to the fiber sensing element, relaxing some of the interrogation system design parameters.

### ***4.1.1. FBG: discrete sensing and multiplexing***

FBGs are a consolidated technology to implement point sensors in optical fibers. The most frequently used FBG technique is by employing a tunable laser and a photodetector to retrieve the spectrum of the FBG in the wavelength domain [1]. As the FBG spectrum shifts when a temperature or strain variation is exerted on the grating region, it is necessary to estimate the peak wavelength (known as Bragg wavelength) from the FBG spectrum and then to track its shift from the reference position to effectively use an FBG to estimate a temperature or strain variation [2]. This method can reach a resolution of 10 pm/°C [3] for temperature measurement. FBGs must be inscribed with different Bragg wavelengths and every peak must be tracked independently to sense at multiple points using peak tracking and single fiber. This method is known as wavelength division multiplexing (WDM) [4-7]. However, this technique has certain drawbacks: firstly, the inscription of gratings with different wavelengths is not a cost-effective solution, it limits the maximum number of independent points that can be monitored in a single fiber and dense arrays of FBGs cannot be

produced to implement a quasi-distributed sensing system. Secondly, the time required to sweep the tunable laser limits the maximum frequency of a detectable dynamic refractive index change. New methods to retrieve information from an array of FBGs were investigated in order to overcome these drawbacks: the use of delay mapping to simplify the implementation of the interrogation system [8]; the fabrication and interrogation of an array of near identical FBGs, in this case, fabricated at the same wavelength [9], using: interferometry [10-15]; microwave photonics [16-17]; wavelength to frequency transform [18]; simultaneous wavelength and time division multiplexing [19]; dual comb spectroscopy [20].

#### **4.1.2. Time analysis: distributed sensing**

A time-based analysis enables the use of distributed and quasi-distributed fiber-based sensors. In this field, the phase sensitive OTDR offers many advantages when performing distributed sensing, with high spatial resolution and the possibility of interrogating many kilometers of standard single mode fiber [21-25]. This sensing technique can coherently sense the Rayleigh backscattered signal in single mode fibers by exploiting the OTDR classical setup and constant phase light pulses. As the backscattered signal is quite low powered ( $< -70$  dB/m), highly sensitive photodetectors must be used. Commercial distributed temperature sensor interrogator achieves a spatial resolution of 12 cm over 50 km [26] and 25 cm over 40 m for acoustic sensing (frequency range 0.01 Hz-50 kHz) [27]. Optical frequency domain reflectometry (OFDR) has also been used in single mode fiber [28] to sense strain and temperature [29-32]. OFDR systems achieve a spatial resolution of 10  $\mu$ m for temperature sensing over 2 km of fiber while a resolution of 10  $\mu$ m in dozens of meters for dynamic strain measurement with a maximum sampling frequency of 3 Hz [33]. Phase sensitive OTDR and OFDR systems are bulky and need the sweep of a laser to perform a measurement; the need to sweep a laser over a long wavelength range limits the maximum frequency of a dynamic refractive index change that can be sensed. This can limit, in practice, the maximum vibration frequency detectable with these techniques. The strength is that a standard

single mode fiber can be used as a sensor, without fabricating any FBGs or reflectors. On the other hand, the possibility to fabricate long gratings or arrays of near identical gratings has open new possibilities in the sensing field, and phase OTDR and OFDR were used to interrogate an array of weak gratings [34-35]. The performance of the systems is improved thanks to the higher backreflected signal.

#### **4.1.3. *Distributed sensing with FBGs***

Implementing a system to perform distributed sensing with FBGs would require the grating to be inscribed along the length of the sensing fiber [36-37]. The idea is to enhance the back reflected signal in fiber using a weak uniform grating. The production of such a device is still a challenge but draw tower gratings are a good alternative. These gratings are created during the drawing process of the optical fiber [38] and make it possible to produce long arrays with a large number of FBGs. If the FBGs are densely assembled in the array a higher backscattered signal can be obtained (as in using a Faint Long Optical Grating [36]) and a distributed sensor can be implemented [39-40]. It is worth fabricating an array of gratings or long grating if the interrogation system can be significantly reduced in dimension and complexity, and/or it is possible to enhance its performance.

The interrogation system presented in this chapter was used to interrogate a dense array of 500, 0.9 cm long, weak gratings separated by 0.1 cm with a short laser pulse to reach high spatial resolution. The higher backreflected signal made it possible to use a photodetector with lower sensitivity than that required for phase sensitive OTDR. The spatial position of the hot point is calculated from the temporal trace by the time of flight. The laser used is a gain switching laser that generates pulses of less than 10 ps without an external electro optical modulator (EOM) [41]. The pulses have a high extinction ratio and low jitter, which is essential to correctly recover the reflected signal evolution in time. Even though the gratings are very weak (nominally around 0.1% reflectivity) the back reflected signal is clearly higher than the Rayleigh backscattering (considering the same



input optical power and fiber length). Two different measurements were made with the same setup. The signal was acquired in the time domain employing an optical oscilloscope for quasi-distributed temperature sensing with sub-centimeter spatial resolution on an FBG array. The second experiment was the measurement of dynamic strain (mechanical vibration). Many studies in the literature have proposed techniques to sense dynamic measurands as vibration using optical fibers. In [42], Cusano et al. describe an interrogation setup using a super-luminescent diode and a grating-based passive filter that can measure vibrations of up to 50 kHz. In [43], two FBGs are used to implement the interrogation system: one to generate a narrow-band signal in wavelength from an incoherent light source and another as a sensing element. A narrow source distributed feedback laser diode (DFB-LD) is used in [44] as the light source to interrogate the FBG vibration sensor. In [45], a fiber ring laser is used to implement the interrogation system of a vibration sensor. Due to the Shannon principle, the factors that limit the maximum frequency in dynamic measurements are laser sweep time (as for the wavelength in WDM), time of flight of the optical pulse in fiber (significant for long fiber sections) and speed of the electronic front end that acquires the signal. The advantage of the system proposed here is that the laser always emits around the Bragg wavelength of the gratings in the array. The vibration signal is obtained by detecting the reflected optical signal with a fast avalanche photodiode. A simple demodulation is used to interrogate the strain-induced Bragg wavelength shift. The proposed interrogation system can measure vibration and reach measured mechanical vibrations of up to 245 kHz with a strain resolution of  $1.2 \mu\epsilon$ .

## 4.2. Interrogation setup and principle of operation

The experimental setup used performs a wavelength-to-time domain analysis, and it is implemented with a gain-switching laser diode module [41]. Gain switching (GS) of a distributed feedback semiconductor laser diode is widely used to generate short optical pulses for time-division

multiplexed optical communication systems, soliton generation and optical signal processing [46]. The module employed uses an attached fiber cavity whose ends are coated with diamond-like carbon (DLC) as a self-seeding pulse feedback circuit (figure 1).

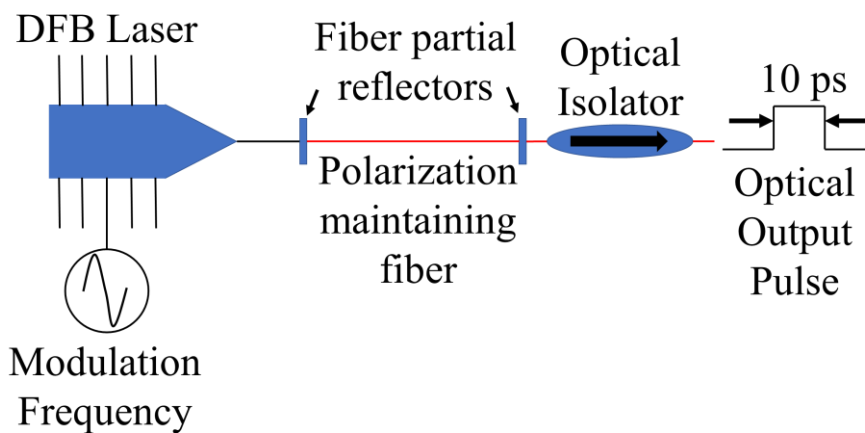


Figure 1. Laser module and optical fiber cavity used for gain-switching implemented with polarization maintaining fiber and two partial reflectors.

A temperature controller is used to change the central wavelength of the optical pulse: the wavelength of the tunable laser used to perform the measurements had previously been calibrated, so that by simply adjusting the thermistor resistance controller the laser wavelength can be easily tuned. The central frequency of the interrogating pulse is precisely controlled by the injection current applied to the laser. The only external signal needed to activate the self-seeding mechanism is a square wave at 5.9 GHz, a much lower frequency than that required to drive an external modulator to generate 10 ps pulses by direct modulation. The setup consists of the laser, described above, a dispersion element (-171 ps/nm at 1550 nm) and an array of 500 weak FBGs (figure 2). The reflected signal was acquired using an oscilloscope with an optical sampling module, triggered by the modulation signal that generates the laser pulses.

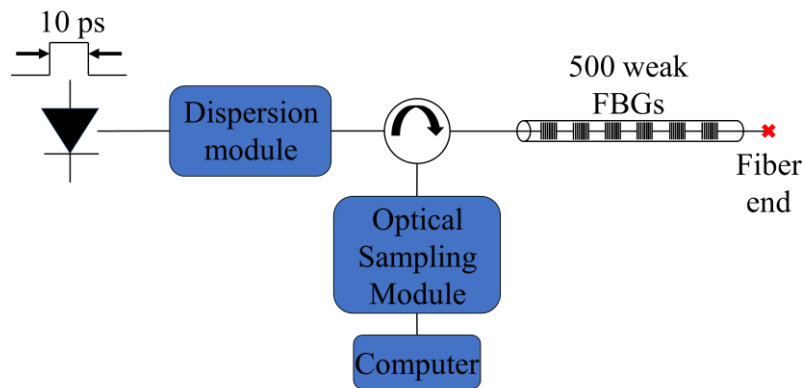
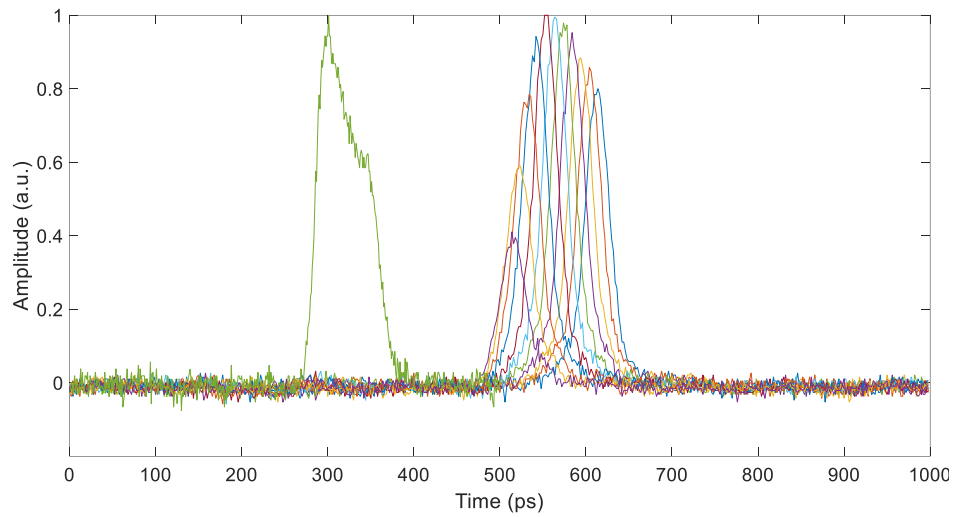
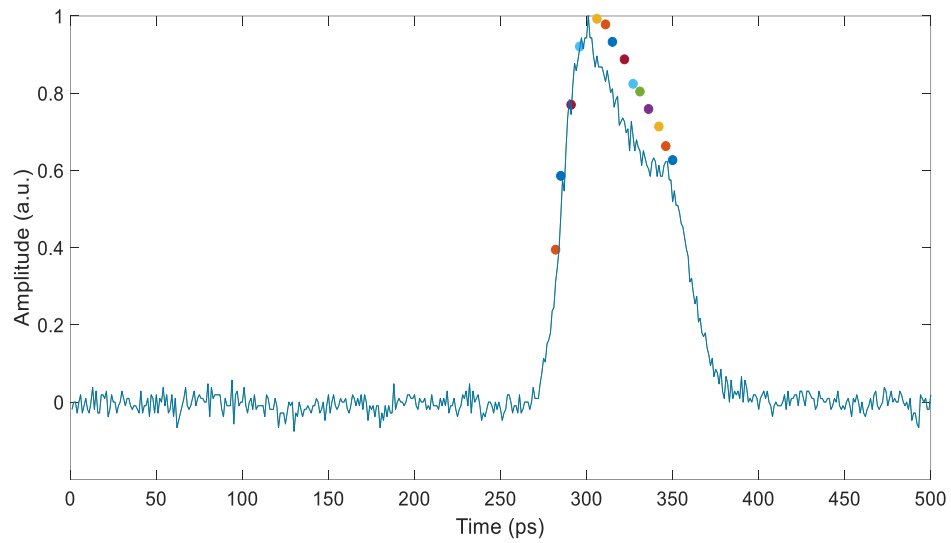


Figure 2. Scheme of the interrogation system and array of 500 weak FBGs.

A dispersion-compensation module, the LL Micro DK-C: 170 manufactured by OFS Fitel, with a total dispersion of  $-171.6$  ps/nm at 1550nm, was used to add dispersion to the optical pulse. The output laser pulse has a short time duration and a broad wavelength spectrum (approximately 1 nm). The dispersion linearly separates the wavelengths of the spectra of the light pulse in time, with a technique known in optical signal processing as time-stretch [47-51]. A single grating was used to illustrate the principle of operation of the interrogation system. The pulse-like signals reflected by the single FBGs carry the amplitude and time delay information associated with the spatial position and Bragg wavelength of each grating. Two events can occur between two instants in time: if no change in the central wavelength is caused by a local change in temperature and/or strain, the amplitude and delay of the reflected pulse do not change. If there is a change in the refractive index, the pulse experiences a time shift and a change in amplitude. Bragg wavelength shift was caused by temperature to demonstrate this principle. Figure 3a shows the plot of the laser pulse after the dispersion element and the reflected pulses, of one FBG, at different temperatures. The maximum of the peak was plotted and superimposed on the interrogation pulse to clearly show the correspondence (figure 3b).



(a)



(b)

Figure 3. (a) Interrogation pulse after the dispersion element (green line) and back reflected pulse from an FBG at different temperatures. (b) The points represent the maximum of the peaks plotted in figure 3a superimposed to the interrogation pulse (blue line).

### 4.3. Temperature measurement

If a temperature change is exerted on a portion of the FBG array, a temperature gradient is obtained. This local refractive index change will result in a local Bragg frequency shift. The hot point on the array, approximately 1 cm long, was obtained using a closed loop temperature controller implemented with a Peltier and thermistor (figure 4).

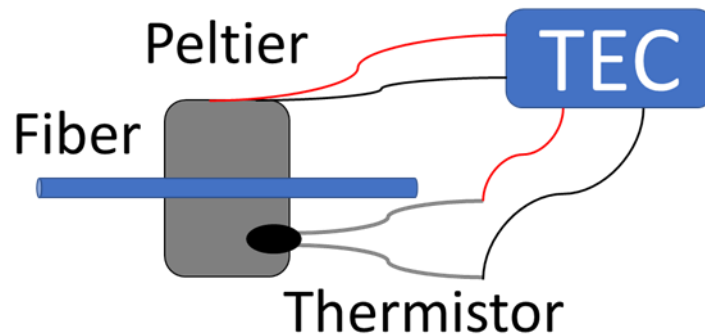
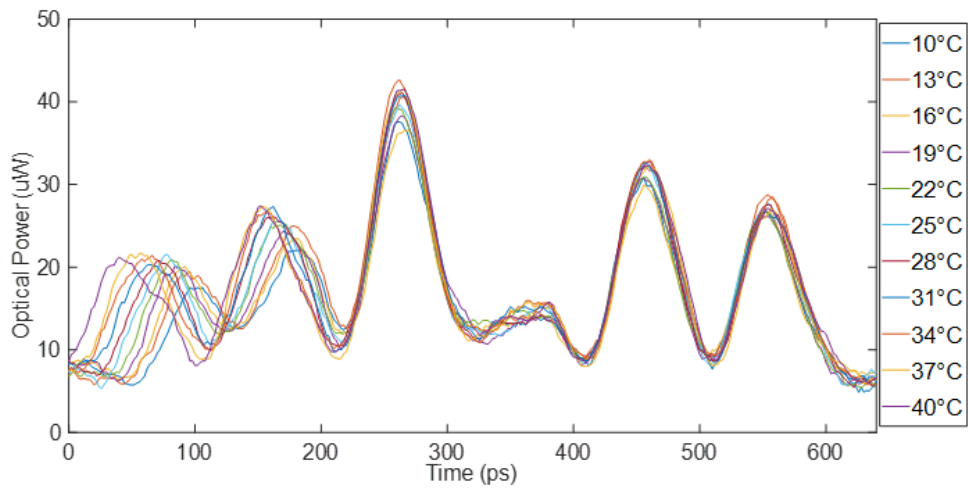
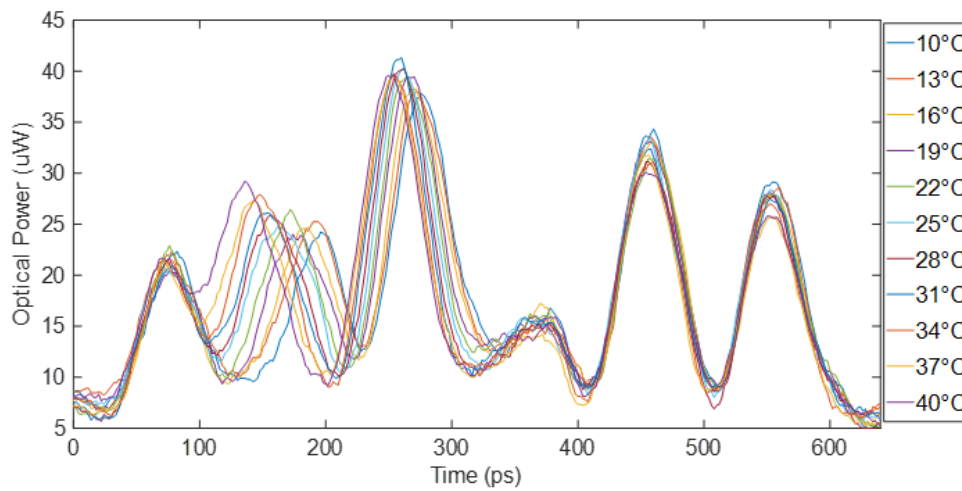


Figure 4. Scheme of the closed loop temperature system. A Peltier with a heatsink was used to set the temperature of the hot spot. The thermistor monitors the temperature. The temperature controller (TEC) provides the current to the Peltier according to the voltage signal of the thermistor.

The temperature was swept from 10°C to 40°C. The nominal shift of the FBGs in the array with temperature is 10 pm/°C. Multiplying this nominal wavelength shift by the dispersion introduced at the laser frequency, the expected dependence of the temporal shift with temperature is obtained 1.702 ps/°C. The hot point was moved along the grating array to interrogate two consecutive gratings (separated by about 1 cm) and verify the sub-cm spatial resolution achieved. Figure 5 shows the reflected spectrum of 6 weak gratings around the hot point when the temperature is swept from 10°C to 40°C in 3°C steps.



(a)



(b)

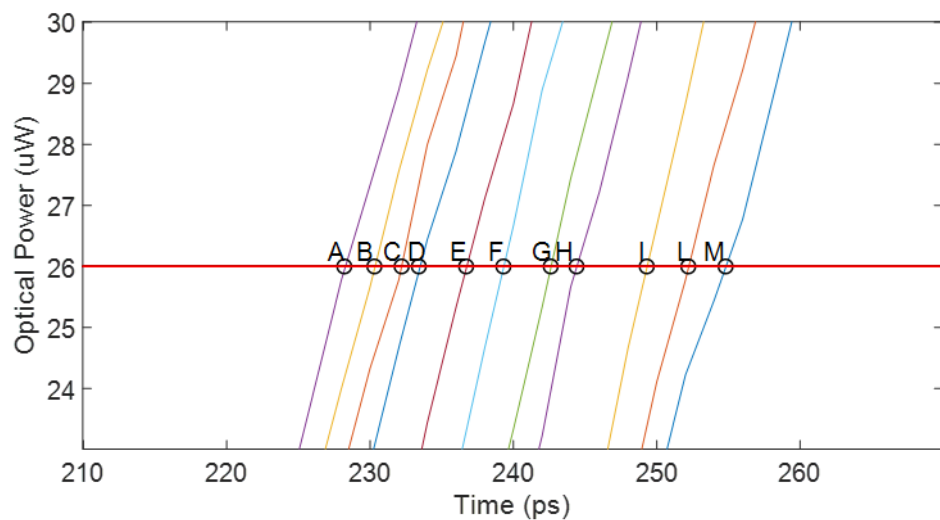
Figure 5. Reflected signal of the array portion under test. The two images show the heating of two points (first point showed in (a), second point showed in (b)) less than one centimeter apart. In both cases, the time shift is visible due to the temperature rising from 10°C to 40°C.

The interrogation pulse has a lower wavelength at the end of the pulse in the time domain. When the temperature is lowered the resonant wavelength of the gratings moves to a lower wavelength, producing a delay of the trace around the hot point.

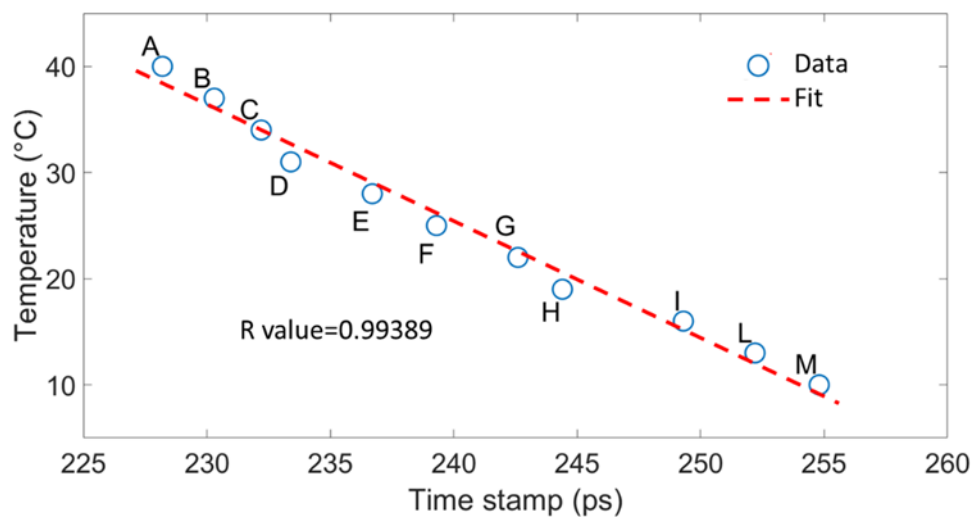
Figure 5 shows the traces of the reflected signal when the temperature sweep is applied at one point (figure 5a) and moved to another grating in the array (figure 5b). The resolution given by the pulse width allows the two cases to be clearly distinguished. This system could not only sense the temperature at the hot point but also the temperature gradient along it as a gradual reduction of the time shift when we moved away from the hot point.

A threshold was fixed to a certain optical power and the time stamp of consecutive traces was derived (figure 6a). The stamps were plotted in relation to the temperature of the hot zone: the results are shown in figure 6b, which shows how the absolute time stamps of the traces are linear with temperature ( $R=0.99389$ ).

The mean value and the standard deviation of the measured time shifts were  $1.9 \pm 0.3505$  ps, close to the expected value of 1.7 ps. The standard deviation is quite high due to the uncertainty of measuring the absolute temperature of the sample with an accuracy better than  $\pm 0.25^\circ\text{C}$  in our lab conditions.



(a)



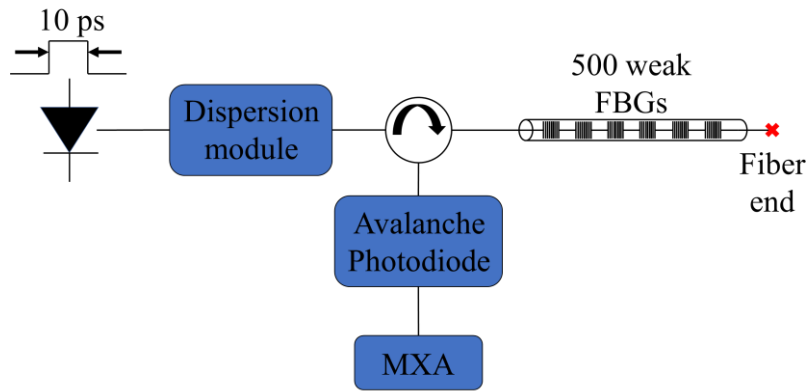
(b)

Figure 6. (a) Evaluation of the response of the sensor to temperature. (b) When the temperature was swept from 10 $^{\circ}\text{C}$  to 40 $^{\circ}\text{C}$  there was a linear relation between time stamps and temperature.

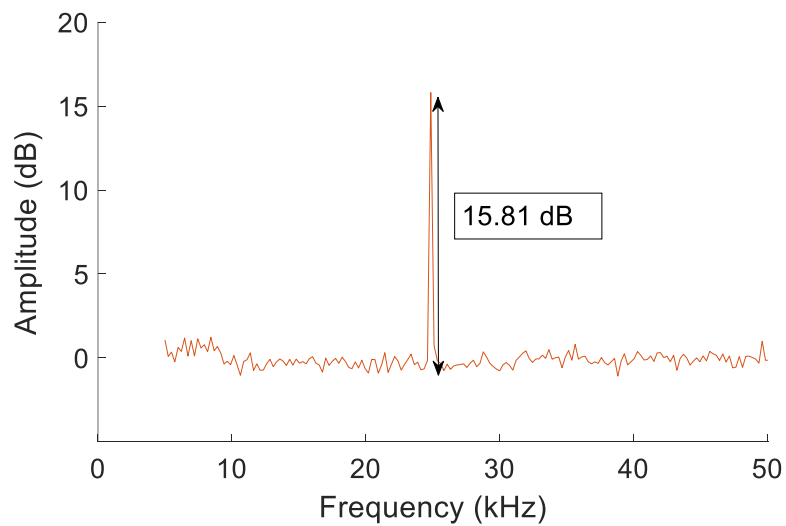


#### 4.4. Vibration measurement

As commented before, the speed of the interrogation system (the sum of the time needed to generate the optical pulse and the acquisition time of the reflected signal) limits the maximum frequency of a dynamic measurement. Since the only active element is the pulsed laser, and the dispersion is added to the interrogation pulse with a passive dispersive element (no active tuning of the laser wavelength is employed), the setup could potentially sense dynamic Bragg wavelength shift at high frequency. In order to test the maximum frequency achievable a vibration was applied to the FBGs of the array. The only modification in the setup is that the reflected signal is now fed to an avalanche photodiode (Thorlabs APD430), which can sense a dynamic change in the optical signal from DC to 400 MHz. The APD electric output is connected to an electric signal analyzer (MXA) (figure 7a). There is a trade-off in the choice of the spectrum width of the light source: a wide spectrum allows to have a high temperature range but lower the strain resolution for vibration sensing. For this reason, a wide light source with a non-flat spectrum was chosen (as it can be observed in figure 3, the amplitude distribution along the pulse has a triangular shape). This spectral feature allows having an amplitude modulation, that the APD can sense when a dynamic strain is applied. The reflected optical signal is constant until a dynamic strain is exerted on the fiber grating. A portion of the sensing element (approximately 5 centimeters) was glued to a piezoelectric (PZT). 10 volts were applied to the PZT, which correspond to a fiber strain of  $38 \mu\epsilon$ . The result of an applied vibration at 25 kHz is shown in figure 7b. The measurement was obtained using a resolution bandwidth of the electric spectrum analyzer of 51 Hz. At this frequency, the signal is 15.18dB over the noise level. An estimated strain resolution of  $6.16 \mu\epsilon$  is achieved at this frequency (if we consider the 30dB achieved at 155 kHz, for example, a resolution of  $1.2 \mu\epsilon$  is obtained). These differences are only given by the non-constant response of the PZT in frequency.



(a)



(b)

Figure 7. (a) Scheme of the interrogation system. (b) Recovered spectra of the photodetector electrical output when a vibration of 25 kHz is applied to the sensing element.

The frequency of the PZT was swept in steps of 10 kHz between 15 kHz and 245 kHz, even for these measurements the resolution bandwidth was of 51 Hz. Figure 8 shows the signal traces of the electrical spectrum

analyzer at different frequencies of the PZT, averaging 10 times. In the frequency range tested, the signal goes from 10 to 30 dB above the noise level, with an obtained resolution of  $1.2 \mu\epsilon$ . The resonances in the PZT response, over the wide frequency range, produce a non-constant response in the frequency domain. For frequency as 55 kHz and 105 kHz the signal is 10 dB, thus the resolution is degraded to  $12 \mu\epsilon$ .

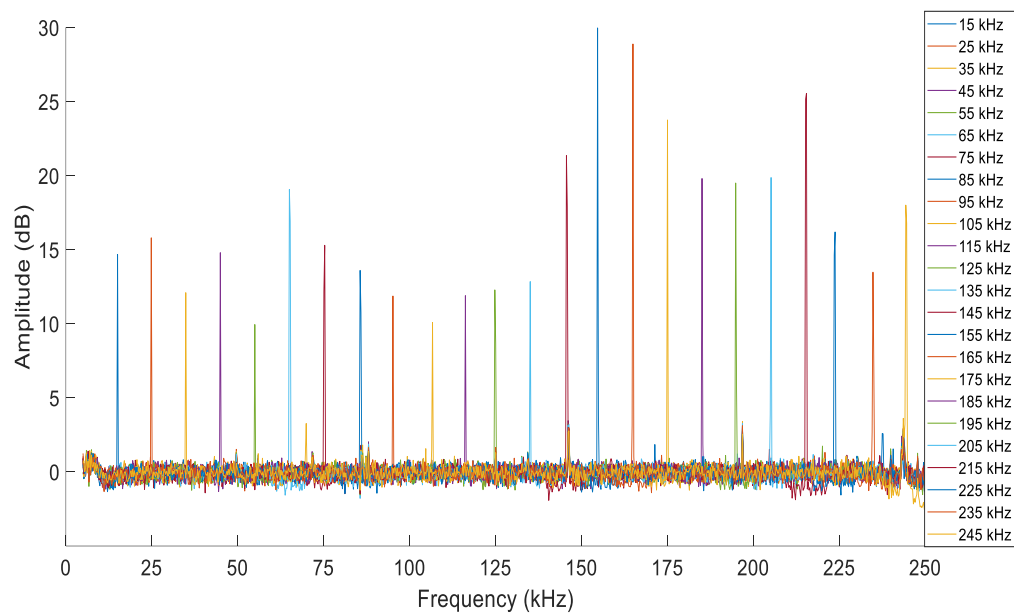


Figure 8. Frequency spectra of the photodetector electrical output when the frequency of the vibration is swept between 15 kHz and 245 kHz.

#### 4.5. Conclusions

A quasi-distributed sensing system of a 5 m long weak grating array was presented in this chapter, using a compact pulsed laser module without an external EOM. The dispersion added to the interrogation pulse can convert any Bragg wavelength shift inside the 500 weak grating arrays in a time shift. A long array of FBGs fabricated at the same wavelength could be interrogated independently. The weak gratings reflect part of the signal thus allowing to measure the temperature and vibration at the same time.

Simultaneous sensing of temperature and vibration could be performed separating, in the frequency domain, the low frequency temperature changes and the high frequency vibration signals. The sensitivity was limited to  $1^{\circ}\text{C}$  due to the maximum sampling rate (2 ps) of the oscilloscope, with a spatial resolution of 1 mm. Temperature sensitivity can be enhanced by applying a higher dispersion to the pulse and using a detection system with a higher sampling rate. Vibration sensing was performed on the same setup, a portion of the sensing element (approximately 5 centimeters) was glued to a PZT. 10 volts were applied to the PZT, which correspond to a fiber strain of  $38\ \mu\epsilon$ . Mechanical strains as low as  $1.2\ \mu\epsilon$ , changing in time to a frequency of 245 kHz exerted on a portion of the weak FBG array, were measured. There is a trade-off in the choice of the spectrum width of the light source: a wide spectrum allows to have a high temperature range but negatively affects the strain resolution for vibration sensing. We chose a wide light source with a non-flat spectrum, thus allowing to have an amplitude modulation when a dynamic strain is applied. The components used to implement the interrogation system for vibration, the pulsed laser module and the reflected signal photodetector are quite compact and allow the whole system to be implemented in a compact frame.

## References

- [1] Hill, Kenneth O., and Gerald Meltz. "Fiber Bragg grating technology fundamentals and overview." *Journal of lightwave technology* 15.8 (1997): 1263-1276.
- [2] Tosi, Daniele. "Review and analysis of peak tracking techniques for fiber Bragg grating sensors." *Sensors* 17.10 (2017): 2368.
- [3] Mihailov, Stephen J. "Fiber Bragg grating sensors for harsh environments." *Sensors* 12.2 (2012): 1898-1918.
- [4] Chan, Peter KC, et al. "Multiplexing of fiber Bragg grating sensors using a FMCW technique." *IEEE Photonics Technology Letters* 11.11 (1999): 1470-1472.
- [5] Morey, William W., James R. Dunphy, and Gerald Meltz. "Multiplexing fiber Bragg grating sensors." *Fiber & Integrated Optics* 10.4 (1991): 351-360.
- [6] Koo, K. P., and A. D. Kersey. "Bragg grating-based laser sensors systems with interferometric interrogation and wavelength division multiplexing." *Journal of Lightwave Technology* 13.7 (1995): 1243-1249.
- [7] Wada, Atsushi, Satoshi Tanaka, and Nobuaki Takahashi. "Partial scanning frequency division multiplexing for interrogation of low-reflective fiber Bragg grating-based sensor array." *Optical Review* 25.5 (2018): 615-624.
- [8] Hervás, Javier, et al. "An interrogation technique of FBG cascade sensors using wavelength to radio-frequency delay mapping." *Journal of Lightwave Technology* 33.11 (2015): 2222-2227.
- [9] Froggatt, Mark. "High density strain sensing using optical frequency domain reflectometry." *Fourteenth International Conference on Optical Fiber Sensors*. Vol. 4185. International Society for Optics and Photonics, 2000.
- [10] Ou, Yiwen, et al. "Large-capacity multiplexing of near-identical weak fiber Bragg gratings using frequency-shifted interferometry." *Optics express* 23.24 (2015): 31484-31495.
- [11] Ou, Yiwen, et al. "Synchronous Reflectivity Measurement of a Weak Fiber Bragg Grating Array Using Frequency-Shifted Interferometry." *IEEE Photonics Journal* 10.2 (2017): 1-9.
- [12] Zhou, Ciming, et al. "Demodulation of a hydroacoustic sensor array of fiber interferometers based on ultra-weak fiber Bragg grating reflectors using a self-referencing signal." *Journal of Lightwave Technology* 37.11 (2018): 2568-2576.
- [13] Ou, Yiwen, et al. "Large WDM FBG sensor network based on frequency-shifted interferometry." *IEEE Photonics Technology Letters* 29.6 (2017): 535-538.
- [14] Bui, Quoc Hung, et al. "Simultaneous multi-point measurement of strain and temperature utilizing Fabry-Perot interferometric sensors composed of low reflective fiber Bragg gratings in a polarization-maintaining fiber." *Optics Express* 28.9 (2020): 13104-13115.

- [15] Liu, Sheng, Xinying Han, and Hongqiao Wen. "Distributed acoustic sensing system using an identical weak fiber Bragg grating array." *Optical Measurement Technology and Instrumentation*. Vol. 10155. International Society for Optics and Photonics, 2016.
- [16] Hervás, Javier, et al. "Microwave Photonics filtering interrogation technique under coherent regime for hot spot detection on a weak FBGs array." *Journal of Lightwave Technology* 36.4 (2018): 1039-1045.
- [17] Ricchiuti, Amelia L., Javier Hervás, and Salvador Sales. "Cascade FBGs distributed sensors interrogation using microwave photonics filtering techniques." *Optics & Laser Technology* 77 (2016): 144-150.
- [18] Liang, Xiao, et al. "Precision dynamic sensing with ultra-weak fiber bragg grating arrays by wavelength to frequency transform." *Journal of Lightwave Technology* 37.14 (2019): 3526-3531.
- [19] Luo, Zhihui, et al. "A time-and wavelength-division multiplexing sensor network with ultra-weak fiber Bragg gratings." *Optics Express* 21.19 (2013): 22799-22807.
- [20] Zhao, Xin, et al. "Dynamic quasi-distributed ultra-weak fiber Bragg grating array sensing enabled by depth-resolved dual-comb spectroscopy." *IEEE Transactions on Instrumentation and Measurement* (2019).
- [21] Pastor-Graells, Juan, et al. "Single-shot distributed temperature and strain tracking using direct detection phase-sensitive OTDR with chirped pulses." *Optics express* 24.12 (2016): 13121-13133.
- [22] Koyamada, Yahei, et al. "Fiber-optic distributed strain and temperature sensing with very high measurand resolution over long range using coherent OTDR." *Journal of Lightwave Technology* 27.9 (2009): 1142-1146.
- [23] Pan, Zhengqing, et al. "Phase-sensitive OTDR system based on digital coherent detection." *Asia Communications and Photonics Conference and Exhibition. Optical Society of America*, 2011.
- [24] Soto, Marcelo A., et al. "Distributed phase birefringence measurements based on polarization correlation in phase-sensitive optical time-domain reflectometers." *Optics Express* 23.19 (2015): 24923-24936.
- [25] Lu, Xin, Marcelo A. Soto, and Luc Thévenaz. "Temperature-strain discrimination in distributed optical fiber sensing using phase-sensitive optical time-domain reflectometry." *Optics Express* 25.14 (2017): 16059-16071.
- [26] "UltimaTM DTS", Silixa Ltd, <https://silixa.com/wp-content/uploads/DTS-datasheet-2018.pdf>
- [27] "iDASTM", Silixa Ltd, <https://silixa.com/wp-content/uploads/iDAS-datasheet-2018-03122018.pdf>
- [28] Eickhoff, Wf, and Rf Ulrich. "Optical frequency domain reflectometry in single-mode fiber." *Applied Physics Letters* 39.9 (1981): 693-695.

- [29] Wang, Shuai, et al. "Distributed fiber-optic vibration sensing based on phase extraction from time-gated digital OFDR." *Optics Express* 23.26 (2015): 33301-33309.
- [30] Chen, Dian, Qingwen Liu, and Zuyuan He. "Phase-detection distributed fiber-optic vibration sensor without fading-noise based on time-gated digital OFDR." *Optics express* 25.7 (2017): 8315-8325.
- [31] Li, Jiong, et al. "High spatial resolution distributed fiber strain sensor based on phase-OFDR." *Optics Express* 25.22 (2017): 27913-27922.
- [32] Li, He, et al. "High-spatial-resolution fiber-optic distributed acoustic sensor based on  $\Phi$ -OFDR with enhanced crosstalk suppression." *Optics Letters* 45.2 (2020): 563-566.
- [33] "OBRTM 4600", Luna Technology, <https://lunainc.com/wp-content/uploads/2012/11/LUNA-Data-Sheet-OBR-4600-V2.pdf>
- [34] Zhu, Fan, et al. "Improved  $\Phi$ -OTDR sensing system for high-precision dynamic strain measurement based on ultra-weak fiber Bragg grating array." *Journal of Lightwave Technology* 33.23 (2015): 4775-4780.
- [35] Clement, Juan, et al. "Interrogation of a sensor array of identical weak FBGs using dispersive incoherent OFDR." *IEEE Photonics Technology Letters* 28.10 (2016): 1154-1156.
- [36] Thévenaz, Luc, et al. "Novel technique for distributed fibre sensing based on faint long gratings (FLOGs)." *23rd International Conference on Optical Fibre Sensors*. Vol. 9157. International Society for Optics and Photonics, 2014.
- [37] Sancho, Juan, et al. "Time-frequency analysis of long fiber Bragg gratings with low reflectivity." *Optics express* 21.6 (2013): 7171-7179.
- [38] Rothhardt, Manfred, et al. "Fabrication and applications of draw tower gratings." *Bragg Gratings, Photosensitivity, and Poling in Glass Waveguides*. Optical Society of America, 2016.
- [39] Westbrook, Paul S., et al. "Continuous multicore optical fiber grating arrays for distributed sensing applications." *Journal of Lightwave Technology* 35.6 (2017): 1248-1252.
- [40] Westbrook, Paul S., et al. "Improving distributed sensing with continuous gratings in single and multi-core fibers." *Optical Fiber Communication Conference*. Optical Society of America, 2018.
- [41] Nonaka, Koji, et al. "Low-time-jitter short-pulse generator using compact gain-switching laser diode module with optical feedback fiber line." *Japanese Journal of Applied Physics* 47.8S1 (2008): 6754.
- [42] Cusano, A., et al. "Dynamic strain measurements by fibre Bragg grating sensor." *Sensors and Actuators A: Physical* 110.1-3 (2004): 276-281.
- [43] Takahashi, Nobuaki, Kazuto Yoshimura, and Sumio Takahashi. "Fiber Bragg grating vibration sensor using incoherent light." *Japanese Journal of Applied Physics* 40.5S (2001): 3632.

- [44] Chang, Jun, et al. "Interrogation a fiber Bragg grating vibration sensor by narrow line width light." *2008 1st Asia-Pacific Optical Fiber Sensors Conference*. IEEE, 2008.
- [45] Tsuda, Hiroshi. "Fiber Bragg grating vibration-sensing system, insensitive to Bragg wavelength and employing fiber ring laser." *Optics letters* 35.14 (2010): 2349-2351.
- [46] Lau, K. Y. "Gain switching of semiconductor injection lasers." *Applied Physics Letters* 52.4 (1988): 257-259.
- [47] Coppinger, F., A. S. Bhushan, and B. Jalali. "Photonic time stretch and its application to analog-to-digital conversion." *IEEE Transactions on microwave theory and techniques* 47.7 (1999): 1309-1314.
- [48] Han, Yan, and Bahram Jalali. "Photonic time-stretched analog-to-digital converter: Fundamental concepts and practical considerations." *Journal of Lightwave Technology* 21.12 (2003): 3085.
- [49] Han, Yan, and Bahram Jalali. "Differential photonic time-stretch analog-to-digital converter." *Conference on Lasers and Electro-Optics*. Optical Society of America, 2003.
- [50] Fuster, J. M., et al. "Single-sideband modulation in photonic time-stretch analogue-to-digital conversion." *Electronics Letters* 37.1 (2001): 67-68.
- [51] Chi, Hao, et al. "Microwave spectrum sensing based on photonic time stretch and compressive sampling." *Optics letters* 38.2 (2013): 136-138.





# Chapter 5

## The role of laser coherence length in microwave photonics fiber sensing

**M**icrowave Photonics (MWP) is an established technology with a wide range of applications such as radio-over-fiber (ROF), optical beam forming, generation of time-delay line, signal processing in microwave, millimeter-wave, and radio frequency (RF) domain. One of the most recent applications of MWP is fiber sensing. MWP offers new solutions for fiber sensing that are intrinsically robust against environmental changes, stable and with good repeatable performance. MWP schemes are also potentially low cost as they are based on low bandwidth RF [1]. However, the phase noise directly affects the amplitude signal retrieved by applying the inverse fast Fourier transform (IFFT) at the frequency response measured using MWP interrogation system. We have studied the performance of MWP schemes with the laser source linewidth interrogating an array of fiber Bragg gratings (FBGs) with an MWP interrogation system under coherent and incoherent regimes [2-3]. First, an insight into the technology and the main application is presented in the chapter. Then, a mathematical model is introduced to explain the conversion of the laser phase noise to amplitude noise. Finally, an experimental work was carried out to measure the influence of phase noise, depending on the relation between coherence length and reflectors spacing (in this case FBGs). Since the amplitude information is used to estimate the change in temperature or strain, the phase noise will affect the minimum detectable strain/temperature.

## 5.1. Microwave photonics

Microwave photonics is a research and technology field based on the interaction of micro and millimeter wave with optic waveguides photonics. In the last decade, this field has attracted a lot of interest and offered new solutions in numerous fields of application. Radio-over-fiber (ROF) is an example of how the introduction of MWP solutions significantly improves the performance: the transport of modulated signal using optical fibers is the best solution for the lossless transfer of signal from a central office to a remote antenna site. MWP have become a leading technology thanks to the improvement in the field of optoelectronic and optical modulation. MWP communication systems offer covering for cellular and WLAN applications from 800 to 2500 MHz, the possibilities to implement stems with multiple antennas [4] and application for 5G up to tens of GHz [5-6]. Optical beam forming can be also be improved using solutions in the microwave domain. From the point of view of the signal transport devices, optical fibers offer a lighter and lower loss solution compared to coaxial cables. For the generation of time-delay lines, needed for this application, chirped and non-chirped FBGs can be used [6-10]. Using chirped FBG it is possible to tune continuously the delay and reconfigure the beam. Another important application of MWP is signal processing in microwave, millimeter-wave and RF domain. The idea is to move part of the entire signal processing from the electronic to the photonic domain, since it allows to implement, for example, reconfigurable and tunable microwave filters [11]. In general, optical signal processing allows working with high bandwidth relaxing the system design. The complexity is transferred from the electronic signal processing to the modulation and detection of optical signal, a field that was greatly improved in the last decade: the use of external cavities and locking technique allows the modulation at tens of GHz [12-15] together with photodetection with high bandwidth [16-18]. Figure 1 shows a schematic of a RF signal processing using MWP, the blue lines

represent the optical signal while the black ones represent the electrical signal.

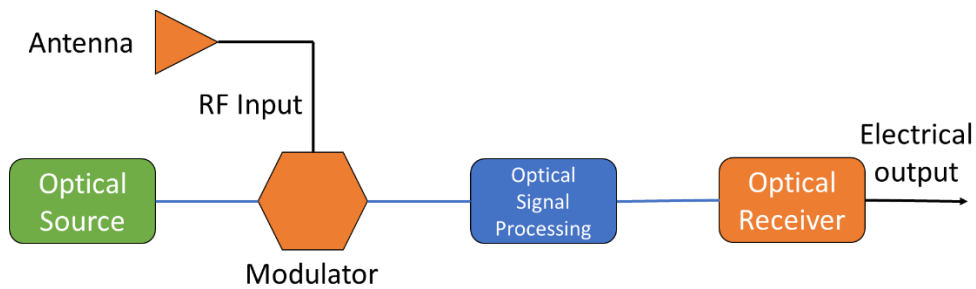


Figure 1. Schematic representation of an MWP system for RF signal processing. The optical signal is represented in blue, while the electrical signal is represented with black lines.

Examples of the advantages of such an RF processing scheme are the results achieved in analog-to-digital conversion. Photonic time-stretch [20-24] enhances the conversion speed of an ADC using a MWP processing: the optical source is a chirped optical pulse, the RF input is the signal that must be converted, the processing consists in a “time-stretched” of the modulated signal using a dispersive element. The stretched signal can be now converted to electrical and to digital, using an ADC with a sampling rate that is  $M$  times lower than the one needed to directly convert to digital the RF input, with  $M$  a factor proportional to the dispersion introduced in the optical processing [25]. MWP was recently applied to the fiber sensing field to implement a novel interrogation system for reflectors and FBGs array.

## **5.2.MWP in optical fiber sensing**

In the last years, MWP have been adopted for sensing applications [1]. Stable and repetitive interrogation systems have been developed for punctual and distributed sensing, implemented with cost-effective components compared to other well established fiber sensing techniques: OTDR in the standard and phase-sensitive implementation required the generation of

ultra-short optical pulses; in OFDR a stable tunable laser is needed, to sweep the wavelength during the measurement. It was demonstrated that MWP allow implementing stable interferometers that can be used for sensing. The concept and implementation of an MWP based interrogation setup for a sensor is shown in figure 2.

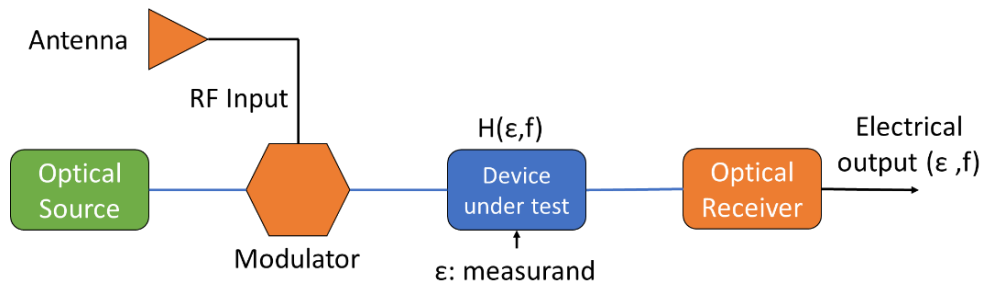


Figure 2. Schematic representation of a generic MWP setup used for sensing.

The concept is the same as for the MWP filters (figure 1), but with a different aim. The signal processing block is substituted with a sensitive element, referred to as device under test (DUT) in figure 2. If the optical properties (e.g. refractive index) characteristics of the DUT are affected by a measurand ( $\epsilon$ ), the electrical output is a function of  $\epsilon$ . MWP filter is designed to obtain a certain pulse response to process the RF input and. Whereas for sensing the RF input and electrical output are compared to retrieve the characteristic of the DUT that acts as a photonic filter. If a relation between the DUT photonic response and the  $\epsilon$  exists, it is possible to retrieve a relation between the electrical output and the measurand and implement a sensor for  $\epsilon$ . The implementation of a generic MWP filter is shown in figure 3.

The signal of a continuous-wave light source (LS) is modulated with an electro-optical modulator (EOM) and split in a number  $n$  of branches, named taps. The signal is weighted by a factor  $\alpha_i$  and delayed a time  $\tau_i$  (being  $i$  the tap number), and then recombined and fed to a photodetector. The response  $H(f)$  can be tuned by changing the number of branches, the values of  $\alpha$  and  $\tau$ , to obtain the wanted MWP filter response. Analogies

can be found between an MWP filter and an array of FBGs interrogated with the setup shown in figure 4. Every FBG of the array can be considered as a single tap of a filter with a  $\alpha$  factor that depends on the grating reflectivity and the  $\tau$  that is the delay of the light reflected by gratings at different locations in the optical fiber [3].

In order to obtain the transfer function of the filter made with an array of FBGs an electric vector network analyzer (EVNA) is used that modulates the input light through port 1 and measure the response of the photodetector (PD) through port 2. Measuring the  $S_{21}$  it is possible to obtain the frequency filter response,  $H(f)$ , which contains information about the Bragg wavelength. This information can be retrieved observing  $H(f)$  in the frequency domain or the time domain response, derived applying the inverse Fourier transform [26].

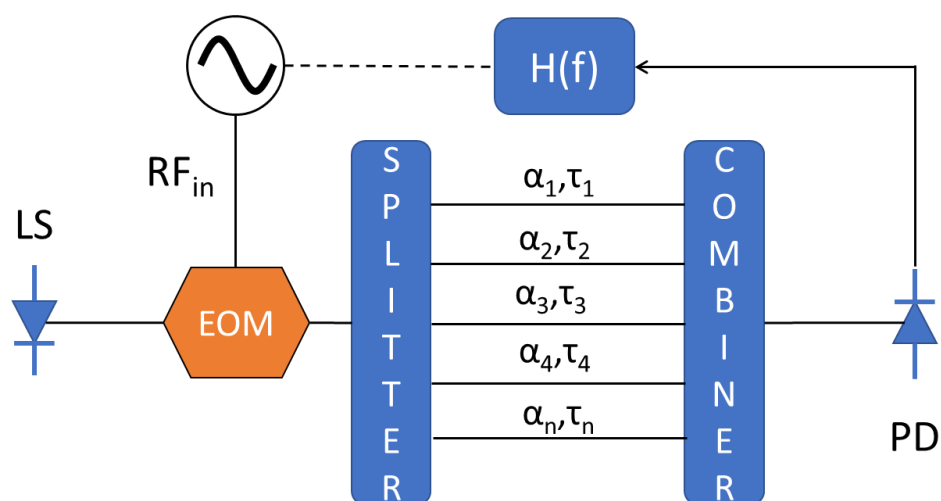


Figure 3. Implementation of a generic MWP filter with  $n$  taps. LS: light source; PD: photodetector; EOM: electro-optical modulator;  $\alpha_n$ : weight of the  $n$ th tap;  $\tau_n$ : delay of the  $n$ th tap;  $H(f)$ : frequency response.

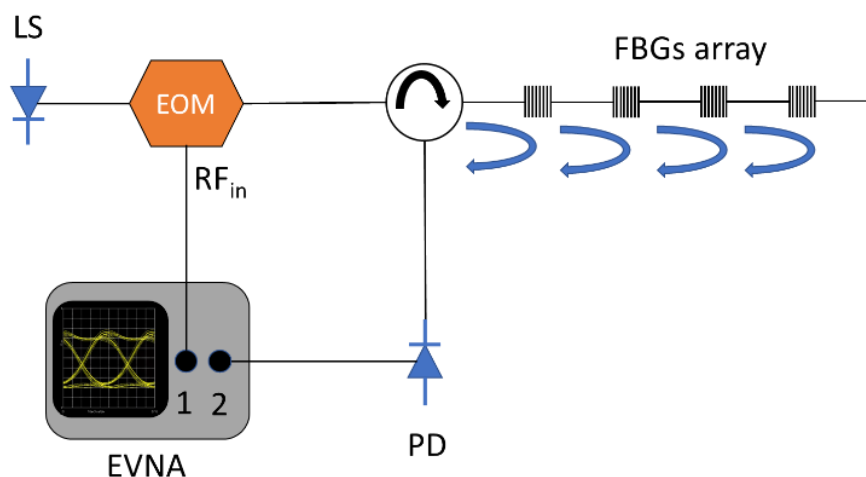


Figure 4. A generic scheme of an MWP based interrogation system for an array of FBGs. LS: light source; PD: photodetector; EOM: electro-optical modulator; EVNA: electric vector network analyzer.

### 5.2.1. Light source linewidth and coherence regime

In general, MWP systems work under incoherent regime since it ensures a stable operation less sensitive to environmental fluctuation [4]. On the other hand, the sensitivity to environmental factors, under coherent regime, is not a constrain for sensing application.

The temperature monitoring of a 500 weak FBGs array using MWP, under incoherent and coherent regime are reported in [3] and [2] respectively. Under incoherent regime, the temperature information of a hot spot is retrieved from filtering the optical source with a bandpass filter and observing the frequency response. The response of the MWP filter depends on the number of taps. The central wavelength of the band-pass filter is swept. This changes the number of minima between two consecutive maxima in the MWP response. Observing the response and the central wavelength of the band-pass filter it is possible to estimate the temperature change between the hot spot and the reference (the portion of the array/long grating not affected by the temperature change) (figure 4).

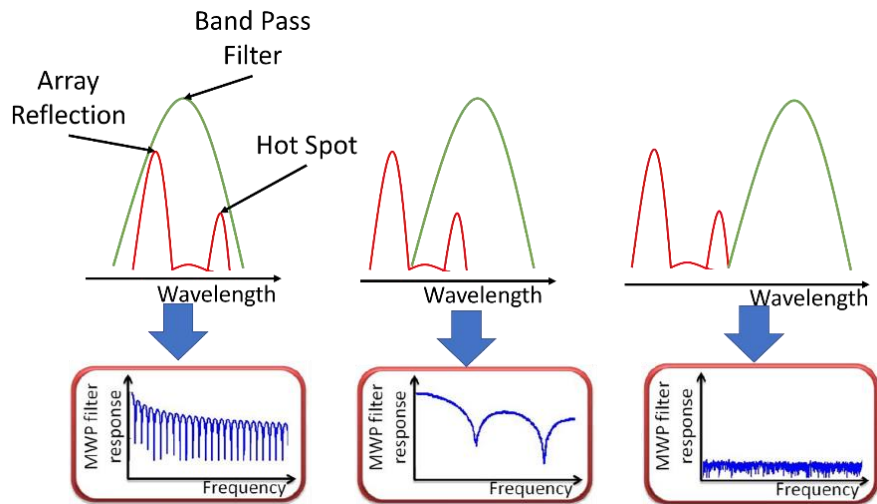


Figure 5. Principle of operation of the interrogation system presented in [3]. Tuning the filter of the light source it is possible to retrieve information about the hot spot in a long FBG.

The accuracy of this method is limited by the fact that the hotspot has to “move” out from the reflection spectra of the whole FBGs array in the wavelength domain, to observe a change in the frequency response, so only significant temperature changes can be sensed. The coherence interrogation of the same array presented in [2], propose a different operation principle to overcome this limitation. The use of a narrow light source permits to convert the Bragg shift of the FBGs of a long array in an amplitude change in the time domain. In this case, no information can be retrieved from the direct observation of the frequency response that has a noisy-like shape. Applying the inverse Fourier transform is possible to retrieve the impulse response in the time domain. It is demonstrated that processing the time-response it is possible to perform distributed sensing of temperature with a sensitivity of  $0.6 \text{ dB}/^\circ\text{C}$ , and a spatial resolution depending on the bandwidth of the EVNA used to perform the measurement.

Phase sensitivity has been investigated in the fiber sensing field: phase sensitive OTDR systems perform distributed sensing over kilometers of fiber with sensitivity down to  $\text{mK}/\text{n}\epsilon$ , in terms of temperature and strain



[27-29]. In OFDR three different regimes are reported in literature: coherent (C-OFDR), incoherent (I-OFDR), low coherent (LC-OFDR). C-OFDR offers a better spatial resolution and higher sensitivity compared to I-OFDR, but a spatial range limited to the coherence length of the light source [30]. LC-OFDR demonstrates that it is possible to maintain the coherent advantages and monitor a length of fiber larger than the coherence length of the source [31].

The coherence regime depends on the relation between the linewidth of the optical source and the  $\tau_i$  of the filter taps considering the generic filter in figure 3 or the distance between the FBGs in figure 4. In [32] it is demonstrated that the coherence length acts as a time-gate and can be used to implement distributed sensing using MWP. An extensive mathematical derivation of the temporal impulse response of a fiber with N reflectors is presented in [32]; the following equation is reported for the amplitude of a pulse in the time domain response:

$$I_n(z_i) = k * [R_i^2 + \sum_{J=1, J \neq i}^N R_i R_j e^{-n|z_i - z_j|/L_c} * \frac{\cos \bar{\omega} n (z_i - z_j)}{c}] \quad (1)$$

With  $z_i$  the travel distance of the light traveling from the EOM to the photodetector, that is reflected by the  $i$ th reflector;  $L_c$  the coherence length of the Lorentzian shaped light source,  $R$  the reflectivity,  $\bar{\omega}$  the central wavelength of the light source,  $n$  the refractive index of the fiber and  $c$  the speed of light. The second term, with the summation, takes into account the interferometers formed by the N reflectors, summed to the amplitude given by the  $i$ th reflectors itself (first term  $R_i^2$ ). It is directly proportional to the exponential to the power of the optical path distance (OPD) between reflectors  $i$ th and  $j$ th ( $n|z_i - z_j|$ ) divided by  $L_c$ . This means that for the incoherent case ( $n|z_i - z_j| > L_c$ ) the impulse response amplitude depends only on the contribution of the  $i$ th reflector, while in the coherent case it depends as well on the contribution of the M reflectors inside the coherence length “gate”, for which  $n|z_i - z_j| < L_c$ . The two extreme regimes were investigated

until now: coherent and incoherent regimes. The influence of the light source linewidth and different reflector spacing under coherent regime are investigated. For this purpose, two arrays of weak gratings were fabricated and interrogated using the MWP setup in the figure. The light source is a tunable laser with coherence control that permits to change the linewidth of the laser.

Under coherent regime, a term should be added to equation (1), to represent the instantaneous signal phase [28]:

$$I_n(z_i, t) = k * \{R_i^2 + \sum_{j=1, j \neq i}^N R_i R_j e^{-n|z_i - z_j|/L_c} * \frac{\cos[\bar{\omega}n(z_i - z_j) + \overline{\phi(t)}]}{c}\} \quad (2)$$

The term  $\phi(t)$  take into account the effect of the light phase, changing in time due to phase noise, in the interferometer between the  $i$ th and  $j$ th reflectors.  $\overline{\phi(t)}$  is the average of the instantaneous phase change. Every point in the frequency response, retrieved with the EVNA, will be affected by phase fluctuation. Calculating the IFFT of the entire frequency response, the contribution of the phase fluctuation is averaged over the number of points of the response. The term  $e^{-n|z_i - z_j|/L_c}$  determines how much these fluctuations affect in terms of time response amplitude. The complete formula that takes into account a limited radio frequency bandwidth  $\Omega_b$  and a central frequency  $\Omega_c$  of the frequency sweep of the EVNA is [30]:

$$F(t_z, t) = \sum_{i=1}^N \Omega_b \text{sinc}[\Omega_b(t_z - \frac{nz_i}{c})] e^{-j\Omega_c(t_z - \frac{nz_i}{c})} I_N(z_i, t) \quad (3)$$

Now that the mathematical model has been determined, the fabrication of the array, the experimental setup and results are presented.

### 5.2.2. Fiber Bragg gratings array fabrication

The gratings arrays were fabricated using the setup of the research group. The fabrication setup consists of:

- A continuous-wave frequency-doubled Argon-ion laser with a peak wavelength of 244 nm and a maximum power of 100 mW. A system of mirror and lenses deviate and focus the laser beam in the fiber core area.
- A phase mask is used to create the interference pattern to inscribe a periodical grating in the fiber core.
- The optical fiber is fixed to two 3D translation stage to place the optical core in the right position. The fiber needs to be aligned and at a minimum distance from the phase mask.
- A core tracking system to maximize the irradiation power in the core of the optical fiber. The system deflects the laser beam moving a piezoelectric with a mirror. The other part of the system is implemented with a photodetector for the 400 nm photoluminescence generated by the UV radiation of the fiber core [33]. The piezoelectric moves the laser beam depending on the power of the radiation produced (figure 6).

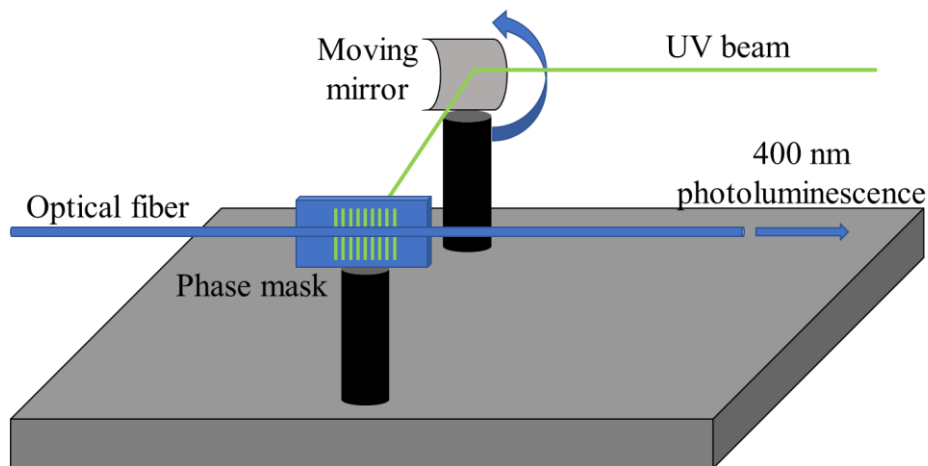


Figure 6. Schematic of the core tracking system. The 400 nm photoluminescence, generated by the UV irradiation, is sensed on one end of the optical fiber during the fabrication. The moving mirror deflects the laser beam to maximize the irradiation.

### **5.3. Coherence length influence on amplitude noise**

Phase noise in semiconductor laser is modeled as the result of three contributions: white, flicker and random walk noise [34-35]. In spectroscopy phase noise has been exploited to investigate a medium without the laser frequency is neither scanned nor modulated [36]. In this case, the power fluctuation due to phase noise is an exploitable phenomenon; a model studying the conversion of laser phase noise to amplitude noise in an optically thick vapor was reported in [37-38]. On the other hand, phase noise normally limited the performance of optical systems in communication and fiber sensing fields. Noise output in an interferometer can limit the sensitivity of a sensor system. Phase noise in interferometric systems was characterized in 1981 for different laser [39], the minimum detectable phase change (that is directly related to the sensitivity of the system) is measured for various interferometer configurations to demonstrate that the effect of phase noise may be reduced, properly choosing the interferometer scheme and design. Distributed fiber sensing systems are affected by phase noise [39-40]. Phase noise cancellation, when possible, improves the performance of fiber-based sensor increasing signal-to-noise ratio of tens of dB [41].

#### **5.3.1. Measurement of amplitude noise**

The study of the effect of phase noise in MWP sensing application could help to improve the performance and help to find out the optimal design of the sensing system, for example with the employment of the proper optical light. For this purpose, two arrays of weak FBGs were fabricated, each consisting of four gratings equally spaced of 20 and 150 centimeters. A typical spectrum in reflection and transmission of an FBG of the arrays is shown in figure 7.

The laser used in the setup has a coherence control. This feature is normally used to eliminate the parasitic interferometers in the optical setup. The whole setup is the one shown in figure 4. The EVNA modulate the light coming from the laser, in a range of frequency of 15 GHz. The EVNA

compared the output current from port 1 with the incoming current at port 2 and retrieve phase and module of the scattering parameter  $S_{21}$ . As in [2] the IFFT was applied to the frequency response measured, to retrieve the time impulse response. In figure 8 are reported the response in the time domain of the two FBGs arrays. Ten measurements were performed to characterize the amplitude change. The peaks amplitude in the time domain, between consequent measurements, changes depending on the coherence of the light source, with a magnitude proportional to the exponential term of equation (2).

As previously discussed, the minimum detectable phase shift (and so the amplitude, due to the phase to amplitude conversion) is limited by the fluctuations due to phase noise [36]. This determines the number of averaging needed to reduce the measurement error under a certain value, and so the speed of interrogation of the sensor. The variance of the peak amplitude was computed for four different configurations: the two arrays were interrogated using the same laser with and without the coherence control, thus permitting to set the linewidth of the laser to 100 MHz (coherence length  $\approx 60$  cm) or 500 kHz (coherence length  $\approx 120$  meters) (Table 1).

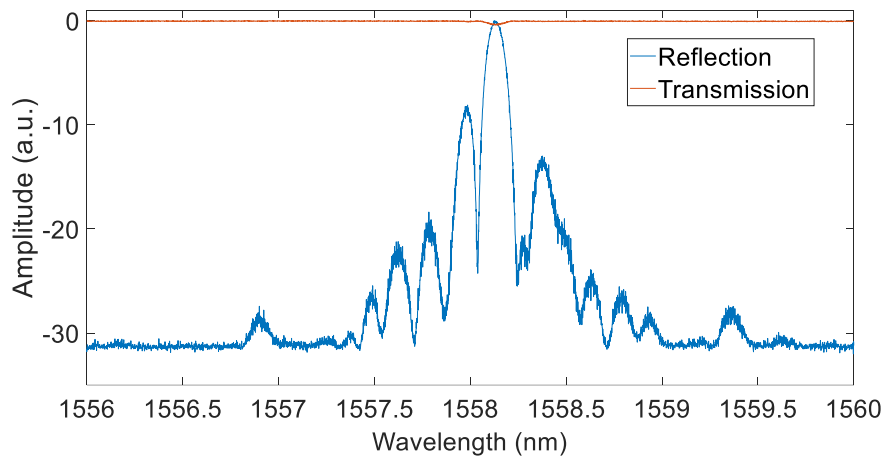


Figure 7. Spectra of a single FBG of the array. The transmitted power drop of 0.5 dB at the Bragg wavelength.

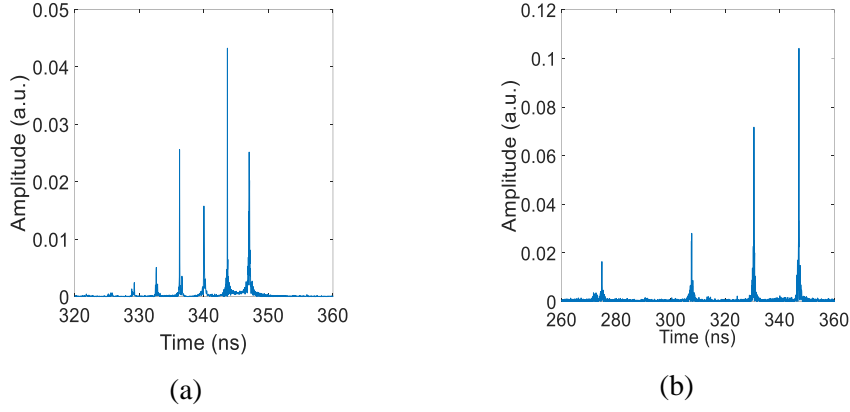


Figure 8. The time domain impulse response retrieved applying the IFFT to the frequency signal measured with the EVNA. In (a) is shown the response of the array with the FBGs spaced of 20 cm, in (b) the response of the array with 150 cm spacing.

Table 1. List of the configuration of FBGs spacing and coherence length for the four measurements

Coherence length (m) Grating spacing (m)	120	0.6
	1.5	Meas. 1
0.2	Meas. 3	Meas. 4

The variance was calculated following the formula:

$$\sigma_I^2 = \sum_{m=1}^M [I_m(z_i, t_m) - \overline{I(z_i, t)}]^2 \quad (5)$$

With  $m$  being the number of measurements of a total of  $M$  measurements performed;  $\overline{I(z_i, t)}$  is the average of  $I_n(z_i, t)$  over different acquisitions. In table 2 are reported the maximum variance for the four configurations. In figure 9 are shown the  $\overline{I(z_i, t)}$  as a blue line and the peak amplitudes of the ten measurements as red circles. As expected, the closer we are to an incoherent state the smaller are the fluctuations, since the fast phase

changes of the incoherent source are averaged out during the frequency sweep of the EVNA.

Table 2. Maximum variance of the peak amplitude for the four configurations

Coherence length (m) Grating spacing (m)	120	0.6
	1.5	$6.29 \cdot 10^{-4}$
0.2	$9.44 \cdot 10^{-4}$	$3.94 \cdot 10^{-4}$

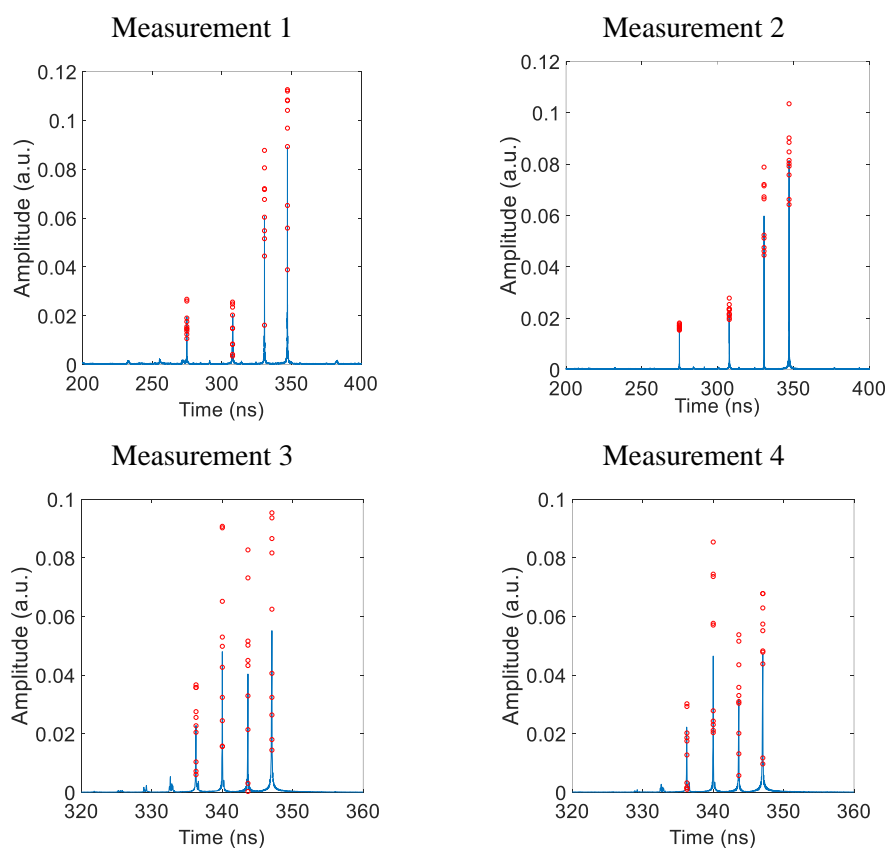


Figure 9. Time average (blue line) and peak amplitudes (red circles) for the 10 measurements performed in the four configurations listed in table 1

The fluctuations are amplitude dependent as described in equation (2). For a distributed system as the one described in [2], the envelope of multiple reflections is considered, and the envelope average change is taken into account to estimate a temperature change. In this case, the choice of the light source will not impact greatly the performance of the sensor while for a punctual sensor it can improve of a factor 10 the minimum amplitude variation detectable. These fluctuations are typical for coherent operation but can be contained by broadening the light source and still maintaining the advantages of working with MWP interrogation under coherent regime.

#### **5.4. Conclusions**

The advantages of MWP technique for sensing applications were presented in this section, a first employment of this technique as an alternative implementation of a C-OFDR has been reported in [2]. The role of laser linewidth, and more in general of the coherence regime the system can operate under, was discussed and a mathematical model was adopted to understand the phenomena and how the setup parameters influence the coherence regime. The fluctuations in the time domain pulse response were studied, to demonstrate how the linewidth of the laser influence the minimum detectable amplitude change, and the role of phase to intensity noise conversion. In the interrogation of a long weak FBGs array, the linewidth of the laser is not so relevant as for a punctual fiber sensor. In the first case, the envelope of multiple reflections is considered to estimate a temperature change, while in the second case the choice of the light source linewidth affected, up to a factor 10, the minimum amplitude variation detectable, due to the phase noise convert to amplitude noise. This is due to the instant phase of the light in time and the coherent beating of the light signal reflected by the FBGs. A correct choice of the light source improves the performance of MWP interrogation system for fiber sensing, that already demonstrates to have performance comparable to well established sensing system with a more stable configuration and potentially implemented with low bandwidth RF components.



## References

- [1] Hervás, Javier, et al. "Microwave photonics for optical sensors." *IEEE Journal of Selected Topics in Quantum Electronics* 23.2 (2017): 327-339.
- [2] Hervás, Javier, et al. "Microwave Photonics filtering interrogation technique under coherent regime for hot spot detection on a weak FBGs array." *Journal of Lightwave Technology* 36.4 (2018): 1039-1045.
- [3] Ricchiuti, Amelia Lavinia, et al. "Microwave photonics filtering technique for interrogating a very-weak fiber Bragg grating cascade sensor." *IEEE Photonics Journal* 6.6 (2014): 1-10.
- [4] Capmany, José, and Dalma Novak. "Microwave photonics combines two worlds." *Nature photonics* 1.6 (2007): 319.
- [5] Yao, Jianping. "Microwave photonics for 5G." *Broadband Access Communication Technologies XIII*. Vol. 10945. International Society for Optics and Photonics, 2019.
- [6] Alavi, S. E., et al. "Towards 5G: A photonic based millimeter wave signal generation for applying in 5G access fronthaul." *Scientific reports* 6 (2016): 19891.
- [7] Molony, A., C. Edge, and I. Bennion. "Fibre grating time delay element for phased array antennas." *Electronics Letters* 31.17 (1995): 1485-1486.
- [8] Zmuda, Henry, et al. "Photonic beamformer for phased array antennas using a fiber grating prism." *IEEE Photonics Technology Letters* 9.2 (1997): 241-243. 241–243 (1997).
- [9] Roman, J. F., et al. "Time-steered array with a chirped grating beamformer." *Electronics Letters* 33.8 (1997): 652-653.
- [10] Zhao, Jiejun, et al. "Configurable Photonic True-Time Delay Line Based On Cascaded Linearly Chirped Fiber Bragg Grating." *2018 International Topical Meeting on Microwave Photonics (MWP)*. IEEE, 2018.
- [11] Zhang, Fan, et al. "Integrated optical true time delay network based on grating-assisted contradirectional couplers for phased array antennas." *IEEE Journal of Selected Topics in Quantum Electronics* (2020).

- [12] Capmany, Jose, Daniel Pastor, and Beatriz Ortega. "New and flexible fiber-optic delay-line filters using chirped Bragg gratings and laser arrays." *IEEE Transactions on Microwave Theory and Techniques* 47.7 (1999): 1321-1326.
- [13] Meng, Xue Jun, Tai Chau, and Ming C. Wu. "Experimental demonstration of modulation bandwidth enhancement in distributed feedback lasers with external light injection." *Electronics Letters* 34.21 (1998): 2031-2032.
- [14] Lau, E. K., Sung, H. K. & Wu, M. C. in *Proc. IEEE Opt. Fiber Commun. Conf. Anaheim, California, USA OTh G2* (2006).
- [15] Zheng, Jilin, et al. "Experimental demonstration of amplified feedback DFB laser with modulation bandwidth enhancement based on the Reconstruction Equivalent Chirp Technique." *IEEE Photonics Journal* 9.6 (2017): 1-8.
- [16] Lau, Erwin K., et al. "Bandwidth enhancement by master modulation of optical injection-locked lasers." *Journal of lightwave technology* 26.15 (2008): 2584-2593.
- [17] Wey, Y. G. et al. Wey, Yih-Guei, et al. "110-GHz GaInAs/InP double heterostructure pin photodetectors." *Journal of lightwave technology* 13.7 (1995): 1490-1499.
- [18] Oehme, M., et al. "High bandwidth Ge p-i-n photodetector integrated on Si." *Applied physics letters* 89.7 (2006): 071117.
- [19] Beling, Andreas, et al. "Miniaturized waveguide-integrated pin photodetector with 120-GHz bandwidth and high responsivity." *IEEE Photonics Technology Letters* 17.10 (2005): 2152-2154.
- [20] Coppinger, F., A. S. Bhushan, and B. Jalali. "Photonic time stretch and its application to analog-to-digital conversion." *IEEE Transactions on microwave theory and techniques* 47.7 (1999): 1309-1314.
- [21] Han, Yan, and Bahram Jalali. "Photonic time-stretched analog-to-digital converter: Fundamental concepts and practical considerations." *Journal of Lightwave Technology* 21.12 (2003): 3085.

- [22] Han, Yan, and Bahram Jalali. "Differential photonic time-stretch analog-to-digital converter." *Conference on Lasers and Electro-Optics*. Optical Society of America, 2003.
- [23] Fuster, J. M., et al. "Single-sideband modulation in photonic time-stretch analogue-to-digital conversion." *Electronics Letters* 37.1 (2001): 67-68.
- [24] Chi, Hao, et al. "Microwave spectrum sensing based on photonic time stretch and compressive sampling." *Optics letters* 38.2 (2013): 136-138.
- [25] Han, Yan, Ozdal Boyraz, and Bahram Jalali. "Ultrawide-band photonic time-stretch A/D converter employing phase diversity." *IEEE transactions on microwave theory and techniques* 53.4 (2005): 1404-1408.
- [26] Hervás, Javier, et al. "An interrogation technique of FBG cascade sensors using wavelength to radio-frequency delay mapping." *Journal of Lightwave Technology* 33.11 (2015): 2222-2227.
- [27] Pastor-Graells, Juan, et al. "Single-shot distributed temperature and strain tracking using direct detection phase-sensitive OTDR with chirped pulses." *Optics express* 24.12 (2016): 13121-13133.
- [28] Zhou, Ling, et al. "Distributed strain and vibration sensing system based on phase-sensitive OTDR." *IEEE Photonics Technology Letters* 27.17 (2015): 1884-1887.
- [29] He, Haijun, et al. "Enhanced range of the dynamic strain measurement in phase-sensitive OTDR with tunable sensitivity." *Optics Express* 28.1 (2020): 226-237.
- [30] Oberson, Philippe, et al. "Optical frequency domain reflectometry with a narrow linewidth fiber laser." *IEEE Photonics Technology Letters* 12.7 (2000): 867-869.
- [31] Zhou, Bin, et al. "Low coherent optical frequency domain reflectometry interrogates fiber Bragg grating sensors." *Journal of lightwave technology* 28.21 (2010): 3049-3054.
- [32] Hua, Liwei, et al. "Coherence-length-gated distributed optical fiber sensing based on microwave-photonics interferometry." *Optics express* 25.25 (2017): 31362-31376.
- [33] Komukai, T., and Masataka Nakazawa. "Fabrication of high-quality long-fiber Bragg grating by monitoring 3.1-eV radiation (400 nm) from

- GeO defects." *IEEE Photonics Technology Letters* 8.11 (1996): 1495-1497.
- [34] Camatel, Stefano, and Valter Ferrero. "Narrow linewidth CW laser phase noise characterization methods for coherent transmission system applications." *Journal of Lightwave Technology* 26.17 (2008): 3048-3055.
- [35] Yabuzaki, T., Takahisa Mitsui, and U. Tanaka. "New type of high-resolution spectroscopy with a diode laser." *Physical review letters* 67.18 (1991): 2453.
- [36] Camparo, J. C. "Conversion of laser phase noise to amplitude noise in an optically thick vapor." *JOSA B* 15.3 (1998): 1177-1186.
- [37] Camparo, James C., and John G. Coffey. "Conversion of laser phase noise to amplitude noise in a resonant atomic vapor: The role of laser linewidth." *Physical Review A* 59.1 (1999): 728.
- [38] Dandridge, A., and A. B. Tveten. "Phase noise of single-mode diode lasers in interferometer systems." *Applied Physics Letters* 39.7 (1981): 530-532.
- [39] Minardo, Aldo, and Luigi Zeni. "Influence of laser phase noise on Brillouin optical time-domain analysis sensors." *Sixth European Workshop on Optical Fibre Sensors*. Vol. 9916. International Society for Optics and Photonics, 2016.
- [40] Urricelqui, Javier, Marcelo A. Soto, and Luc Thévenaz. "Sources of noise in Brillouin optical time-domain analyzers." *24th International Conference on Optical Fibre Sensors*. Vol. 9634. International Society for Optics and Photonics, 2015.
- [41] Fernández-Ruiz, María R., et al. "Laser phase-noise cancellation in chirped-pulse distributed acoustic sensors." *Journal of Lightwave Technology* 36.4 (2018): 979-985.



**Chapter 6**  
**Summary,**  
**conclusions and**  
**open research lines**

## 6.1. Summary and conclusions

As described in the objectives of this Ph.D. two research lines were followed, to implement new interrogation systems and sensors using: plastic optical fibers and glass fibers.

In chapter 1, the introduction contextualizes this work in the optical fiber sensing field. Distributed and discrete fiber sensing have been presented and the breakthrough of long FBGs arrays for quasi-distributed sensing has been assessed. The state of the art for fiber sensing using plastic fiber was presented as well. The most common fabrication methods have been reported. The techniques and interrogation systems used to exploit POFs as sensors have been introduced.

In chapter 2, an intensity based POF sensors is presented for the monitoring of vital signal monitoring (movements, breath rate). The implementation of the sensor using commercial POFs and electronic components is reported. The experimental tests confirm the possibility to use the sensor in a real application. The first circuit was then re-designed to be scaled to a compact version with smaller dimensions and two PCB were fabricated with new components. Custom 3D printed mechanical pieces were produced to substitute the bulky connector-less LED used in the first design. The new boards had very small dimensions (10x3.5 cm and 3x2 cm) and are equipped with a Bluetooth module and batteries holder, making the device portable.

In chapter 3, the fabrication and experimental validation of a new bend-direction and rotation sensor have been presented. Extrusion from pellet was investigated as a novel method to fabricate plastic optical fiber for sensing. An extensive experimental work was carried out, first with circular fibers, to study the effect of the process parameters on the optical losses of the obtained POFs. A custom extrusion die was designed to obtain a three lobe POF. The results of the mode confinement simulations demonstrate that this kind of fiber can be used to estimate the bend-direction. An

experimental setup was used to demonstrate the possibility to use the three lobes POF as bend-direction and rotation sensor. The fabricated fibers can be embedded in textiles or composite thanks to their mechanical properties and used to monitor the presence of curvature or rotation inside the material, monitoring the light intensity transmitted in the POF sensor proposed.

In chapter 4, a novel interrogation system for dense FBGs array is presented. A compact laser module was adopted to generate ultra-short optical pulse without the employing of external electro-optical modulation. A dense array of nearly identical 500 FBGs, fabricated using draw tower technology, was interrogated. The higher backscattered signal was detected using a photodiode and processed offline. A dispersion was added to the input optical pulse. When a change in the refractive index occurs in a grating area, the pulse back reflected experiences a time shift and a change in amplitude. Comparing consecutive traces, it is possible to derivate the temperature change from the time delay. The setup was modified to sense vibration as well. The back reflected signal was fed to an avalanche photodiode connected to an electric signal analyzer. The temperature was measured with sub-cm spatial resolution and  $1^\circ$  of resolution. Wide frequency range vibrations were sensed using the modified setup, between 15 and 245 kHz.

In chapter 5, MWP filter technique applied to fiber sensing is introduced. The coherence regime depends on the relation between the linewidth of the optical source and the optical path between the reflectors. Incoherent and coherent regimes influence greatly the operation in the interrogation of weak fiber Bragg gratings array. Two arrays of four FBGs, with different grating spacing, were fabricated and interrogated using a MWP scheme and a light source with two different linewidths. The effect of the phase noise on the amplitude noise was studied and the experimental results were presented.



## 6.2. Open research lines

Some of the work presented in this thesis may be improved in the future:

- Plastic optical fiber sensors:
  - The compact interrogation board presented in chapter 2 can be improved in terms of sample frequency and sensitivity for new applications.
  - New simulation results may indicate other POF shapes that can be interesting for sensing purposes. The fabrication of new core shapes and multicore POFs could be an interesting challenge for the fabrication method used to fabricate the three lobes POF.
  
- Weak fiber gratings array interrogation systems
  - The compact robust components used to implement the interrogation system of chapter 4, allow designing a compact interrogation system. This can be a novel solution for the interrogation of weak fiber gratings.
  - Interferometric methods showed potential as an alternative to the most common interrogation systems for fiber sensors. The possibility to implement an interferometric interrogation system using MWP may be studied.

## Appendix 1

### Glossary

POF: plastic optical fiber  
OTDR: optical time domain reflectometry  
OFDR: optical frequency domain reflectometry  
 $\Phi$ -OTDR: phase sensitive optical time domain reflectometry  
FBG: fiber Bragg grating  
WDM: wavelength division multiplexing  
mPOF: microstructured plastic optical fiber  
PMMA: poly methyl methacrylate  
MWP: microwave photonic techniques  
DAC: digital to analog converter  
ADC: analog to digital converter  
PCB: printed circuit board  
SMD: surface mount device  
SMF: single mode fiber  
TFBG: tilted fiber Bragg grating  
PP: polypropylene  
PVDF: polyvinylidene fluoride  
EOM: electro optical modulator  
DFB-LD: distributed feedback laser diode  
GS: gain switching  
DLC: diamond like carbon  
TEC: temperature controller  
APD: avalanche photodiode  
MXA: electric signal analyzer  
PZT: piezoelectric  
ROF: radio over fiber  
IFFT: inverse fast Fourier transform  
DUT: device under test  
EVNA: electric vector network analyzer  
OPD: optical path distance

## **Appendix 2**

### **Author's publications**

#### **Scientific publications in journals**

Sartiano, Demetrio, and Salvador Sales. "Low cost plastic optical fiber pressure sensor embedded in mattress for vital signal monitoring." *Sensors* 17.12 (2017): 2900.

Sartiano, Demetrio, and Salvador Sales. "Monitoring temperature and vibration in a long weak grating array with short-pulse generation using a compact gain-switching laser diode module." *Optics Express* 27.26 (2019): 38661-38669.

Sartiano, Demetrio, Geernaert, Thomas, Torres Roca, Elena, and Sales, Salvador. "Bend-Direction and Rotation Plastic Optical Fiber Sensor." *Sensors* 20.18 (2020): 5405.

#### **Scientific publications in congresses**

Sartiano, Demetrio, Salvador Sales, and Elena Torres Roca. "Three Lobes Plastic Optical Fiber Bending and Rotation Sensor." *Multidisciplinary Digital Publishing Institute Proceedings*. Vol. 15. No. 1. 2019.

Sartiano, Demetrio, Javier Madrigal, and Salvador Sales. "Sub-cm Temperature Monitoring of 500 Weak Gratings Array Through Chirped Ultra-Short Light Pulses." *Optical Sensors*. Optical Society of America, 2019.

Pérez-Galacho, Diego, Demetrio Sartiano, and Salvador Sales. "Fronthaul links based on Analog Radio over Fiber." *2019 European Conference on Networks and Communications (EuCNC)*. IEEE, 2019.

Perez-Galacho, Diego, Demetrio Sartiano, and Salvador Sales. "Analog Radio over Fiber Links for Future 5G Radio Access Networks." *2019 21st International Conference on Transparent Optical Networks (ICTON)*. IEEE, 2019.

Sartiano, Demetrio, et al. "On the Use of Microwave Photonics Techniques for Novel Sensing Applications." *2019 21st International Conference on Transparent Optical Networks (ICTON)*. IEEE, 2019.

## **Participation in research projects**

- FINESSE
  - Financing entity: European commission
  - Duration from: Oct 2016 - Sept 2020
  - Grant value: 3,880,324.44 €
  
- DIMENSION
  - Financing entity: Ministerio de Economía y Competividad
  - Duration from: Jan 2018 – Dec 2020
  - Grant value: 203,280 €